

ABSTRACT

Title of Document: DETERMINATION OF MIXED-MODE
ENERGY RELEASE RATES IN
LAMINATED CARBON FIBER
COMPOSITE STRUCTURES USING
DIGITAL IMAGE CORRELATION

Ensign Joseph F Puishys III, USN,
Mechanical Engineering, 2013

Directed By: Dr. Hugh A. Bruck
Professor, Department of Mechanical
Engineering

Carbon fiber composites have recently seen a large scale application in industry due to its high strength and low weight. Despite numerous beneficial attributes of composite materials, they are subject to several unique challenges; the most prevalent and troubling is delamination fracture.

This research program is focused on developing an appropriate damage model capable of analyzing microscopic stress strain growth at the crack tip of laminated composites. This thesis focuses on capturing and identifying the varying stress and strain fields, as well as other microstructural details and phenomena unique to crack tip propagation in carbon fiber panels using a novel mechanical characterization technique known as Digital Image Correlation (DIC).

DETERMINATION OF MIXED-MODE ENERGY RELEASE RATES IN
LAMINATED CARBON FIBER COMPOSITE STRUCTURES USING DIGITAL
IMAGE CORRELATION

By

Ensign Joseph F. Puishys III, USN.

Thesis submitted to the Faculty of the Graduate School of the
University of Maryland, College Park, in partial fulfillment
of the requirements for the degree of
Master of Science
2013

Advisory Committee:
Professor Hugh A. Bruck, Chair
Dr. Abhijit Dasgupta
Dr. Sung Lee

© Copyright by
Ensign Joseph F. Puishys III, USN
2012

Preface

This research was conducted at the University of Maryland, College Park under the direction of Dr. Hugh A. Bruck from January 2012 until December 2012 as part of a cooperative program between the United States Naval Academy, and the University of Maryland wherein students are allowed to begin their masters coursework while still an undergrad. Students are allowed precisely one calendar year to complete graduate work before being sent to their next duty station, where Naval officers will use their experience, classroom education, and research skills to further advance the United States Navy as the most technologically advanced force in the United States' arsenal. Funding for this research and coursework is made possible by the Office of Naval Research, and the Department of Defense.

Dedication

I wish to dedicate this work to my shipmates, those who are serving this country both at home and abroad, as well as the soldiers, sailors, and airmen who have gone before me and given the ultimate sacrifice.

“Only our individual faith in freedom can keep us free” – Dwight D. Eisenhower

Acknowledgements

I wish to acknowledge the following for their assistance, consultation, and instruction which have made my work possible:

Dr. Hugh Bruck, University of Maryland, Mechanical Engineering

Sandip Haldar, University of Maryland, Mechanical Engineering

Prakhar Singh, University of Maryland, Mechanical Engineering

Ananth Virakthi, University of Maryland, Aerospace Engineering

Dr. Peter Joyce, United States Naval Academy, Mechanical Engineering

Fanny Planes, University of Maryland, Mechanical Engineering

Alex Zahn, University of Maryland, Mechanical Engineering

I also wish to acknowledge Ms. Krystal Kenney for providing me much support throughout my research program, as well as transportation to and from the University of Maryland, without which this course of study would not have been possible.

Lastly, I wish to acknowledge my mother, Mrs. Kathi Puishys, and my father, Mr. Joe Puishys for all of the love, encouragement, and support they have provided over the last 22 years.

This work was supported by NAWCAD in Pax River, MD through cooperative agreement N00421-98-H-1116 with the University of Maryland.

Table of Contents

Preface	ii
Dedication	iii
Acknowledgements	iv
Table of Contents	v
List of Tables	x
List of Figures	xi

Chapter 1: Introduction

1.1 Introduction.....	1
Introduction.....	1
Research Program Focus.....	2
1.2 Thesis Outline	3

Chapter 2: Literature Review

2.1 Composite Materials	4
2.2 Laminate Damage Mechanisms	5
2.3 Fracture	8
Introduction to Fracture	8
Fracture Modes	8
Griffith's Criterion and Energy Approach.....	9
2.4 Crack Tip Displacement Theory.....	11
Crack Opening Displacement	11
Crack Shear Displacement.....	11
2.5 Digital Image Correlation	13
2.6 Closing Remarks.....	15

Chapter 3: ASTM Standard and the Wyoming Test Fixture

3.1 Introduction.....	16
3.2 Nomenclature and Definitions	17
3.3 Geometric Relations.....	17
3.4 Loading Parameters	18
Test Schematic	19
3.5 Specimen Properties.....	19
3.6 Special Parameters for Experimental Analysis.....	19
Transverse Modulus Correction Parameter	19
Crack Length Correction Parameter	20
3.7 Variation in Mode Mixture for Wyoming Test Fixture	20
3.8 Pure Mode I Testing.....	21
Wyoming Test Fixture MMB limitations	21
Double Cantelever Beam Test	21
Double Cantelever Beam Test Theory.....	22
3.9 Identification of Laminated Composite Specimens for Testing	23
Estimated Deflection.....	24
Estimated Load	24
3.10 Preparation of Unidirectional Laminated Composite Test Specimens	24
Criteria for Manufacturing.....	24
Ply Lay-up Process	26
Composite Cure Cycle	27
Sample Post Processing	28
3.11 Determination of Material Properties for Unidirectional Carbon Fiber	30
3.12 ASTM Standard for Calculation of Mode Mixity.....	33
Introduction.....	33
Calibration Factors.....	34
Fiber Modulus Calculation	37
Fracture Parameters Calculation.....	38

Chapter 4: New Test Protocol for Conducting Mixed Mode Fracture

Tests using Wyoming Test Fixture and DIC

4.1 Test Protocol Introduction	39
Introduction.....	39
Imaging the Speckle Pattern	40
4.2 Digital Imaging and Microscopy	42
Equipment Overview	42
4.3 Test Protocol	45
Test Setup.....	46
Image Collection and Data Tracking	46
Data Analysis	47
4.4 Test Protocol Summary.....	48
Introduction.....	48
Delimited Task List.....	48
4.5 Testing Protocol Conclusions	51

Chapter 5: Initial Multi-scale Mixed-Mode Fracture Experiments

5.1 Load Displacement Data From Typical Experimentation	52
Introduction.....	52
Load Displacement Data.....	53
5.2 Attempts to Arrest Crack Growth and Induce Stability.....	52
5.3 Analytical Methods for Determination of Fracture Parameters.....	52
5.4 Analysis of Analytically Obtained Fracture Parameters.....	63
5.5 Mixed Mode Fracture Experiments Analyzed Using Crack Tip Displacement	64
COD and CSD analysis from DIC	65
5.6 Crack Tip Displacement Results From DIC Analysis	67
COD and CSD analysis from DIC	70
5.7 Crack Tip Displacement Analysis and Conclusions.....	75
Crack Tip Displacement Results.....	76

Chapter 6: Fracture Parameters Extracted Using Synthetic Data from

FEA Model

6.1 FEA Modeling of Mixed Mode Fracture Fixture	77
Introduction.....	77
FEA Model.....	78
6.2 Crack Tip Displacements Using Synthetic Data.....	79
6.3 Full Field Analysis with Synthetic FEA Data	82
6.4 Synthetic Data Results Extracted from FEA Modeling.....	80
0% Mode Mixture.....	80
50% Mode Mixture.....	83
50% Mode Mixture.....	89
100% Mode Mixture.....	92
6.5 Discussion of FEA Results	94

Chapter 7: Full Field Fracture Analysis Using DIC

7.1 Full Field Displacement analysis of Mixed Mode Fracture.....	99
Introduction.....	99
Typical Results.....	100
7.2 Refined Full Field Analysis	105
7.3 Full Field Analysis for 0% Mode Mixture DIC Data	112
7.4 Full Field Analysis for 22% Mode Mixture DIC Data	116
7.5 Full Field Analysis for 22% Mode Mixture DIC Data After Crack Propagation	121
7.6 Full Field Analysis for 50% Mode Mixture DIC Data	128
7.7 Full Field Analysis for 100% Mode Mixture DIC Data	130
7.8 Analysis of Fracture Parameters Extracted from Full Field DIC Displacement Data.....	135

Chapter 8: Scientific and Technical Contributions

8.1 New Test Protocol for Obtaining Mixed Mode Energy Release Rates using a Wyoming Test Fixture and DIC	137
---	-----

8.2 Measurement of Mixed Mode Energy Release Rates.....	137
8.3 Measurement of Mixed Mode Crack Growth using New Test Protocol	140
8.4 Development of Accurate Fitting Function for Fracture Parameters.....	141
Chapter 9: Future Work	
9.1 Characterization of Fiber Bridging and its Effect on Fracture Parameters.....	142
9.2 Characterization and Testing of Multidirectional Laminate Structures.....	142
9.3 Fatigue Fracture Testing of Composite Laminates	143
References.....	144

List of Tables

Table 1: Material properties of unidirectional carbon fiber laminate.....	33
Table 2: Strain energy release rate calculated from CTD analysis.....	75
Table 3: Fracture parameters for synthetic data from FEA model compared to ASTM standard.....	96
Table 4: Difference in slope of load displacement curve for FEA model, and experimental data.....	97
Table 5: Fracture parameters for DIC data compared to ASTM standard, 0% Mode Mixture during crack growth.	114
Table 6: Fracture parameters for DIC data compared to ASTM standard, 22% Mode Mixture before crack growth.	117
Table 7: Fracture parameters for DIC data compared to ASTM standard, 22% Mode Mixture post initial crack growth.....	120
Table 8: Fracture parameters for DIC data compared to ASTM standard, 50% Mode Mixture	127
Table 9: Fracture parameters for DIC data compared to ASTM standard, 100% Mode Mixture	130
Table 10: Fracture parameters from DIC data compared to ASTM Analysis	134
Table 11: Summary of fracture parameters for 0% Mode Mixture	137
Table 12: Summary of fracture parameters for 22% Mode Mixture.....	137
Table 13: Summary of fracture parameters for 50% Mode Mixture.....	137
Table 14: Summary of fracture parameters for 100% Mode Mixture.....	138

List of Figures

Figure 1: Transverse tensile failure in Unidirectional Carbon Fiber, taken with scanning electron microscope. Baral, [4]	6
Figure 2: Catastrophic delamination of glass fiber composite , Medford, [5].....	6
Figure 3: Fracture Modes, Image Courtesy of Robinson [8]	9
Figure 4: MMB Test schematic	18
Figure 5: Lever arm length and mode mixture	20
Figure 6: Schematic for Double Cantilever Beam Test, Balzani [19]	21
Figure 7: Typical Cure Cycle for Pre-Preg Carbon Fiber.....	27
Figure 8: Specimen configuration for Mixed-mode fracture characterization with loading tabs affixed. [15]	28
Figure 9: Test Specimen and complete Wyoming Test Fixture for MMB setup for 22% Mode Mixture Test.....	30
Figure 10: Load-displacement curves for 3 point bend tests in axial and transverse fiber directions.....	32
Figure 11: Example of poor speckle pattern for DIC.....	40
Figure 12: Example of ideal speckle pattern for DIC.....	41
Figure 13: Camera set up using traditional camera lens for far field DIC analysis...	42
Figure 14: Edmond optics microscope mounted in translating microscope stand...	43
Figure 15: Ring mounted high output light for illuminating test samples.....	44
Figure 16: Theoretical values of GI, and GII as a function of Load.....	52

Figure 17: Raw Load-displacement data for 22% Mode Mixture unidirectional test specimen (red), and compliance corrected load-displacement (blue).....	53
Figure 18: Raw Load-displacement data for 50% Mode Mixture unidirectional test specimen (red), and compliance corrected load-displacement (blue).....	54
Figure 19: Raw Load-displacement data for 100% Mode Mixture unidirectional test specimen (red), and compliance corrected load-displacement (blue).....	55
Figure 20: Change in crack length-displacement data for a 22% mode mixture unidirectional test.....	58
Figure 21: G_{IC} versus change in crack length data for a 22% mode mixture.....	59
Figure 22: Shear Fracture Toughness for 22% mode mixture test.....	60
Figure 23: Shear Fracture Toughness for 50% mode mixture test	61
Figure 24: Shear Fracture Toughness for 100% mode mixture test.....	61
Figure 25. A typical cracked specimen showing orientation of CSD and COD.....	65
Figure 26. DIC results showing (left) near-field displacements transverse to the crack, and (right) far-field shear strain at the crack tip with various length scales.....	67
Figure 27. CSD (left) and COD (right) extracted from a 50% Mode II test using DIC and subsequent fits using equations (5) and (6).....	67
Figure 28. COD (top) and CSD (bottom) extracted from 22% Mode Mixture test using DIC and subsequent fits using equations (5) and (6).....	69
Figure 29: Crack Opening Displacement data and fit for near field solution (Top) and Crack Shear Displacement and fit for near field solution (Bottom).....	67

Figure 30: Crack Opening Displacement data and fit for perfect synthetic data at 79 N (Top) and Crack Shear Displacement and fit (Bottom).....	74
Figure 31: Illustration of the model constructed in ABAQUS.....	78
Figure 32: Test specimen model with meshing region.....	78
Figure 33: FEA modeling crack tip displacement data with analytical fit. For 22% mode mixture case at 28.14 N load.....	80
Figure 34: FEA modeling for crack tip displacement analysis for 22% mode mixture case at 79 N load.....	81
Figure 35: V and U fields from FEA and analytical solution at 21.84 N Load, 0% mode mixture.....	83
Figure 36: V and U fields from FEA and analytical solution at 56.28 N Load, 0% mode mixture.....	84
Figure 37: V and U fields from FEA and analytical solution at 84.42 N Load, 0% mode mixture.....	84
Figure 38: V and U fields from FEA and analytical solution at 112.56 N Load, 0% mode mixture.....	85
Figure 39: V and U fields from FEA and analytical solution at 21.84 N Load, 22% mode mixture.....	86
Figure 40: V and U fields from FEA and analytical solution at 56.28 N Load, 22% mode mixture.....	86

Figure 41: V and U fields from FEA and analytical solution at 84.42 N Load, 22% mode mixture.....	87
Figure 42: V and U fields from FEA and analytical solution at 112.56 N Load, 22% mode mixture.....	87
Figure:43 Shear Fracture Toughness extracted from Analytical Full Field Solution compared to ASTM for 22% FEA Test.....	88
Figure 44: Shear Fracture Toughness extracted from Analytical Full Field Solution compared to ASTM.....	88
Figure 45: V and U fields from FEA and analytical solution at 21.84 N Load, 50% mode mixture.....	89
Figure 46: V and U fields from FEA and analytical solution at 56.28 N Load, 50% mode mixture.....	89
Figure 47: V and U fields from FEA and analytical solution at 84.42 N Load, 50% mode mixture.....	90
Figure 48: V and U fields from FEA and analytical solution at 112.56 N Load, 50% mode mixture.....	90
Figure:49 Shear Fracture Toughness extracted from Analytical Full Field Solution compared to ASTM for 50% FEA Test.....	91
Figure 50: V and U fields from FEA and analytical solution at 21.84 N Load, 100% mode mixture.....	92

Figure 51: V and U fields from FEA and analytical solution at 56.28 N Load, 100% mode mixture.....	92
Figure 52: V and U fields from FEA and analytical solution at 84.42 N Load, 100% mode mixture.....	93
Figure 53: V and U fields from FEA and analytical solution at 112.56 N Load, 100% mode mixture.....	93
Figure 54: Shear Fracture Toughness extracted from Analytical Full Field Solution compared to ASTM for 50% FEA Test	94
Figure 55: Crack Tip displacement fits at 76 N load for 22% Mode Mixture Test....	99
Figure 56: DIC and Analytical solution for full field displacements in U and V fields 76 N load for 22% Mode Mixture Test.....	94
Figure 57: Full Field measured DIC displacement, and Fit functions for a “good” quality fit of 22% mode mixture fracture test.....	106
Figure 58: Full Field measured DIC displacements in v and u field for 50% test at 270 N load.....	108
Figure 59: Full Field DIC displacements in v and u field for 50% test at 270 N....	109
Figure 60: Fitted displacements in v and u field for 50% test after data seeding....	109
Figure 61: DIC and fitted displacements for v and u field for 50% test after data seeding and addition of crack rotation parameters.....	110
Figure 62: Final optimal fit for displacements in v and u field for 50% test.....	111
Figure 63: Load displacement curve for 0% Mode Mixture fracture test (DCB)....	112
Figure 64: Crack length with respect to displacement during DCB test.....	113

Figure 65: Strain energy release rate G_I with respect to crack length for 0% DCB test.....	113
Figure 66: V and U fields from DIC and Analytical fit at 40 N, 0% Mixture.....	114
Figure 67: V and U fields from DIC and Analytical fit at 50 N, 0% Mixture.....	115
Figure 68: V and U fields from DIC and Analytical fit at 60 N, 22% Mixture.....	117
Figure 69: V and U fields from DIC and Analytical fit at 70 N, 22% Mixture.....	118
Figure 70: V and U fields from DIC and Analytical fit at 79 N, 22% Mixture.....	118
Figure 71: Fracture Parameters calculated from DIC data compared with ASTM Standard for LEFM region of 22% mode mixture fracture test.....	119
Figure 72: V and U fields from DIC and Analytical fit at 40 N, 22% Mixture.....	120
Figure 73: V and U fields from DIC and Analytical fit at 50 N, 22% Mixture.....	121
Figure 74: V and U fields from DIC and Analytical fit at 60 N, 22% Mixture.....	121
Figure 75: Fracture Parameters calculated from DIC data compared with ASTM Standard after initial crack propagation of 22% mode mixture fracture test.....	122
Figure 76: Strain energy release rate with increasing load and crack length for a 22% mode mixture test.	123
Figure 77: Strain energy release rate with increasing crack length for a 22% mode mixture test.	124
Figure 78: Strain in xx (left) yy (right) and xy orientation (bottom).....	125
Figure 79: Fiber bridging in a 22% mode mixture test analyzed for DIC.....	126

Figure 80: V and U fields from DIC and Analytical fit at 200 N, 50% Mixture.....	128
Figure 81: V and U fields from DIC and Analytical fit at 299 N, 50% Mixture.....	128
Figure 82: Fracture Parameters calculated from DIC data compared with ASTM Standard after initial crack propagation of 50% mode mixture fracture test.....	129
Figure 83: V and U fields from DIC and Analytical fit at 300 N, 100% Mixture...	130
Figure 84: V and U fields from DIC and Analytical fit at 350 N, 100% Mixture...	131
Figure 85: V and U fields from DIC and Analytical fit at 380 N, 100% Mixture...	131
Figure 86: Fracture Parameters calculated from DIC data compared with ASTM Standard after initial crack propagation of 100% mode mixture fracture test.....	132
Figure 87: Strain in xx (left) yy (right) and xy orientation (bottom) for 100%.....	133

Chapter 1: Introduction

1.1 Introduction

The past four decades have seen remarkable changes in the manner in which industry utilizes materials. Particularly prevalent in the military industry, is a marked shift away from heavy, homogenous, and well understood metallic materials, to more versatile, and lightweight polymer matrix composites. Structures that were traditionally metal I beams are often replaced with composite sandwich structures. Structures which were sheet metal are now often replaced with laminates. The need for low cost and lightweight materials for use in aviation platforms, automotive industry, and marine vehicles has spurred tremendous advances in composite technology. Composite engineering has come a long way from the thatched straw and mud bricks used by the Egyptians some 4000 years ago, though the principles have remained relatively unchanged. The first fiberglass-epoxy systems were developed in 1935, however these were still too weak for industrial application. It wasn't until the 1970's when carbon fiber structures were developed that could match and outperform the strength of some metals. Today, composites are a state of the art material; extremely versatile and offering limitless potential. In particular, carbon fiber has become an industry and high design favorite, often applied in weaves with high performance resins such as PEEK, carbon fiber has found itself in almost every imaginable application. Such tremendous advances in technology however, are not without disadvantage. Carbon fiber composites, by nature, are a highly directional material, and one which exhibits favorable characteristics in only discrete directions.

The major drawback to the use of composite laminates is their predisposition to fracture failure. Very little is known about crack propagation in composite laminates, and until recently only global load conditions and displacements have been measured.

This research program is focused on developing an appropriate damage model, capable of analyzing microscopic stress strain growth at the crack tip of laminated composites. This course of study intends to capture the varying stress and strain fields, as well as other microstructural details and phenomena unique to crack tip propagation in unidirectional carbon fiber panels using a novel mechanical characterization technique known as Digital Image Correlation (DIC). Using DIC and very fine resolution cameras enables detection and quantification of strain fields present in mixed mode fracture. These details are then used to enhance existing models by providing critical details and explanations on the failure mechanisms and fracture growth which occurs under loading.

This research represents the first attempt to utilize DIC to extract fracture parameters of composite laminate structures under mixed mode I and mode II bending conditions with the Wyoming Test Fixtures, MMB-52 fixture. The analysis presented within this research affirms the successful use of DIC for applications with fracture mechanics, as well as the limitations of such techniques. This research also presents a systematic and comprehensive protocol for conducting DIC under mixed mode bending for composite laminate structures.

1.2 Thesis Outline

A literature review is presented in subsequent pages, briefly describing the fundamentals of composite materials engineering, the most common failure mechanisms involved with them, as well as an introduction to the principles behind Linear Elastic Fracture Mechanics. Also presented in the literature review are the basic principles behind DIC, and its application for this course of study. Following the discussion of these principles comes the mathematical analysis used for traditional analysis of fracture parameters, followed by a detailed test protocol which shows an in depth method for conducting fracture tests using the Wyoming Test Fixtures MMB apparatus. Theoretical analysis using traditional methods, crack tip displacement analysis, full field data analysis, as well as synthetic data acquired through Finite Element Analysis are presented in the results section. Conclusions about the use of DIC for extraction of fracture parameters are made. Lastly, future work and suggested improvements to this course of study finish the thesis.

Chapter 2: Literature Review

2.1 Composite Materials

Composite materials are engineered materials made from two primary components known as constituents, which remain separate and distinct within the finished structure, but combine to create a super lightweight yet amazingly resilient structure. The first material is typically a pattern weave of fibrous material called the reinforcement, usually consisting of extruded glass fibers, carbon fibers, Kevlar fibers, metal or in some cases ceramic particles. These fibers are then embedded in a much softer matrix. The matrix may vary with the use of select soft metals, epoxy resins, or even ceramics. This course of study however focuses explicitly on the use of polymer matrix compositions as they are commonly found in the aerospace industry. The reinforcement material is what gives the composite its high axial strength and other favorable properties, while the matrix serves to transfer the load among the reinforcements, and hold the reinforcement in an orderly and continuous fashion. The reinforcement may vary with orientation with the fibers all in one orientation, known as a unidirectional composite, or in two directions, known as a bidirectional weave. Non-continuous fibers are also used for composite materials, and the reinforcement may vary from short randomly spaced fibers to discrete particles, however only continuous fibers are investigated in this research program. Composites may also be comprised of numerous discrete fiber orientations; this is most commonly referred to as a laminate. Laminates make use of the directional

properties of the reinforcement, and by stacking several plies in multiple directions a much stronger structure is formed, resistant to stresses in multiple directions.

Characterization of the stacking sequence is intrinsic to understanding the nature of a particular laminate under investigation. Laminate stacking sequence is reported for each test specimen used in corresponding tests. Puishys, [1] This course of study primarily analyzes unidirectional carbon fiber composite laminates.

2.2 Laminate Damage Mechanisms

Though good strength to weight ratios may be fundamentally positive characteristics of composite laminates, they are not without significant drawbacks. The directional nature of fiber reinforcement puts special emphasis on the engineer to properly design composite components for its expected load, and application. Unidirectional laminates are particularly weak when loaded transverse to the fiber direction, and take on the strength characteristics of the matrix only. This is predominantly troubling when a laminate is loaded in bending. Nikbakht, [2] Defects in the composite's matrix, such as voids, contaminants, resin pockets, and ply drop off, combined with defects in the fibers themselves such as broken fibers, fiber slacks, kinks, misalignments, and deboned areas are all issues unique to composite engineering. Scale, [3] The ultimate strength rarely is effected by such defects, however the failure mechanisms of composite materials are drastically impacted.

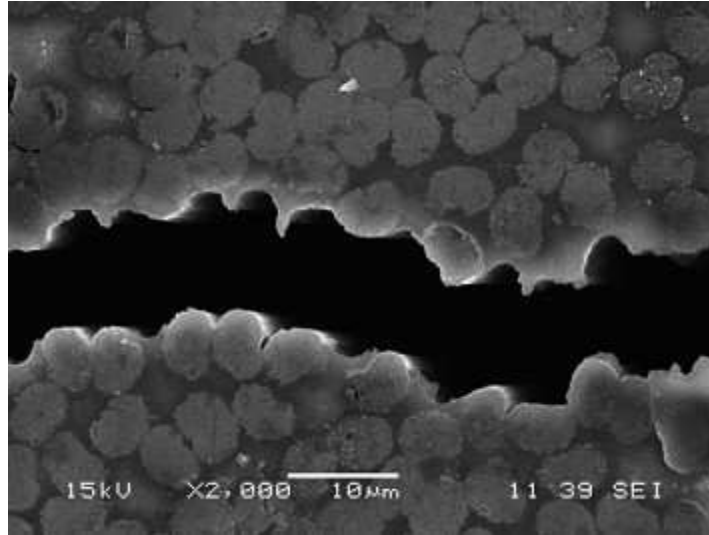


Figure 1. Transverse tensile failure in Unidirectional Carbon Fiber, taken with scanning electron microscope. Baral, [4]

Such unique problems truly differentiate composite laminates from homogenous materials. Though many failure mechanisms are not specifically unique to composites, the propensity for delamination certainly is. *Figure 1* demonstrates the propensity for crack propagation to occur in the matrix material. *Figure 2* shows catastrophic delamination failure in composites.



Figure 2. Catastrophic delamination of glass fiber composite laminate, Medford, [5]

The most predominant failure mechanism of composite material systems is the physical failure of the matrix material bonds in interlaminar failure. Delamination, is the result of stress which breaks the the cohesive matrix holding together the reinforcement, forming separate and discrete layers with a significant loss to the

mechanical strength of the laminate. [1] Though it is the engineer's duty to ensure that a composite system is designed to carry the bulk of the load in the fibers, the matrix still proves essential in maintaining the structural integrity of the system, as well as transferring and distributing load across the entire specimen. Fracture in the matrix, and the subsequent debonding of lamina may not be catastrophic for a composite laminate as is the case in *figure 2*, however, delamination does reduce structural stiffness, and results in a loss of the system's integrity. [2] As previously stated, delamination is not usually the structural failure, rather the point for further damage to the system. Typical delamination in composite laminates are initiated by compressive loads, something which composites are notoriously poor at withstanding. Buckling and bending, especially with a large cross sectional area results in large displacements which are different for each lamina ply. The simple thought experiment may be applied where one attempts to compress a phone book from binding to the loose end. Imagine how the pages bow outward, and free space develops between the individual pages. When composites are loaded in compression, or in bending, plies on the compression side of the neutral axis are subject to large loads that to pull the individual lamina apart and increase stress the matrix. The initial delamination is now a localized area of debonded material, and in short, a crack defect. This defect under continued load will result in crack propagation and ultimately fracture if critical loads are exceeded. Thusly, delamination is a process in the overall failure of a laminate while fracture is the ultimate destruction of the structure. [2] Delamination is closely linked to the primary damage mechanism of

fracture, and is the main failure mechanism which will be investigated in this course of study.

2.3 Fracture

Fracture is the separation of an object into two or more subsequent pieces. Fracture can occur globally, as is the case for a specimen which has completely parted, or locally as in the case for cracks which propagate across the length of a specimen. Crack propagation and initiation always accompanies fracture of materials; the rate at which it occurs, all depends upon the loading condition as well as material properties. Fracture in homogeneous materials can undergo transgranular fracture, or intergranular fracture; however, in composite materials crack propagation is usually limited to the matrix material as it offers the path of least resistance. Matrix materials tend to fail in a brittle manner, and cracks spread rapidly with little or no plastic deformation. Adams [6] This becomes an issue for tracking crack growth under unstable loading conditions.

Fracture is generally characterized in one of three basic modes, or a combination of two modes as seen in *figure 3*. The first is Mode I, or opening mode fracture, where load is applied in tension to separate layers of the material. The second is Mode II, in plane shear, or sliding mode. And the last fracture mode is Mode III, out of plane shear, or tearing mode. Mixed mode fracture could refer to any combination of these three modes; however, is generally limited to a combination of Mode I and Mode II, as is the case for this course of study. All of which may

generally be tested using methods pioneered by Williams, Carlson and Reeder, [6, 7] such as the Double Cantilever Beam (DCB) test, discussed in greater detail later, as well as the Mixed Mode Bending (MMB) method, first developed for use by NASA in 1988. [6]

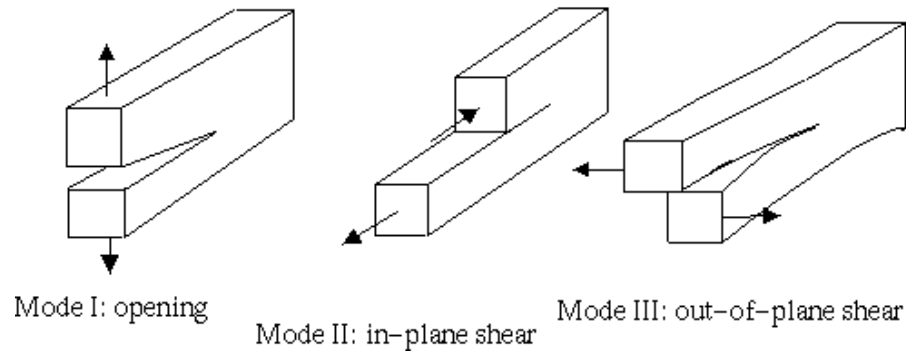


Figure 3: Fracture Modes, Image Courtesy of Robinson [8]

The traditional means of determining parameters governing crack propagation was first examined by A. A. Griffith. Griffith's criterion for quasi-static loads explains crack propagation with stress intensity factors, and by comparing energy stored in the deformed crack tip. Haslach et al. [9] Using Griffith's approach it is possible to conduct tests and calculate the strain energy release rate, as well as the stress intensity factors directly from test data, material properties, and geometry. Williams's asymptotic solution for wedge cracks in conjunction with Michell's stress and displacement solutions are an accurate representation for homogenous materials with a wedge initiated crack. Bruck, [9, 10] For such materials, solutions for stress intensity factor, and stress are known. According to Tada, Paris and Irwin [11] the exact solution for Tensile cracks (Mode I) is:

$$K_I = \sigma^\infty \sqrt{\pi a} \quad (1)$$

$$\sigma_{22} = \frac{\sigma^{\infty} x_1}{\sqrt{x_1^2 - a^2}} \quad (2)$$

And the Exact solution for shear cracks (mode II) is:

$$K_{II} = \tau^{\infty} \sqrt{\pi a} \quad (3)$$

$$\sigma_{12} = \frac{\tau^{\infty} x_1}{\sqrt{x_1^2 - a^2}} \quad (4)$$

This may be applied to provide solutions for mixed mode fracture and crack propagation quite easily; however this all operates under the assumptions of homogenous materials. This is certainly not the case for composite laminates, where numerous other effects cause the estimated value for strain energy release rate to be skewed.

Priel [12] demonstrated that delamination and fracture is usually initiated by high interlaminar stresses [2] at geometric discontinuities. This discontinuity, usually in the form of an intentionally implemented delamination insert, results in stress concentrations and further crack growth. Many of these experiments have been successfully affirmed with Cohesive Zone Modeling (FEA) and numeric Finite Element Analysis (FEA) using modern computer programs. Though there are limitless opportunities for improving the determination of material behavior, the most common, and universal method is to use energy based approaches for fracture mechanics in composite materials. [2, 6, 7, 9, 10, 11] This course of study will analyze the fracture using both linear elastic fracture mechanics, and energy based approaches for fracture mechanics, but will confirm these values with a much more precise means of interrogating near field fracture phenomena using DIC.

2.4 Crack Tip Displacement Theory

Poursartip, et al. [13] were amongst the first to investigate measurements of crack tip displacement fields in composite laminates, specifically focusing their analysis on the crack opening, as well as crack shearing displacement. Poursartip, et al. writes with much concern over the practical limitations of existing methods for determination of shear fracture toughness in mixed mode loading. Problematic phenomena such as friction in Mode II dominate cases, and fiber bridging in Mode I dominate cases greatly influence the behavior of crack propagation. [13] Even the ASTM standard used as the basis for this experiment [14] operates under the assumption that fiber bridging is negligible, a significantly incorrect assumption to make, when experiment shows its presence for high Mode I loading. Poursartip [13] makes the case that crack tip displacement analysis can accurately account for these anomalies while still providing accurate results with minimal assumptions. The difficulty though of Poursartip's proposed solution lies in accurate measurements of these displacements, something he relies on a scanning electron microscope for. The expressions for COD and CSD in the crack tip region for orthotropic bodies was previously developed by Lekhnitskii and Sih [15] are as follows for an orthotropic specimen:

$$\text{COD} = \left[4(2)^{1/4} \frac{(a_{11}a_{22})^{1/4}}{\sqrt{\pi}} \left(\frac{2a_{12} + a_{66}}{2a_{11}} + \sqrt{\frac{a_{22}}{a_{11}}} \right)^{1/4} \right] \sqrt{G_1} \sqrt{r} \quad (5)$$

$$\text{CSD} = \left[4(2)^{1/4} \sqrt{\frac{a_{11}}{\pi}} \left(\frac{2a_{12} + a_{66}}{2a_{11}} + \sqrt{\frac{a_{22}}{a_{11}}} \right)^{1/4} \right] \sqrt{G_{11}} \sqrt{r} \quad (6)$$

This analysis goes a few steps beyond simple beam theory, and correction factors, and other problems associated with large displacement tests which limit the effects of far field loads. The analytical framework set forth here is the basis for the initial DIC work collected in my research, and as you will see does not apply particularly well to composite laminate structures. Poursartip et al. concludes that this analysis using COD and CSD profiles are well suited for evaluation of strain energy release rate [13]. They also conclude the stress singularity is of order $r^{-1/2}$, as predicted by linear elastic fracture mechanics. Poursartip also concludes that “the global [applied] strain energy release rate equals the local strain energy release rate seen by the crack tip for the tested specimens.” [13] This is a conclusion which is not affirmed by my results using multi scale crack tip displacement measurements. The level of K dominance as discussed in chapter 5 is simply not the same. This is in no small part due to Pourssartip’s assumption that composite specimens are homogenous, neglecting the individual layers of the composite laminate. [13] This course of study will be focused on affirming the potential to use crack tip displacement theory for extracting fracture parameters in composite laminate structures, while also identifying several severe deficiencies in this analysis. Additionally, this course of study will examine techniques which may be used to mitigate the issues common with crack displacement analysis for this barrage of test specimens.

2.5 Digital Image Correlation

DIC is a novel technique used for identifying and measuring displacements in materials. In essence, DIC is an optical method for tracking and registering discrete changes between two or more images. This may be applied for both two dimensional and three dimensional measurements. The technique was first pioneered by H. Bruck, S. McNeil, and M. Sutton in the 1980s, and has since been an ideal tool for obtaining accurate displacement measurements at multiple length scales. The application of crack tip displacement measurements, and DIC together is truly elegant. Using DIC programs like Vic-2D by correlated solutions allows users to quickly measure displacements in a specimen for many different length scales. Mogadpalli et al. [16] used DIC to determine stress intensity factors for cracks in orthotropic composites. Mogadpalli discusses previous experiments where strain gauges were used to successfully measure strain and calculate stress intensity factors for cracked laminates. DIC is important because it removes the additional analysis and uncertainty present with the use of strain gauges. Strain gauges, though common, require a complex and meticulous application process. In some cases, the presence of a strain gauge, and the mounting glue may alter the fracture properties of the sample being measured. DIC has become a useful tool for measuring displacements because of the minimal effort for surface preparation, but its scope is limited to surface displacements only, or anywhere a series of images may be captured [16]. McNeil et al. [17] was the first to use DIC to determine stress intensity factors for cracks, however this research was limited to homogenous materials. Mogadpalli et al. [16] to was the first to use DIC to determine stress intensity factors for cracks in orthotropic

composites. The key difference between this research and that pioneered by Mogadpalli, is that he was investigating pre cracked, transverse axially loaded composites, and not studying delamination in composite laminates. This course of study is much more useful as it investigates a more challenging and common failure mechanism. The advantage of using DIC is that it negates the necessity for using compliance correction in calculation of the material properties. In tests like the DCB and MMB tests, the compliance of the load frame and testing apparatus must be calculated and accounted for to prevent results from being skewed. Because the measurements in DIC are collected directly from the specimen itself there is no need to consider deformations in the load fixture. This step becomes ancillary for DIC testing, but necessary for analyzing tests with LEFM methods. The use of DIC also negates the necessity of many assumptions used in previous methods, like Poursartip's assumption that composite specimens are homogenous [13], or the ASTM standard's assumption that fiber bridging is negligible, and friction in mode II cases should not be considered [15]. DIC enables measurements of displacement relative to a zero load image, regardless of what anomalies, contrary to assumptions, are present in the test. The result is pure measurement for more refined results and analysis. The drawback is that DIC requires a relatively stable platform, and that the same local area be monitored for all tests. Using the DCB test, and MMB test, some cases result in large displacements, and keeping the camera in focus on the exact location of the crack tip requires extreme prejudice, a cunning eye, and steady hands. A task made easier after the acquisition of a traveling x-y-z microscope stand. DIC is also useful at numerous length scales, from high magnification, to global conditions.

This enables observation and characterization of crack propagation at both global and local scales. The successful implementation of DIC to measure crack propagation has been affirmed by Mogadpalli, Tippur, and McNeil. [16, 18, 17] Though DIC has been previously used to accurately extract fracture parameters of orthotropic materials, it has not yet been used to analyze the near field crack tip phenomena common in composite laminates. This course of study intends to prove the viable use of DIC to capture, analyze and explain unique phenomena in fracture of non-orthotropic materials such as carbon fiber laminates.

2.6 Closing Remarks

There has been significant ground work that has established the theory which makes this research possible. DIC has been successfully used to characterize all kinds of materials under different loading conditions. DIC is particularly ideal for applications with fracture mechanics, enabling the user to characterize fracture at multiple length scales all while neglecting common assumptions required for previous analysis. Using DIC combined with displacement theory for fracture mechanics. This research will establish an innovative new means of accurately characterizing fracture parameters for laminated composite materials.

Chapter 3: ASTM Standard and the Wyoming Test Fixture

3.1 Introduction

During the literature search, several competitive methods for measuring the shear fracture toughness of various materials were identified, however, the ASTM standard D6671 [15] was designed specifically for aerospace and aircraft composite materials in mixed mode bending. The test was developed in the 1980s by Don Adams in association with NASA as a means of describing the interlaminar fracture toughness of continuous fiber composite materials. Otherwise known as the Mixed-Mode Bending Test (MMB), this is a means of subjecting composite materials at varying degrees of both Mode I and Mode II fracture. This is opposed to individually loaded specimens using the Double Cantilever Beam test (DCB), and the End Notched Flexure test (ENF) which only allow composite materials to be subjected to a single fracture mode at a time. The process for Mixed Mode Bending fracture testing is summed up in ASTM Standard D6671 [15], and summarized below with annotations as to the most effective means of conducting the mixed mode bending test with applications for DIC. The following describes one possible method to determine the inter-laminar fracture toughness of continuous fiber-reinforced composite materials in mixed mode bending, the testing rig and its basic operation, as well as test itself. The testing rig was obtained from Wyoming Test Fixtures, and is classified as the WTF-MM-35.

3.2 Nomenclature and Definitions:

Mode I strain energy release rate: G_I “the loss of strain energy associated with Mode I deformation in the test specimen per unit of specimen width for an infinitesimal increase in delamination length, ∂a ” [15]

Mode II strain energy release rate: G_{II} “the loss of strain energy associated with Mode II deformation in the test specimen per unit of specimen width for an infinitesimal increase in delamination length, ∂a ” [15]

Strain Energy Release Rate: G the total shear fracture toughness, may be calculated by the sum of G_I , the Mode I component, and G_{II} , the mode II component.

3.3 Geometric Relations:

In this section I intend to clarify the different nomenclature used for fracture testing. There are several competing methods for nomenclature, the one I have chosen to use for the entirety of this course of study is as follows:

Crack Length: a

Initial Delamination Length: a_o (measured from loading tab)

Specimen Width: b

Lever Arm Length For Rest Apparatus: c

Lever Arm Length to Center of Gravity: c_g

Half Thickness of Specimen: h

Half Span Length of MMB Apparatus: L

Slope of Load Displacement Curve: m

Fiber Volume Fraction: V

Non-dimensional Crack Length Correction Parameter: β

Crack Length Correction Parameter: x

3.4 Loading Parameters

Applied Load: P

Weight of Lever and Attached Apparatus: P_g

Critical Load at Nonlinear Point of Curve: P_{nl}

Load on the Loading Tab: P_{tab}

Critical Observed Load: P_{vis}

Load Point Deflection: δ

Compliance: C

Coefficient of Variation: CV

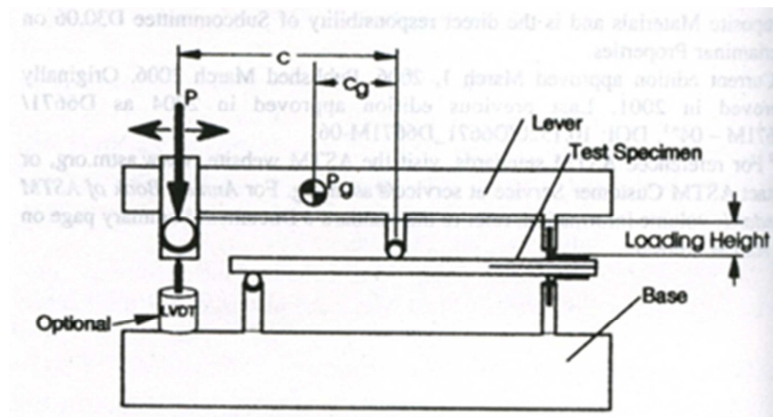


Figure 4. MMB Test schematic [15]

3.5 Specimen Properties

Longitudinal Modulus of Elasticity: E_{11}

Transverse Modulus of Elasticity: E_{22}

Shear Modulus (out of plane): G_{13}

Sear Modulus (in plane): G_{12}

Total Strain Energy Release Rate: G

Strain Energy Release Rate (Mode I): G_I

Strain Energy Release Rate (Mode II): G_{II}

Total Mixed Mode Fracture Toughness: G_c

Mode Mixture: $\frac{G_{II}}{G}$

3.6 Special Parameters for Experimental Analysis:

Transverse Modulus correction Parameter: $\Gamma = 1.18 \frac{\sqrt{E_{11}E_{22}}}{G_{13}}$

Crack length correction parameter: $x = \sqrt{\frac{E_{11}}{11G_{13}} \left[3 - 2\left(\frac{\Gamma}{1+\Gamma}\right)^2 \right]}$

3.7 Variation in Mode Mixture for Wyoming Test Fixture:

Using the ASTM standard, the appropriate mode mixture is selected. The length of the lever arm “c” compared to the possible mode mixture is displayed in

figure 5 below. It can be seen that unreasonable values of c are needed to achieve mode mixture below 0.2, so this represents the limit of our current testing system. In any case, the Wyoming Test Fixtures Mixed Mode Bending apparatus has a maximum possible length of c limited to 107 mm.

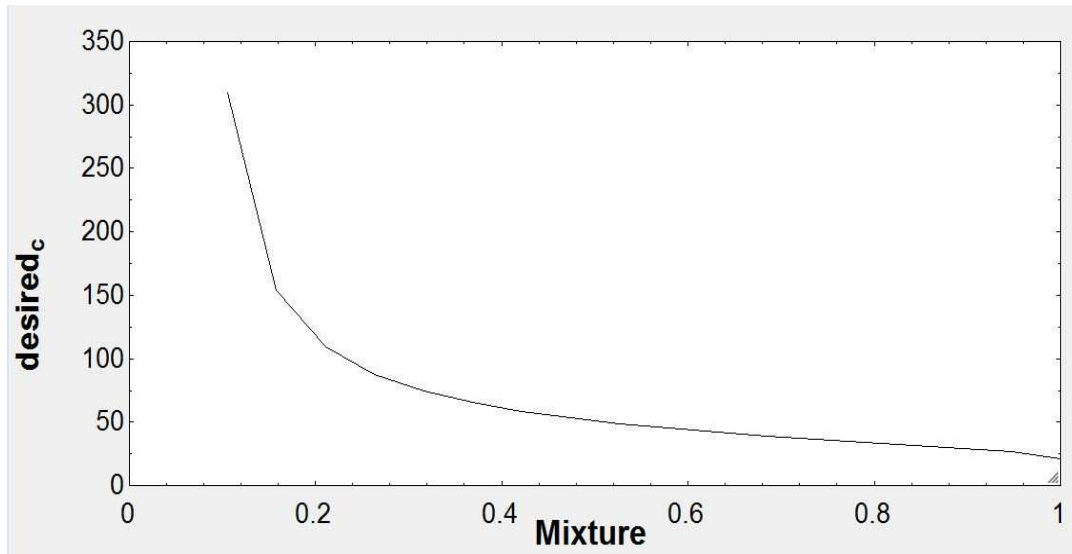


Figure 5: Lever arm length and mode mixture

As a consequence, 0% mode mixture is not possible with the MMB apparatus from Wyoming Test Fixtures, and the closest to a pure Mode I test possible, is limited to nearly 20% mode mixture. For this course of study, three levels of mode mixture are to be investigated: (a) 22% (close to Pure Mode I), (b) 50%, and (c) 100% (Pure Mode II). These were selected as the levels with the most interesting and reproducible results. Due to the nature of the experiments there is only a very narrow range for which data may be acquired using high power microscopes and DIC, however

different methods may be applied to effectively calculate the shear fracture toughness. This is discussed at length in chapter 5, Initial Multi-Scale Testing.

3.8 Pure Mode I Testing:

The nature of the Wyoming Test Fixture is to provide Mixed Mode conditions for composite laminate structures, however, for calibration purposes, as well as the necessity to be comprehensive in my course of study, I was compelled to analyze specimens in a pure Mode I scenario. *Figure 5* demonstrates how achieving a 0% mode mixture with the Wyoming Test Fixture would require an infinitely long lever arm, considering the maximum value of “c” possible with this fixture is 107mm it is impossible to apply a pure 0% mode mixture test with this setup.

The most ideal way to achieve a Mode I fracture testing is the test principle wherein the Wyoming Test Fixture replaced with a simple pair of clamps intended to apply a load and displacement at the edge of a specimen in pure opening. This test setup, known as a Double Cantilever Beam (DCB) test used may be seen in *figure 6*.

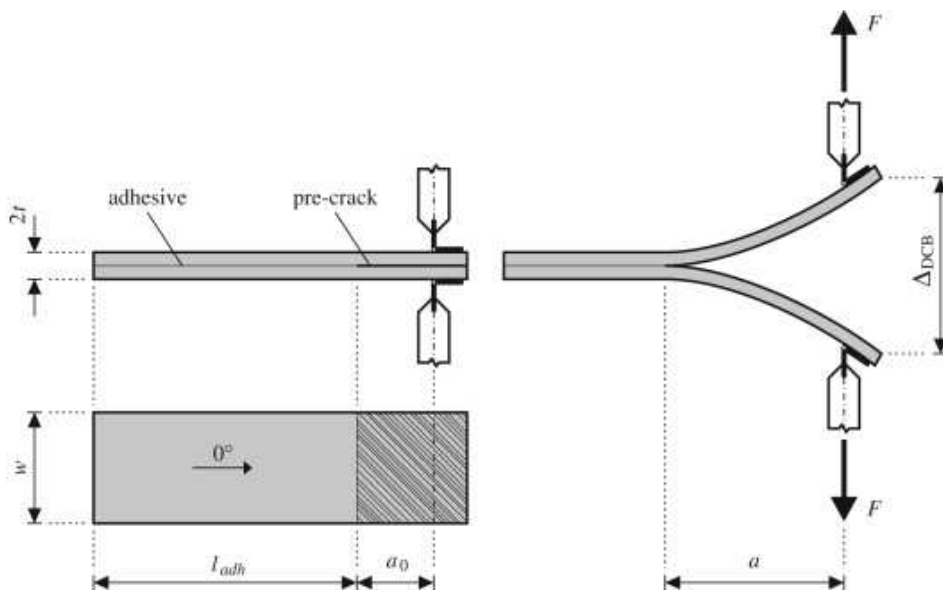


Image 6: Schematic for Double Cantilever Beam Test, Balzani [19]

Testing with this setup enables measurements of slow and consistent crack growth of composite laminates. Using the same parameters discussed in previous sections, the load point compliance of the DCB specimen must be calculated as:

$$C = \frac{\delta}{P} = \frac{2a^3}{3E_1fI} \quad (7)$$

The strain energy release rate, G which is only a function of G_I only, as G_{II} is by definition 0 for a double cantilever beam test. Thusly, G becomes:

$$G = \frac{P^2}{2w} \frac{dC}{da} \quad (8)$$

The combination of the two above equations yields:

$$G = \frac{P^2 a^2}{wE_1fI} \quad (9)$$

In order for this test condition to have stable crack growth, the change in G with respect to crack length must remain below 0. [11] This test, much like the Wyoming Test Fixture for Mixed Mode Bending must be performed under prescribed displacement conditions only for stability to exist. All other geometric relations not specifically listed above are assumed to be the same between Mixed Mode Bending Test, and the Double Cantilever Beam test. Specimen processing, as well as output data, is collected in a consistent manner between the two tests.

3.9 Identification of Laminated Composite Specimens for Testing:

ASTM Standard D6671 is limited to use with composites consisting of unidirectional carbon fiber tape laminates. It is possible to apply different configurations of composite types with the test fixture, but for consistency purposes

only unidirectional laminates were considered for this test. Because this technique will be used with DIC, restrictions on use of the global conditions for obtaining the localized mixed-mode fracture conditions with this standard can be obviated. Though the ASTM standard equations will be used for a baseline result for comparison, a much more accurate means of calculating local fracture parameters will be achieved, negating the necessity to use only unidirectional samples. Despite these extenuating circumstances, several material assumptions present in the analysis used to calculate task critical parameters are: (1) a brittle and tough single phase polymer matrix must be used, (2) reinforcement must be long and continuous, and (3) delamination must be initiated with an insert. [15] Linear Elastic Fracture Mechanics (LEFM) behavior is assumed in the calculation of fracture toughness for the ASTM standard, but as indicated previously is not necessarily an assumption with the use of DIC for localized displacement field measurements near the crack tip. Typically, this assumption would be valid only if the damage zone, where ideally minimal plastic deformation is present at the crack tip propagation, is small relative to the specimen thickness. This is consistent with the assumption that a brittle polymer matrix is used. Another requirement of successful use of the Wyoming Test Fixture is that displacements are kept to acceptable values. The following equations with estimated critical load, and estimated load point of deflection may be used to determine the specimen thickness to achieve permissible amounts of displacement:

$$\delta^{est} = \frac{p^{est}}{8bE_{11}h^3L^2} [4(3c - L)^2(a + hx)^3 + (c + L)^2(2L^3 + 3(a + 0.42hx)^3)] \quad (10)$$

$$p^{est} = \sqrt{\frac{\frac{3}{4}G_c^{est}b^2E_{11}h^3L^2}{(3c-L)^2(a+hx)^2 + \frac{3}{4}(c+L)^2(a+0.42hx)^2}} \quad (11)$$

Using these equations, specimens were manufactured to have 24 plies, resulting in a nominal manufactured thickness of 3.11 mm with a variation of no more than .1 mm. Any specimens which fall outside the acceptable parameters were rejected and subsequently not used for fracture testing.

3.10 Preparation of Unidirectional Laminated Composite Test

Specimens:

Specimens were prepared and layed up in accordance with manufacturer specifications, and ASTM Standard D5528 [20]. For ease of manufacturability, and to reduce the amount of time dedicated to sample preparation, as well as a desire for a consistent fiber content between all samples, unidirectional pre-impregnated carbon fiber tape was purchased from the “Composites Store Inc” to be used as the material in this course of study. The pre-impregnated material was bought in a 24 inch wide roll, and immediately stored with dry ice until it could be cut down small enough to fit inside the lab’s freezer. Rather meticulously, the roll was cut into 6 inch by 6 inch squares, and then individually packaged in plastic wrap for protection against moisture infiltration as well as possible foreign contaminates. These 24 ply precut packs were then placed in a freezer at 0°C until they were ready to be used. The one drawback with the use of pre-impregnated composites is that the resin begins to cure

as soon as it is manufactured. Though heat is used to speed up the process, low temperatures are required to prevent a premature cure. At 0°C, the material used has a manufacture rated shelf life of one year. Any samples used for testing were manufactured with materials that were no older than six months. With proper care, moisture prevention, and acceptable levels of cooling, there is no degradation of performance within the polymer resin.

Composite manufacturing has a propensity to attract foreign objects and particulate matter, particularly because of the tackiness of the resin used. Extreme prejudice was taken to ensure a clean workstation, devoid of dust and debris. Before any sample was manufactured, the workstation was vacuumed clean, wiped with a mold release agent, and coated with a clean protective layer of paper. Proper personal protective equipment including gloves were used at all times to prevent oils from contaminating the specimen. All precautions were taken to avoid the addition of any contaminants to the system which may induce stress concentration factors and impact fracture tests.

Samples must contain an even number of plies in order to prevent asymmetric loading, and geometric discontinuities. Baseline calculations discussed in Chapter 4 proved that a thickness of 3.11 mm, an equivalent of 24 plies after curing, achieved the desired stiffness characteristics required for testing. The square precut sheets of carbon fiber were layed up in the 0 degree orientation (all fibers aligned in the same direction) to ensure that crack propagation occurs consistently for all fibers. A 13 micron, 0.0005 in, sheet of Teflon film was inserted in between the 12th and 13th layer of the composite. The film was carefully placed to extend 2 inches into the length of

the carbon fiber panel. Layers 13 through 24 were inverted compared to the orientation of layers 1 through 12. This is done to ensure that micro residual stresses present in the fibers from its manufacturing as they are pressed through rollers, shipping, and even storage are arranged symmetrically within the composite about the central axis. This negates these micro stresses and prevents warping in the finished product. Not inverting the second half of the composite typically results in a slight curvature of the laminate after curing, resulting in a sample which is warped and looks more like a “Pringle” potato chip than like a flat plate. Any samples manufactured with appreciable curvature were rejected. Specimens manufactured were at least .2 inches thick to avoid large displacements and geometric nonlinearity. [15]

Once the square 24 ply laminate with Teflon insert was manufactured, two thick sheets of Teflon were placed on the outer sides of the sample. The completed arrangements were then placed between two fine polished aluminum platens, and pressed to 2000 lbs. A large number of C clamps were then used to maintain the load on the completed assembly. Additionally, the aluminum platens were cleaned of any excess resin before each manufacturing. The platens and composite sample are then placed in an oven at 200 °C for 1 hour. The oven temperature is then increased to 300 °C and held for 2 hours to ensure the thick structures are properly cured. The oven which was used was a vacuum oven, and any air remaining in the oven was removed during the curing process. This is another step taken to prevent contamination of the sample during the manufacturing process. *Figure 7* is a diagram of the exact cure

schedule of the resin used. This information was provided by the manufacture for best results.

Typical Cure Cycle

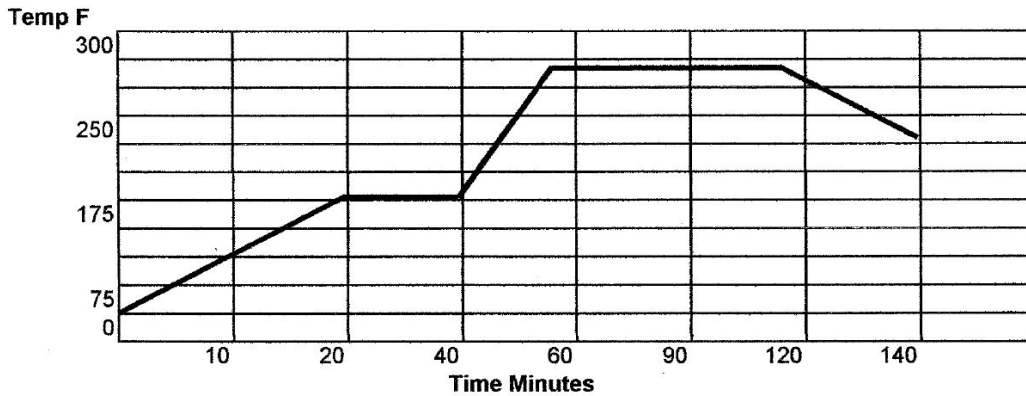


Figure 7: Typical Cure Cycle for Pre-Preg Carbon Fiber

Once cured the composite plate is removed from the oven, and the location of the Teflon film insert is carefully annotated. It is important to note that the specimen dimensions are not critical for testing, and a significant variation in the geometry of each specimen is actually permissible, so long as careful measurements are made before each test, a necessary though potentially redundant part of experimental testing. Each plate, nominally 6 inches by 6 inches, was inspected for viable use. Then the rough edges of excess resin were cut off and the edges were sanded down to a fine grain. This is a necessary step in order to prevent unwanted fiber splinters from piercing and becoming lodged in the skin while handling. Following this step, a band saw was used to cut in the direction of the fibers to form six samples. Nominally the samples were to be one inch wide, and six inches long, though losses during the cutting process usually resulted in 5 good specimens, and one particularly undersized

specimen. These smaller specimens were generally not used for testing, and discarded as waste. After final cutting, these specimens are then carefully processed with sand paper to have smooth edges. The top and bottom surface of the specimens on the same edge as the delamination insert were then sanded for one inch from the edge. This served to roughen the surface and promote better adhesion to the loading tabs.

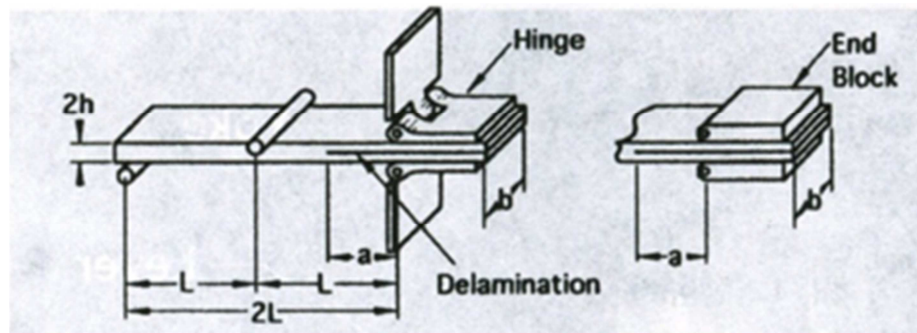


Figure 8: Specimen configuration for Mixed-mode fracture characterization with loading tabs affixed. [15]

Tabs were applied to the ends of the specimen to transfer the loads required for testing. The sample's outer skins are sanded to provide a better bonding surface, and standard piano hinges are affixed using high strength cyanoacrylate glue. Tab locations are such that the load is applied exactly 1 inch away from the edge of the delamination insert. Though there is some uncertainty as to the location of the exact crack tip, this can be measured more accurately during testing, and once measured can be used in calculations to determine special fracture parameters. Special care was taken to ensure that the tabs were aligned parallel with the specimen as well as with each other. While the adhesive was curing, the loading tabs were clamped together

with a C-clamp. The whole assembly was left for at least 6 hours before any loads were applied. A completed specimen with hinges affixed can be seen in *Figure 8*. The hinges used were standard type thin hinges procured at any local hardware store. A grinder was used to remove excess material which would prevent them from lying flat upon the surface of the specimen, and several holes were drilled with a drill press in order to affix the loading tabs to the Wyoming Test Fixture mixed mode bending apparatus.

Once the loading tabs were applied to the samples, a brittle white paint was painted on the outer edge of the composite to provide better resolution for non – DIC testing. This white paint was then marked sequentially at mm intervals so that crack propagation if any for the test could be easily recorded with high speed photography. For tests using DIC the brittle white paint was not used, and the sanded and cleaned edges of the specimen were then speckled using a combination of black and white spray paint.



Figure 9. Test Specimen and complete Wyoming Test Fixture for MMB setup for 22% Mode Mixture Test.

Figure 9 shows the complete experimentation setup for the Wyoming Test Fixture as would be expected for a 22% Mode Mixture Test. This specimen does not have a speckle pattern painted on it, and the microscope used for collecting images in DIC is not depicted here.

3.11 Determination of Material Properties for Unidirectional Carbon

Fiber Test Specimens:

As Linear Elastic Fracture Mechanics (LEFM) is being used as a baseline for the experimental characterization of mixed mode bending, proper analysis requires the determination of the transversely isotropic elastic properties. Although these properties can usually be assumed to be consistent with the generally accepted values reported in the literature for the given matrix and carbon fibers, it is good practice to verify the validity of these assumptions. This was done via numerous tests to include: tensile testing, 4 point bending, 3 point bending, and extensive literary searches and theoretical calculations. It is important to note that this is also necessary for use with DIC, as these material properties are manifest in the fitting equation as constants for material properties explained later in this section. These constants may be assumed, and optimized but this adds more degrees of freedom to the analysis and knowing them generally results in more accurate calculations.

The carbon fiber laminates used in this course of study were all made using the same lot of pre-impregnated carbon fiber. The reinforcement for all specimens

used in testing had a designation of: X534-SR-150/35. This would be an SGL 50K fiber, with a standard modulus of 34000 ksi, and a tensile strength of about 580 ksi. These standard modulus fibers are very similar to the more common AS4 fibers used in industry. The matrix material used is the Aldila AR250 Resin System. According to the manufacturer Aldila, AR250 is a “controlled flow toughened epoxy resin system.” AR250 is 99.5% solids and ideal for low outgassing applications. AR250 resin is a phenol novolac epoxy which is very similar to bisphenol F. This resin system has a specific gravity of 1.2 g/cc, a tensile strength of 11.4 ksi, a tensile modulus of 450 ksi, and a flexural strength of 17 ksi. The cure process does require the use of an oven or other heat source. The overall composite used has 150 grams of resin per square meter fiber, resulting in a nominally 35% by volume resin content. The aerial weight is 150 gms. This unidirectional composite system if manufactured properly, will retain the properties commonly associated with other prevalent industry standard composite fiber-epoxy systems. In order to calculate higher order effects of material fracture in crack opening displacement, the material constant matrix must be known. [16] This matrix requires knowledge of the following material properties:

E_I = Axial Stiffness

E_{II} = Transverse Stiffness

G_{12} = In Plane Shear Stiffness

ν_{12} = Major Poissons Ratio

ν_{21} = Minor Poissons Ratio

A standard 3 point bend test was used to tabulate the load displacement data, and generate a slope “m.” Equation 12 was then used to calculate the young’s modulus in both the axial and transverse directions. Results can be seen in *Figure 10*, and the modulus can be calculated using the equation:

$$E = \frac{L^3}{4wh^3} * \frac{\Delta p}{\Delta \delta} \quad (12)$$

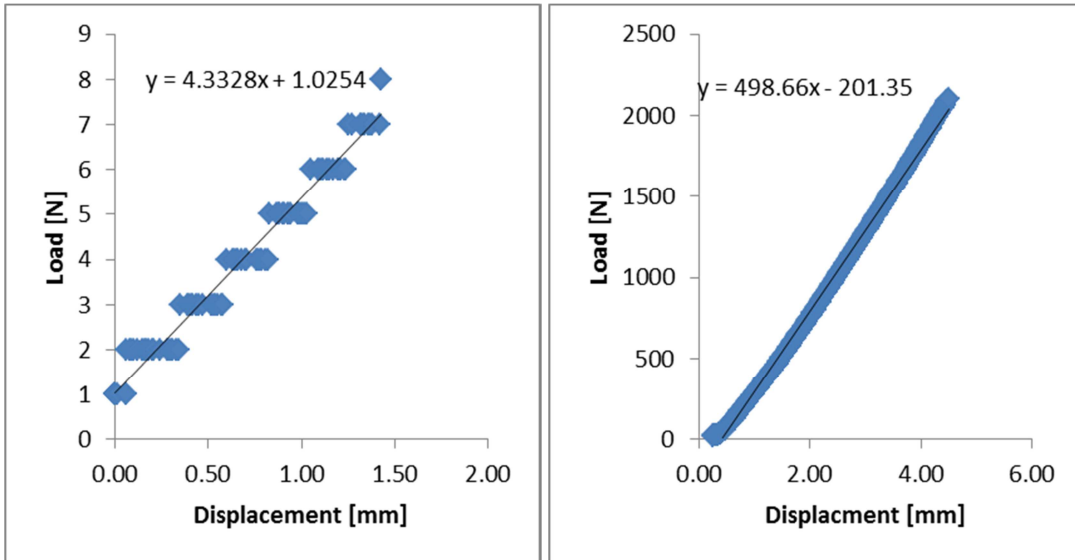


Figure 10: Load-displacement curves for 3 point bend tests in transverse loading (left) and axial loading (right) with respect to fiber directions.

The test results from *figure 10* resulted in values within acceptable levels of material variation reported in the literature. [6, 7] Therefore, the following measured material properties were assumed to be true for all of the composites that will be used in subsequent tests.

E_I	Axial Stiffness	138 GPa
E_{II}	Transverse Stiffness	10.3 GPa
G_{12}	In Plane Shear Stiffness	5.9 GPa
ν_{12}	Major Poisson's Ratio	0.3
ν_{21}	Minor Poisson's Ratio	0.0224

Table 1: Material properties of unidirectional carbon fiber laminate

The transversely isotropic elastic constants are therefore defined as [16]:

$$\begin{bmatrix} \epsilon_1 \\ \epsilon_2 \\ \gamma_{12} \end{bmatrix} = \begin{bmatrix} S_{11} & S_{12} & 0 \\ S_{12} & S_{22} & 0 \\ 0 & 0 & S_{66} \end{bmatrix} * \begin{bmatrix} \sigma_1 \\ \sigma_2 \\ \tau_{12} \end{bmatrix} \quad (13)$$

Where

$$S_{ij} = \begin{bmatrix} 7.25E^{-6} & -2.2E^{-6} & 0 \\ -2.2E^{-6} & 9.71E^{-5} & 0 \\ 0 & 0 & 1.45E^{-4} \end{bmatrix} \quad (14)$$

These parameters are used in the Crack Tip Displacement (CTD) analysis, as well as material constants in the full field DIC fit solutions. discussed in Chapter 7.

3.12 ASTM Standard for Calculation of Mode Mixity

Experimentation is very straight forward, so long as careful precaution and slow methodical work ethic is induced. Because of the nature of this multi-scale investigation, a myriad of different imaging techniques were used through the course

of study. Various standard optical cameras, with zooming lenses were used to capture global conditions, while microscope mounted cameras were used to investigate the crack tip at local conditions. Length scales varied for different tests. Some were conducted at global measurement scales along the full length of the test specimen in order to obtain the macro scale deformation conditions assumed for the energy-based mixed mode analysis using LEFM. Some tests were conducted at high magnifications, local to the crack tip in a region no greater 2 square mm. The assumption behind how much zoom is enough to meet assumptions present in the LEFM analysis, is that the area under investigation must be much less than the specimen width to be indicative of the mixed-mode near field response. The complete test set-up can be seen in *Figure 9*.

In order to calculate accurate data using the aforementioned experimental analysis, using LEFM, a calibration factor must be added to account for the compliance of the testing fixture, as well as the load frame, and hinges which transfer load to the specimen. Another significant advantage of using DIC is that data collection occurs directly from the specimen, and no compliance correction is necessary for the displacements during those tests. To account for this, a calibration specimen of known modulus must be used in the MMB rig; it is also important to recalibrate each time the setup of the system is changed, or if the lever arm length “c” is adjusted. An aluminum bar with a modulus of 70 GPa and dimensions that are nominally the same as those used for the composite was manufactured. The loading tabs were affixed in the same manner as they would be for the carbon fiber specimens, and the test is run until failure is achieved. Because there is no crack, or

crack propagation, and the adhesion between the tabs and the aluminum is not as good as it is with the carbon fiber, the failure always occurs at the upper loading tab, and well before any plastic deformation in the calibration bar is present. The calibration specimen must be a homogenous specimen with a known modulus. For calibration purposes, any homogeneous isotropic material with known modulus can be used, so an aluminum specimen was chosen. Listed below are the parameters used in the calculation of the calibration compliance [15]:

b_{cal} = Calibration bar width

t = Calibration bar thickness

C_{cal} = Calibration Compliance

E_{cal} = Modulus of Elasticity of calibration sample

m_{cal} = Slope of load displacement curve for calibration sample

$$C_{cal} = \frac{2L(c+L)^2}{E_{cal}b_{cal}t^3} \quad (15)$$

$$C_{sys} = \frac{1}{m_{cal}} - C_{cal} \quad (16)$$

The loading rate is to be set at a constant displacement of .5 mm/min. The output data for the calibration test should be the load – displacement data at the crosshead of the load frame which applies load to the yoke/ saddle interface. This load – displacement data is collected for all subsequent tests as well, and is not

limited only to the calibration tests. When conducting tests with pre-cracked specimens, the test is stopped once the crack propagates to the central support span, at which point the load is removed, and the test is complete. This test can be repeated to collect load and displacement field data at all various levels of mode-mixture desired.

Mode Mixture of the test specimen is determined predominantly due to the geometry of the fixture. The saddle may be adjusted from dominate Mode I (double cantilever beam test) to pure Mode II (end notched flexure testing). The position of the saddle is represented by the variable “c,” and is measured from the roller bearing which takes load, to the central support span. Initially, this experiment will be run with dominate Mode 1, dominate Mode 2, and eventually various levels of Mixed Mode conditions. Note the slots and additional holes along the top of the MMB apparatus in *Figure 9*. By adjusting the saddle to the end of the beam, high Mode I opening is observed, and adjusting the saddle to the other end of the testing fixture, the mode mixture can up to 100%. If the saddle is positioned even more to the right, and aligned directly over the central support span, then the sample is loaded in pure 3 point bending, at which point the geometry of what fracture mode is dominate seems to vary with the load. There is no test protocol for having a lever arm length of “c” as it is very similar to an End Notched Flexure Test, however, the loading tab on the upper specimen induces an opening component in addition to the in plane shear stresses. This configuration is not useful, and does not produce repeatable and stable crack growth, and is thusly not considered for testing.

Once load and displacement data is reported, the slope of the linear elastic region of the load – displacement curve is measured, all geometric properties are

observed, and the compliance of the system is measured, equation 17 may be employed to calculate the modulus of elasticity in the fiber direction for the unidirectional carbon fiber laminate test specimen. This value should be within 5% of the accepted property value for the tensile modulus in the fiber direction. If there is an appreciable distance between the property value and the calculated value for E_{1f} , then this is an indication that the compliance correction factor determined with equations 15 and 16 may be incorrect. Alternatively it may be an indication of a poorly made composite specimen, and the other specimens manufactured from the same batch should be inspected for consistency, and high quality. The equation used for calculating E_{1f} is listed below as *equation 17* [15] :

$$E_{1f} = \frac{8(a_o+xh)^3(3c-L)^2+[6(a_o+0.42xh)^3+4L^3](c+L)^2}{16L^2bh^3\left(\frac{1}{m}-C_{sys}\right)} \quad (17)$$

Equations for fracture toughness may be calculated, so long as displacement is kept to a minimum; this is consistent with the assumptions made for LEFM.

Violation of this assumption results in geometric nonlinear errors, and the errors associated with the test shall exceed permissible values. The shear fracture toughness is based upon the geometric properties of the laminate specimen, the calculated elastic modulus in the fiber direction (17) as well as the crack length and load.

Theoretically, the shear fracture toughness at any load level be determined using these equations, typically

The Mode I component of strain energy release rate may be calculated in [kJ/m^2] via:

$$G_I = \frac{12P^2(3c-L)^2}{16b^2h^3L^2E_{1f}} * (a + xh)^2 \quad (18)$$

The Mode II component of strain energy release rate in [kJ/m²] may be calculated via:

$$G_{II} = \frac{9P^2(c+L)^2}{16b^2h^3L^2E_{1f}} * (a + .42xh)^2 \quad (19)$$

Total mixed mode strain energy, G, is the sum of G_I and G_{II} , and Mode Mixture I is defined as the percent of the total strain energy that is mode I:

$$\frac{G_I}{G} = \frac{G_I}{G_I + G_{II}} \quad (20)$$

These afore mentioned theoretical calculations are able to predict strain energy release rate, and even shear fracture toughness for a specimen at various load levels with a known load displacement curve, and crack geometry. This LEFM analysis combined with other more specific local characterization of fracture parameters is important for an accurate determination of composite laminate material failure. A more enhanced understanding of these state of the art materials is required for their successful widespread implementation.

Chapter 4: New Test Protocol for Conducting Mixed Mode Fracture Tests using Wyoming Test Fixture and DIC

4.1 Test Protocol Introduction:

Throughout this course of study I have manufactured several hundred carbon fiber composite laminate structures for use as test samples. Additionally I have made several hundred more carbon fiber laminates during my time at the Naval Research Laboratory, and United States Naval Academy while conducting research in laser irradiated composite sandwich structures. In my time working with composites I have learned that composite engineering is often similar to baking, where even slight variations in procedure can produce dramatically different results in the quality of the test samples being made. The same is true for the process required to collect fracture parameters during testing. Over the past year, my team and I have painstakingly discovered many ways to conduct unsuccessful tests, and countless more on how to invalidate any results gleaned from experimentation. As such a meticulous procedure has been developed for conducting DIC on composite laminates using the Wyoming Test Fixture for Mixed Mode Bending. I cannot stress enough the importance for following this procedure. It should also be of note that a meticulous nature and attention to detail will go a long way, not only for enhancing the quality of test results, but this is necessary to prevent any geometric non-linearities.

Primarily, the test requires the use of a fully calibrated test specimen. Strict adherence to the ASTM standard is a good start at ensuring minimal disturbances in

the successful implementation of this kind of test. Calibration should be conducted with an un-cracked specimen of known modulus with nominally the same dimensions. The only measurement which must be extracted from such a calibration specimen is the load displacement somewhere well before any plastic deformation occurs in the specimen. This goes into the linear elastic fracture mechanics equations used for ASTM standard calculations. The most important part of specimen preparation is ensuring the laminate has a proper speckle pattern. Ideally the smaller the speckle pattern, the better. It is important to ensure that there are no large swathing areas of single colors. *Figure 11* is an example of a poor speckle pattern. Though it is usable, and some data may be gleaned from its analysis, this pattern is anything but ideal, and is subsequently prone to errors in data processing.

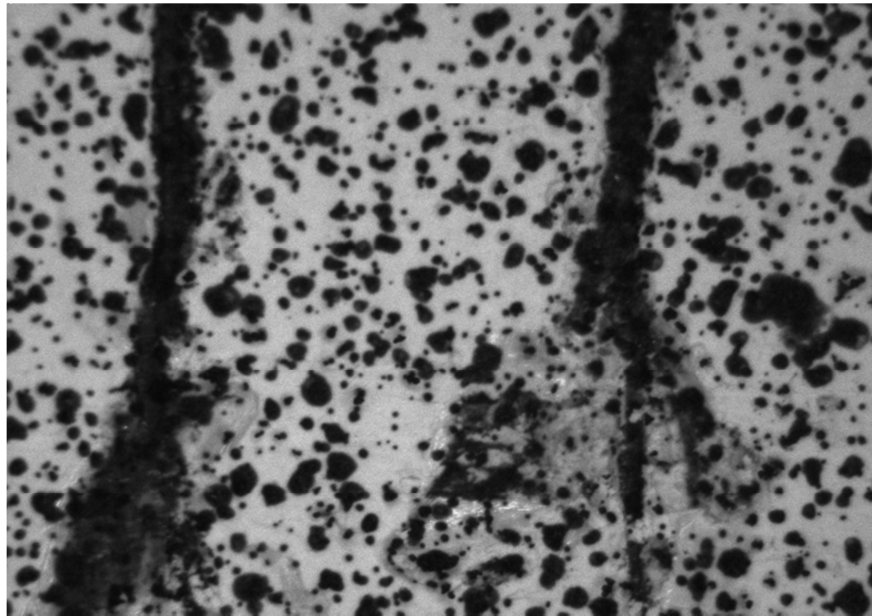


Figure 11: Example of poor speckle pattern for DIC.

Notice the large portions of the sample which are devoid of any features. This results in poor image correlation, as there is very little information for the program to measure. In this particular image, the two large black lines were added with razor

slashes to provide a reference for image scaling. The two razor marks are approximately one mm apart resulting in a scale of 304 mm per pixel. An Ideal speckle patten would have patterns no larger than 15-25 pixels, and no further than 15 pixels apart. *Figure 12* is an example of a nearly perfect speckle pattern.

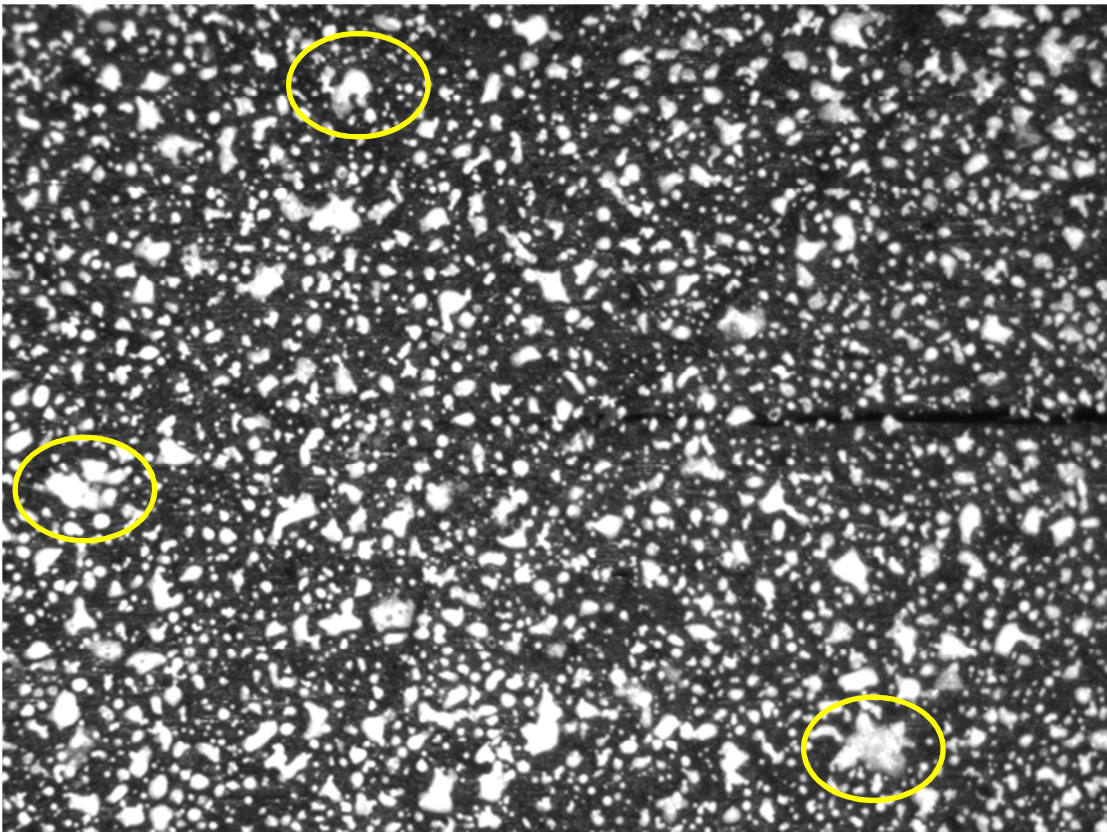


Figure 12: Example of ideal speckle pattern for DIC.

In *figure 12*, the largest features are 25 pixels in diameter, and are all in the far field. Most features are significantly smaller, and very well-spaced apart. Many speckles are extremely small, and highly concentrated at the crack tip. This is ideal for measuring fracture parameters, as the most data, and particularly accurate data will be capture in these dense regions. The larger features, though bad for DIC, are also important for conducting the test. This will be readily apparent in later sections of this chapter.

4.2 Digital Imaging and Microscopy:

The imaging in this course of study is conducted almost entirely with cameras from Point Grey Optics. These cameras are ideal because they easily connect to a variety of lenses for different length scales, and are compatible with numerous computer imaging programs such as Vic Snap, and fly-cap. Of the competing camera setups, only two were used for this actual research not including the digital camera used to take images of the test set up. The first depicted in *figure 13* is of a traditional camera lens set up. The lenses used were Tamron 75-300 mm adjustable zoom lenses. This system is adjustable for a range of field investigations, and if desired, can fit the entire length of the test specimen in the field of view.



Figure 13: Camera set up using traditional camera lens for far field DIC analysis

This set up is particularly useful for the far field tests, though is not of much importance for data analysis. This equipment was also used for measuring and recording crack growth with respect to displacement in the test rig.

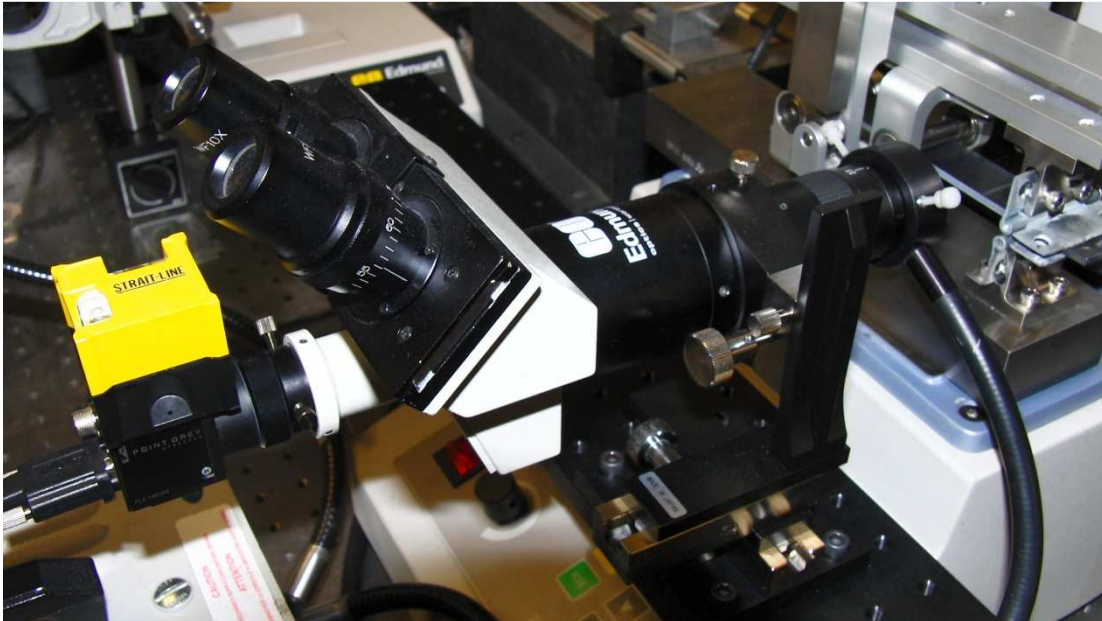


Figure 14: Edmond optics microscope mounted in translating microscope stand.

Near field tests were conducted using an Edmond Optics microscope. This setup shown in *figure 14* was an ideal solution as it interfaces rather nicely with the cameras used for this course of study. The digital camera and microscope set up must be mounted on a translating microscope stand to promote ease of focus and image tracking. In some testing configurations, a significant amount of translation and displacement occurs at the crack tip. Though this may be as little as 2 or 3 millimeters, when the observed area being imaged at high magnification is only 2mm in height, the crack tip will easily be moved out of the field of view. It is necessary during testing to keep adjusting the position of the microscope lens in order to maintain the crack tip.

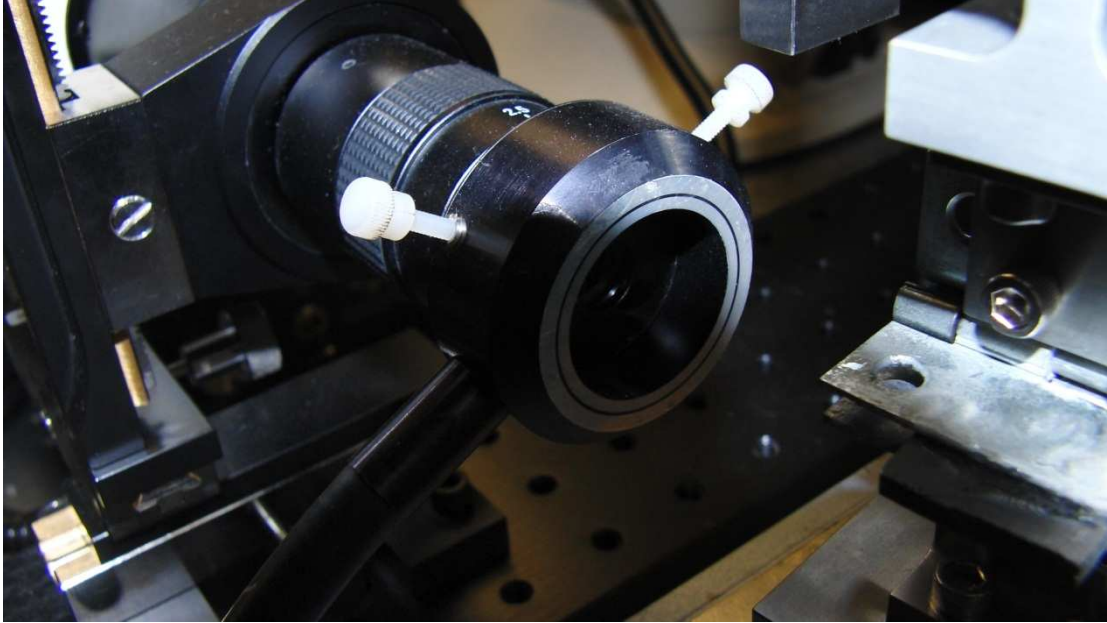


Figure 15: Ring mounted high output light for illuminating test samples.

Illumination of the laminate specimens is provided by a high output halogen projector lamp. The light is transferred via fiber optic cable to a ring mount light which fits at the end of the microscope shown in *figure 15*. The light intensity is adjustable, as are the aperture, shutter speed, and frame rate, and gain of the camera. All of these factors are adjusted for optimal performance. Ideally, the image will be clear, sharp, and not so bright that the white speckle patterns become washed out. With proper focus, light levels, and alignment, the images captured during a test should be comparable to that shown in *figure 12*. One of the most common issues with imaging, and most easily correctable, includes blurred edges. This is an indication that the camera is not perfectly level, or that the specimen is not aligned properly within the testing fixture. In this case, the camera is focused on a particular plane, but because of the slight angle, is out of focus for another plane. The use of levels, and straight edges is highly recommended to improve imaging results.

4.3 Testing Protocol:

Once the complete imaging set up and testing fixture is in place, all components are properly aligned and calibrated, sample images may be captured and the test may be conducted. It is possible to run the test in two ways, but setting displacement speed of the compression machine, or manually adjusting the displacement. DIC does not require the use of videos, but rather still images collected at discrete unique loading conditions. Best results were obtained by manually adjusting the displacement on the Imada compression testing machine, with force and displacement readings captured in real time. These load displacement readouts are very instrumental in determining LEFM parameters for the composite samples. Even if the test is paused, this data should still be collected, as loading and unloading of the specimens while recording this data are a good check for hysteresis.

Applying a slight load to the testing fixture before the test is conducted is a good means of identifying the crack tip location. The idea is to capture as much of the near field region as possible, and provide a reasonable amount of area for crack propagation to occur. The crack tip should be located about 1/3 of the way across the images being captured on the right side of the screen, assuming that the crack grows from right to left. This enables imaging for the opening regions, as well as provides enough room for the crack to grow and still be within the image. It is also important to note that the visually identifiable crack tip is likely not the true location of the crack tip. Once this area is found, the load may be removed, and camera adjusted to keep the crack in the same location. The next step is to identify unique features in the

speckle pattern. This serves as a means of tracking displacements in the specimen. Using a grease pen, at least three or four of the larger white speckles are outlined and filled in. As the specimen displaces during the test, the microscopes translating x-y-z stand may be used to ensure that the colored marks on the computer screen always line up with the unique speckles. The red circles in *figure 12* indicate good features to use as reference nodes. At least three should be used. A slight variation in the alignment of these features is permissible, but the more displacement that is observed in an imaged specimen, the more potential data points are lost. The first image must always be of the specimen with a zero load state. This is the reference image, for which all other images are compared to. As compressive load is applied to the Wyoming Test Fixture, images are taken and saved with the load displacement data in their title. This is for ease of reference in the post processing of the images. Extreme care is taken to keep the loading speed under .5 mm per min, and the test is periodically paused to acquire images and adjust the position of the microscope setup. Each test is different, but approximately 10-50 images are collected per test, the frequency of the images captured usually increases as the specimen is leaving the LEFM region, and crack propagation is expected. If fracture extends all the way to the central support span once crack propagation begins, then the test is completed, and may be unloaded. If the crack only propagates slightly, and then subsequent crack growth is arrested, i.e. stability exists, then the last image should be taken of the fully expanded crack growth, and the load-displacement levels for crack propagation should be noted. At this point, the microscope may be adjusted to put the new crack tip location at the ideal spot for data acquisition. Additionally, the new crack length

should be noted from the load pins to the crack tip. Once the new crack tip location is in view for the microscope, the specimen must be fully unloaded to the zero load, and zero displacement condition. For any further DIC data to be accurate this must be compared to the baseline “un-deformed” sample. The testing procedure can then be repeated for the new, longer crack. Images collected here should be saved in a different location and analyzed as post initial crack growth. This data is usually only measureable for very stable High Mode I tests.

Once the images are collected, and load displacement data curves are generated, the ASTM standard may be used to calculate estimates for the fracture parameters of the test configuration. The images are then loaded into the DIC program Vic-2D. The image area is selected and a reference node must be selected. The best reference nodes are those which can be easily identified by the human eye. A unique looking shape which has relatively little displacement between the image series is important; if the software has a difficult time recognizing this feature in later image frames, you will be required to do so manually. Once all images are calibrated with the system, and accurately identifiable with the computer program, then the correlation may be run in the simulation, and point displacements may be reported. The displacement values are output in an excel sheet in units of pixels. The X and Y location in pixels is reported, as well as the u and v field displacements. These location and displacement data are then input into a fitting function in Microsoft Excel. The theoretical displacements are calculated and then compared to the measured DIC displacements. The mean squared difference between the fit, and DIC data is then minimized with various fracture parameters as variables. Once the

optimal fit is acquired, they may be plotted on contour plots to check consistency, and finally reported.

4.4 Testing Protocol Summary:

The following is a brief delineated list summarizing the test protocol used in this course of study for obtaining fracture parameters. More in depth analysis on composite test specimen fabrication is delineated in Chapter 3, and more in depth analysis on data processing is described in Chapter 7. The steps will be listed in numbered form with the assumption that all material properties for the composite sample to be tested are known.

- 1.) Create composite lay-up with 12 plies
- 2.) Create second lay-up also with 12 plies
- 3.) Apply delamination insert to last 2 inches of one of the lay-ups
- 4.) Combine the two 12 ply lay-ups into one 24 ply lay up
- 5.) Compress lay-up between platens to keep shape, secure with clamps
- 6.) Insert completed assembly into oven set to 185 °C for 1 hour
- 7.) Increase oven temperature to 310 °C and bake for 2 hours
- 8.) Turn off oven and remove sample
- 9.) Leave sample in platens for 12 hours as assembly cools
- 10.) Remove laminate, and cut into 1 inch wide by 6 inch long strips ensure smooth edges by sanding specimens after cutting
- 11.) Apply loading tabs one inch from crack tip as shown in figure 8
- 12.) Allow adhesive on loading tabs sufficient time to dry, at least 12 hours

- 13.) Apply speckle pattern to test specimen, ensure that spray pattern is a fine mist which completely covers inspection area
- 14.) Adjust load lever arm length to desired mode mixture
- 15.) Affix calibration specimen to Wyoming Test Fixture
- 16.) Apply displacement to generate the slope of the load displacement test for this configuration
- 17.) Record all pertinent data, geometric properties and adjustable lengths.
- 18.) Affix composite test specimen with loading tabs to Wyoming Test Fixture, and place apparatus in Imada compression test.
- 19.) Adjust microscope to focus on region near predicted crack tip
- 20.) Adjust light levels as appropriate
- 21.) Apply small load (no greater than 30 N) to end of load fixture
- 22.) Adjust microscope to have the edge of the crack tip slightly to the right of the center. (assuming crack growth will be to the left)
- 23.) Focus as needed to provide clear sharp image
- 24.) Remove load from test fixture
- 25.) Mark reference speckles as needed on screen with grease pen
- 26.) Take reference image at 0 load (unreformed state)
- 27.) Begin applying displacement to testing fixture at a rate not to exceed .5 mm/min.
- 28.) Adjust microscope as needed throughout test to maintain crack tip location in original position.

- 29.) Record digital images as desired noting displacements and loads as they are recorded
- 30.) Record load displacement data at real time during test
- 31.) Continue adding displacement and adjusting microscope as needed to maintain crack tip in center of the image
- 32.) If crack propagates, stop test, unload specimen
- 33.) Re-adjust microscope as needed
- 34.) Repeat steps 22 through 30 as desired if crack propagates outside field of vision for microscope.
- 35.) Conclude physical test, unload specimen and remove fixture from load frame
- 36.) Import digital images into Vic-2D
- 37.) Conduct DIC analysis on speckled images
- 38.) Export data files
- 39.) Import extracted data into fitting file
- 40.) Seed fitting file as appropriate for expected values
- 41.) Conduct analysis using fitting file and observe returned contour plots until satisfied with data correlation
- 42.) Report fracture parameter values after confirming results.

4.5 Testing Protocol Conclusions:

The test protocol briefly delineated above represents a refined process for conducting mixed mode fracture testing using the Wyoming Test Fixture analyzed with DIC. For more specific details on extracting and refining the fracture parameters

extracted through DIC please consult Chapter 7 of this report. Strict adherence to this protocol is essential for guaranteeing consistent results of the highest and most accurate quality.

Chapter 5: Data Analysis for Multi-scale Mixed-Mode Fracture Experiments using New Test Protocol

5.1 Load Displacement Data From Typical Experimentation

If executed properly, the Tests will provide data consistent with the ASTM standard. The following reported data is all for tests conducted consistently with the procedure described in Chapter 4. All composite laminates used for testing were inspected to be of the highest quality, all calibration data was completed properly, and all anomalous testing conditions or errors during the testing process were eliminated entirely. When configured with a loading arm length “c” = 98 mm, the Mode I and Mode II energy release rates, seen in Figure 16, can be calculated from the ASTM standard at various loads. The maximum load achieved during the test before crack propagation can therefore be used to determine the critical strain energy release.

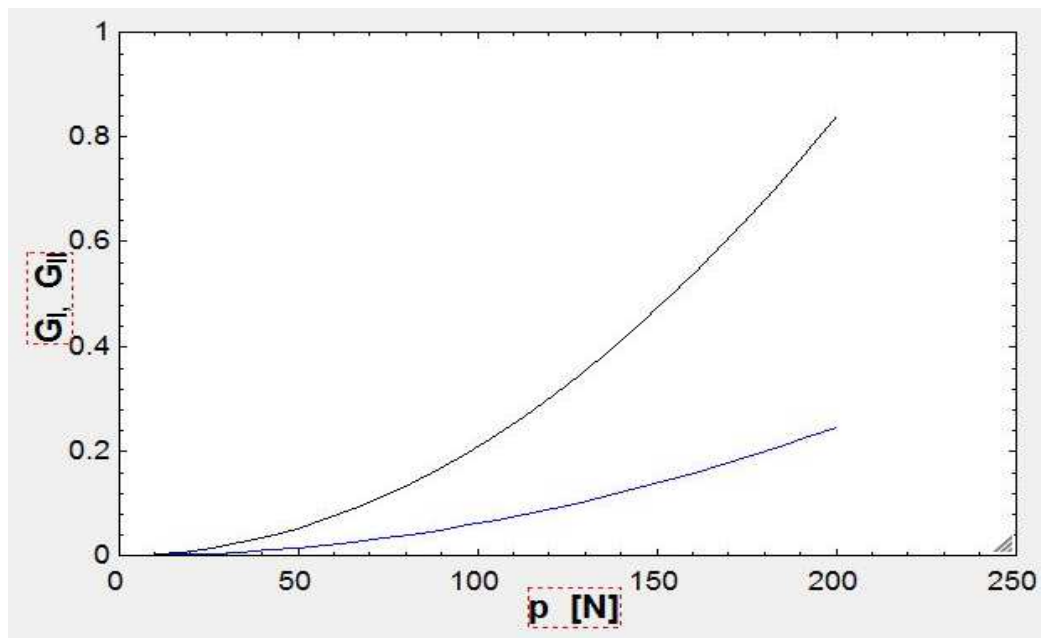


Figure 16: Theoretical values of GI, and GII as a function of Load. $c = 97.35$ mm

The initial crack growth proves to be highly unstable, that is because the initial delamination is more of a notch then a sharp crack, as per ASTM standards. Even though the film insert is only $13 \mu\text{m}$ thick, it still drastically affects the initial crack propagation. As a consequence, there is more crack growth at a higher load level for initial crack growth than would be expected from a perfect, standard test. As noted from the load-displacement data in *figure 17* obtained during the same Mode I dominate, 25% mixture test as shown in *figure 16*. The large jump discontinuities shown in *figure 17*, are an indication of unstable crack growth. An ideal fracture curve will have a smooth peak, and a slow leveling off of the load displacement until maximum displacements are achieved; additionally, there would be no significant jump discontinuities in the data. In this fracture test, the change in energy noted by the first sharp drop is an overestimate of the shear fracture toughness for this configuration.

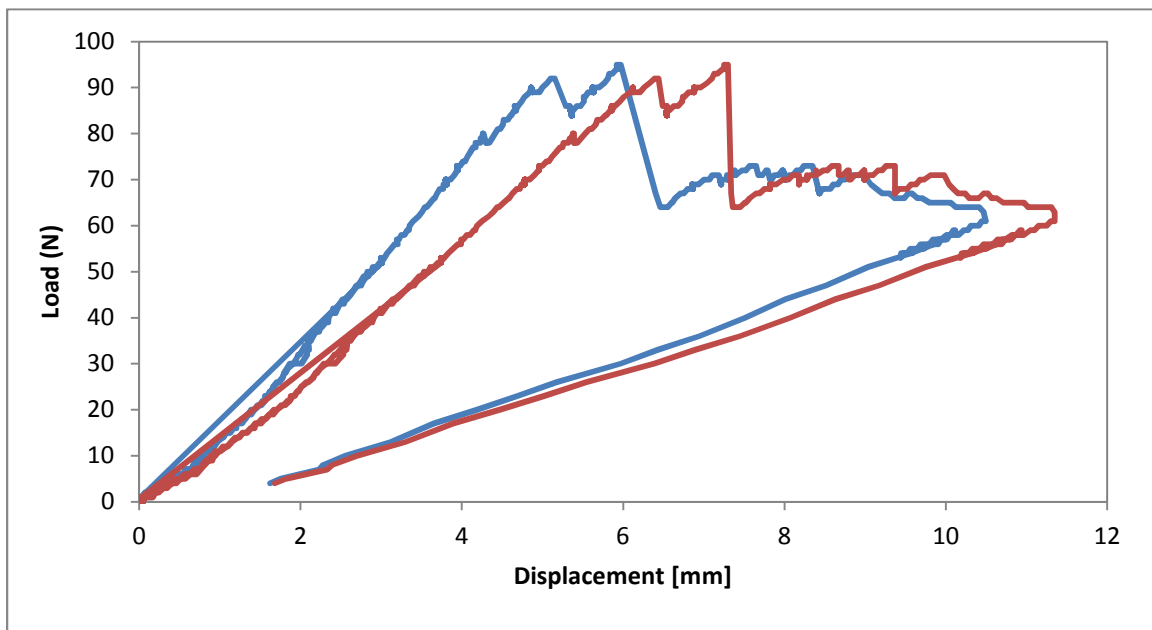


Figure 17: Raw Load-displacement data for 22% Mode Mixture unidirectional test specimen (red), and compliance corrected load-displacement (blue)

A preliminary approach to avoiding large jump discontinuities was to eliminate any potential notch effect from the delamination insert. One way that was attempted involved driving a fine wedge, like a razor blade, into the notch to grow the crack using displacement-controlled boundary conditions on the crack faces to physically breaking the matrix material in the cohesive zone at the center of the specimen plate. This did not work well as it induced asymmetric crack growth, and increased the likelihood for fiber bridging to occur, a phenomena discussed in detail later in this report. Ultimately this solution was abandoned as I could not notice any appreciable decrease in the propensity for sudden and unstable crack growth. This method was also completely ineffective for Mode II fracture testing. The nature of shear dominated tests is to have unstable crack growth. This is visible with the load displacement data for a 50% mode mixture test, *figure 18*, and the load displacement data for a 100% mode mixture test, *figure 19*.

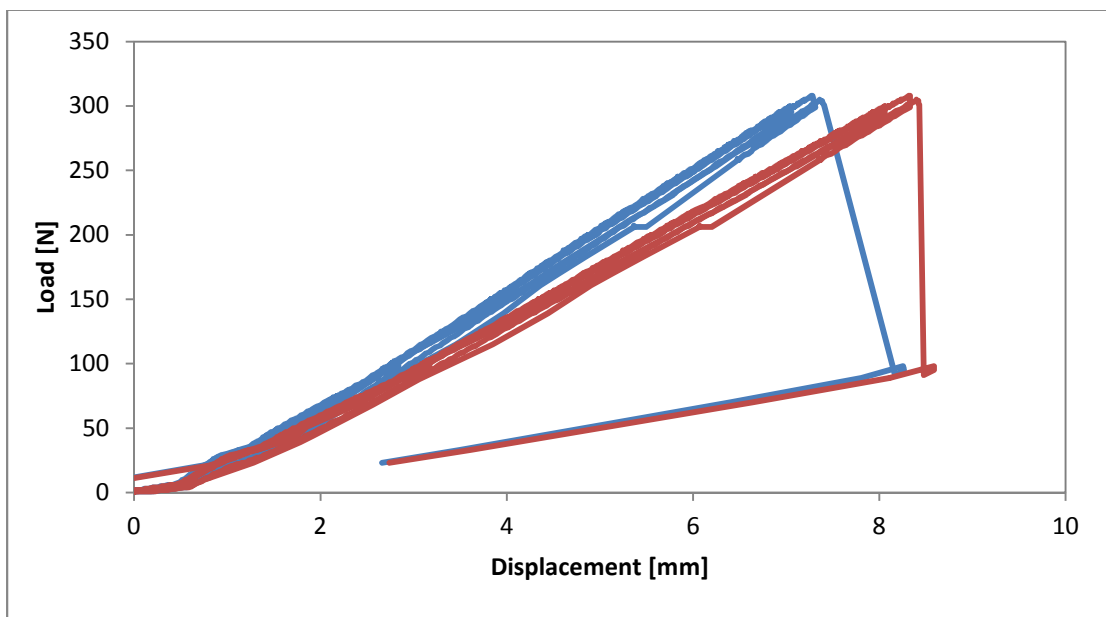


Figure 18: Raw Load-displacement data for 50% Mode Mixture unidirectional test specimen (red), and compliance corrected load-displacement (blue)

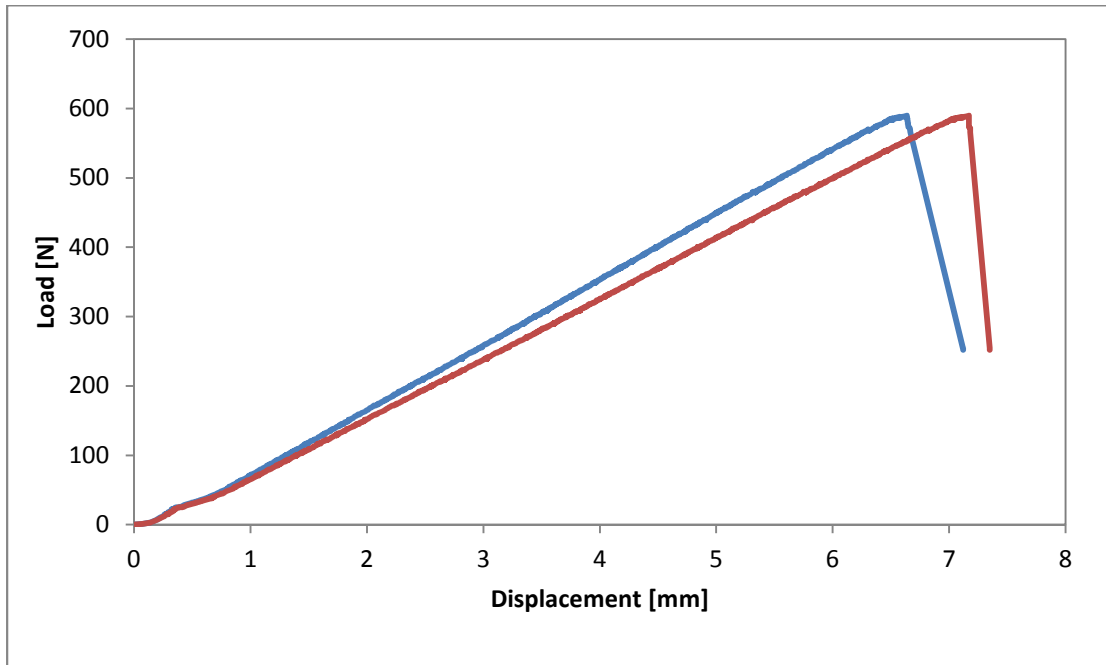


Figure 19: Raw Load-displacement data for 100% Mode Mixture unidirectional test specimen (red), and compliance corrected load-displacement (blue)

5.2 Attempts to Arrest Crack Growth and Induce Stability

Figures 18 and 19 rather clearly illustrate the rapid crack growth present in the high Mode II cases of fracture toughness. As was the case for all tests, regardless of load speed, machine compliance, and method for delamination insert, the 50%, and 100% mode mixture cases resulted in rapid and unstable crack growth all the way to the central support roller. This served to arrest crack growth, but subsequently invalidates any equations and assumptions made about the fracture beyond this point. The result is that while using the Wyoming Test Fixtures, Mixed Mode Bending apparatus for conducting MMB tests, only a certain portion of the material may be

investigated. With high Mode II cases, only the linear elastic region, before crack propagation may be investigated. If one is particularly lucky, an extremely small amount of crack propagation may be observed with the 50% mode mixture case. This is visible in *figure 18*, as there is a slight drop in load right before the critical load is reached. With the 100% mode mixture case this hope is completely removed as rapid crack growth across the entire length of the specimen is almost always present.

The high Mode I test cases offer a very unique opportunity. The experiment, if conducted carefully may show natural crack growth so long as the displacement is increased very slowly, allowing time for the specimen to settle while testing. Once some amount of crack growth is allowed the microscope may be refocused on a different area. Subsequent investigation with DIC by completely unloading and reloading the specimen at the new crack tip allow DIC to be used on the natural crack growth, after the initial notch effects have been negated, and are no longer an effect in the analysis.

The second method considered for avoiding notch effects in the data was to attempt to propagate the crack through approaches like fatigue loading. Cyclic and especially slow loading and unloading of the specimen would result in plastic deformation at the crack tip, and potentially allow for extremely slow crack growth, particularly for Mode II dominant tests. This concept and its subsequent investigation was beyond the scope of this investigation.

The notch effects are also confirmed in literature searches, as shear fracture toughness values reported for the same material typically show G_C values which are 10% higher when the delamination is initiated by an insert as opposed to fatigue crack

growth [6]. Unfortunately there are no known means for slowing crack growth in shear dominate cases to acceptably slow levels. The only potential solution to this issue would be to enhance laboratory equipment. Extremely high speed imaging equipment might be able to capture the crack propagation, a better resolution force transducer would be required to accurately report load displacement data in real time as well.

5.3 Analytical Methods for Determination of Fracture Parameters:

Also seen in *Figure 18*, is an unloading curve. This is obtained after the initial crack growth wherein the load and displacement is measured while the specimen with new crack geometry is unloaded and re-loaded. The purpose of doing this is to determine any initial change in slope due to contact effects in the test fixture, and therefore obtain the true compliance after crack growth. This is also a means of checking for hysteresis. The change in slopes along with crack length may be used in order to measure the critical energy release rate, G_c , from the standard formula:

$$G_c = b\Delta C/\Delta a \quad (21)$$

To obtain the true specimen compliance, it must also be corrected for the system compliance using the standard aluminum calibration specimen. From the unloading data in *figure 17*, it is important to note that there is very little hysteresis from the unloading curve, even after crack growth, and the initial change in slope occurs very close to zero displacement. This is further proof that the test

configuration is very stable and can provide accurate and reliable results.

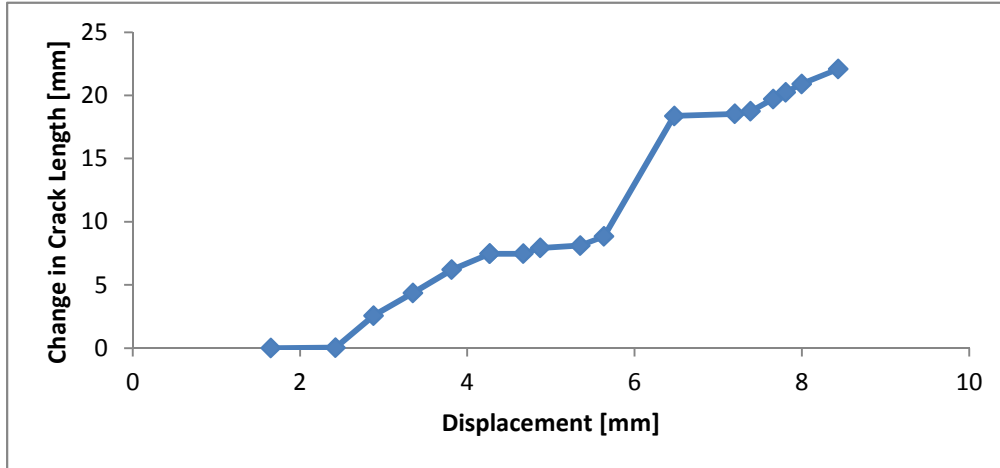


Figure 20: Change in crack length-displacement data for the same Mode I unidirectional test specimen in Figure 6. These displacements are compliance corrected.

To obtain the critical energy release rate, it was also necessary to determine the change in crack length with displacement, which was easily obtained from digital images of the test, and can be seen in *figure 20* for the same 22% Mode Mixture test specimen with load displacement data from *figure 17*. Results for G_{IC} obtained at various changes in crack length can be seen in *figure 17*. It is also important to note from *figure 20* that displacement values above 8 mm, we begin to see a flattening of the load-displacement curve. This is due to the crack tips approach to the central loading point of the test fixture. This serves to arrest the crack growth and induce an artificially low value for G_{IC} , as a result, only the data between 6 and 8 mm of displacement should be considered for calculation of Mode I fracture toughness. The values of G_{IC} in *figure 21*, which ranged from 250 to 370 J/m² were also found to be close to the ASTM calculations for G_C (*Equation 20*) obtained from the critical load, 320 J/m². The fact that the critical load only begins to match ASTM predictions after

appreciable crack growth may be considered to be a part of the notch effects present in the testing specimen. It should also be of note that the test specimen used in testing to generate *figure, 17, 20, and 21* fractured at an unusually high load level compared to other 22% mode mixture tests.

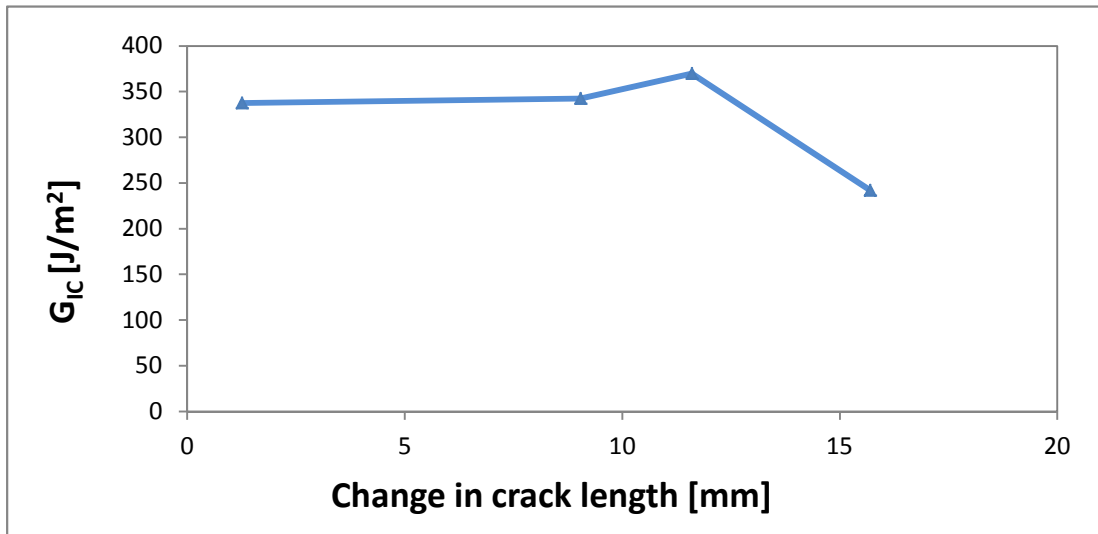


Figure 21: G_{IC} versus change in crack length calculated from data shown in *figure 17*.

Note that this is from raw data and is not compliance corrected.

Using multiple forms of data collection, the critical value for shear fracture toughness may be ascertained. It can be conclusively stated that shear fracture toughness may be determined with the aforementioned traditional techniques using Linear Elastic Fracture Mechanics, however, there is much opportunity for improving the quality and consistency of the results.

Using the load displacement data for *figures 17, 18, and 19*, at three different mode mixture cases of 22%, 50%, and 100%, the ASTM standards were utilized to generate curves which show the Mode I and Mode II fracture toughness's, G_I and G_{II} , at various loads for a standard sized test specimen. *Figures 22, 23, and 24* show this

data for the three afore mentioned tests. The critical fracture toughness is denoted on the curves by a red x, and the value for G_I is depicted with a black line, while the value for G_{II} is depicted with a blue line.

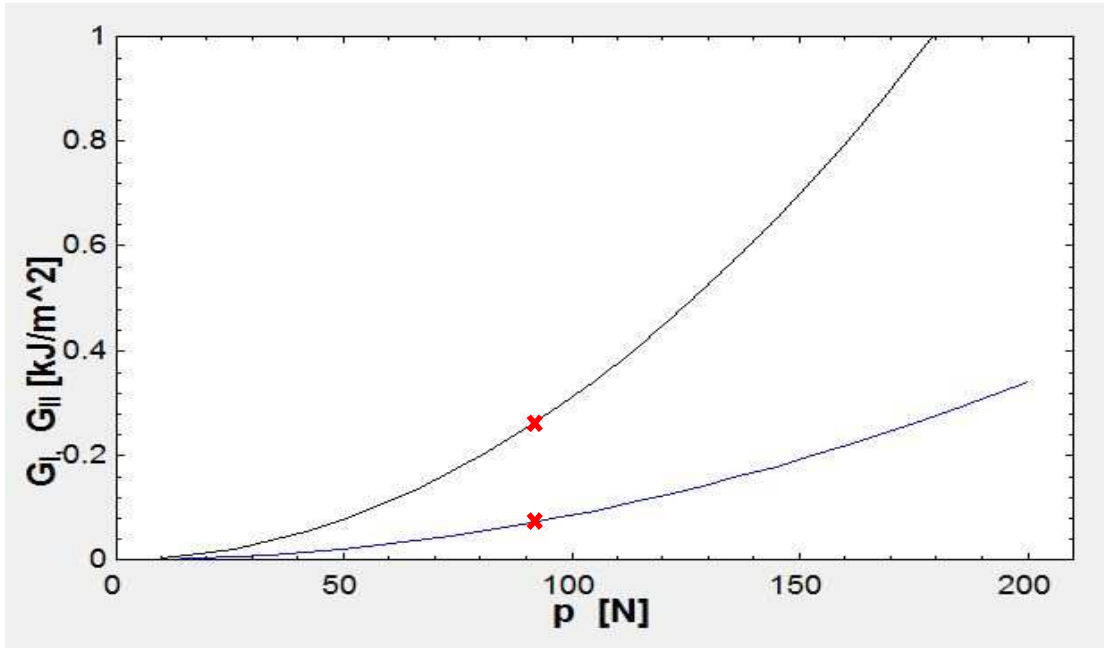


Figure 22: Shear Fracture Toughness for 22% mode mixture test.

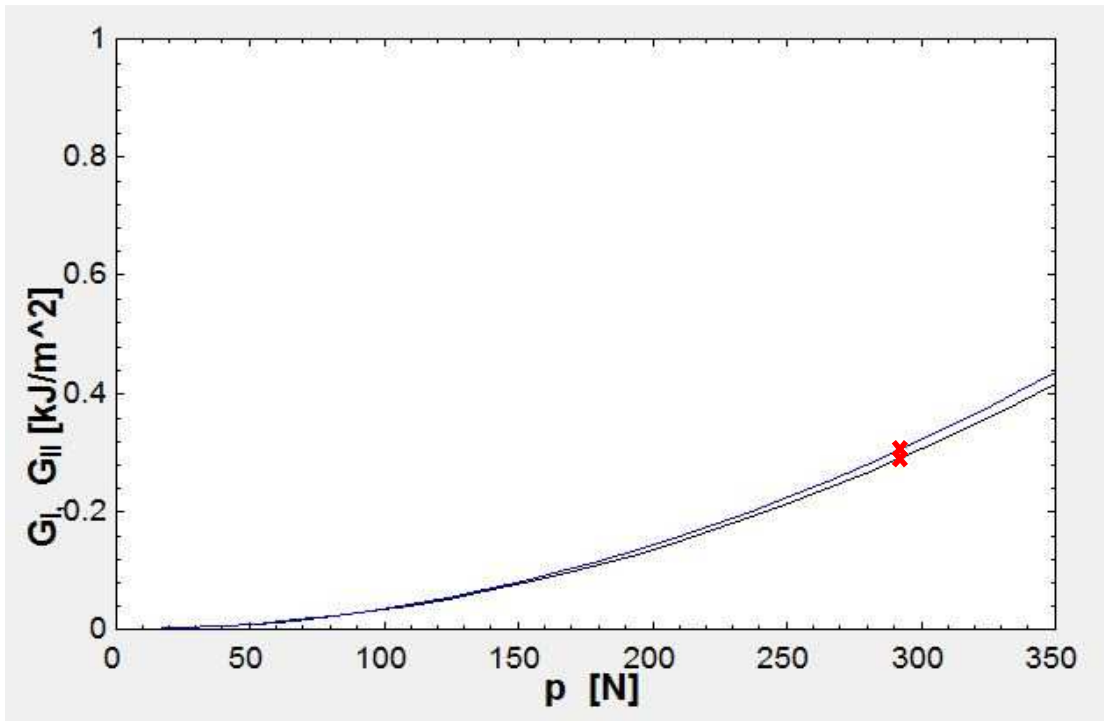


Figure 23: Shear Fracture Toughness for 50% mode mixture test.

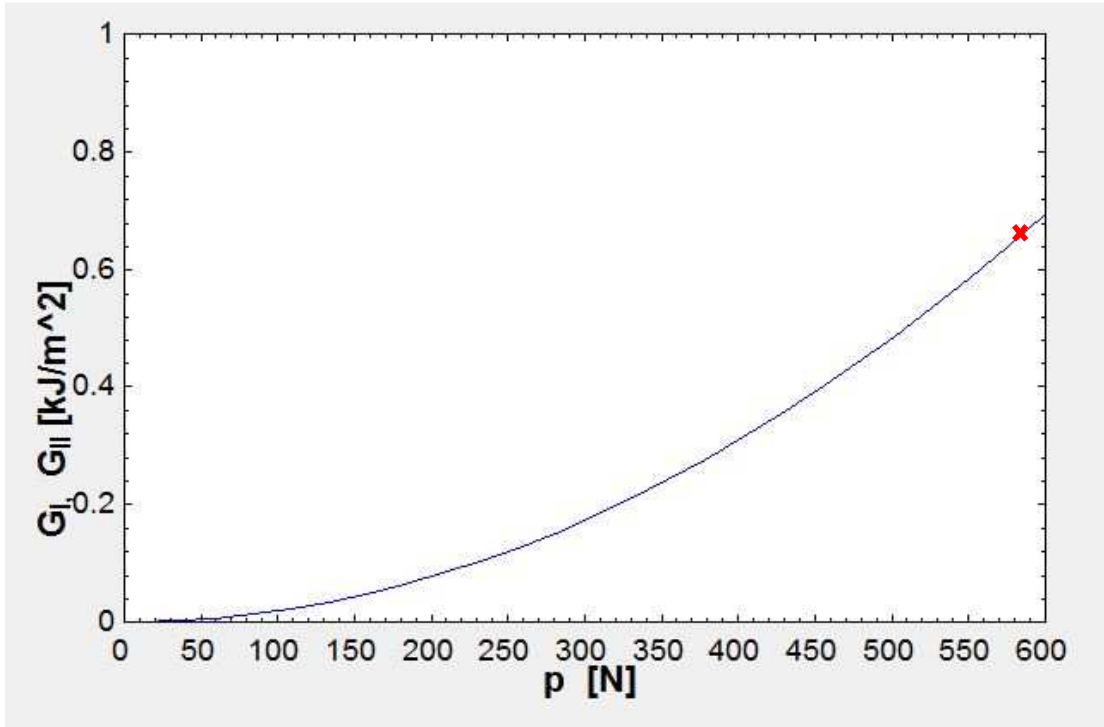


Figure 24: Shear Fracture Toughness for 100% mode mixture test.

Several trends are immediately and readily visible from the initial ASTM analysis. Firstly, the level of Mode II fracture toughness increases with the mode mixture. Secondly, the more that shear fracture dominates a mixed mode bending test with the Wyoming Test fixture, the higher critical fracture load may be expected. This is noted by the red “x” on the previous figures. For the 22% mode mixture case, fracture and crack propagation occurred at 90 N resulting in a critical shear fracture toughness of $231 J/m^2$. It should be noted here that this particular test appeared to be weaker than previous tests of the same configuration, as other 22% mode mixture cases usually grew at load levels of upwards of 100 N. This is acceptable though, as DIC will be able to confirm the proper value for shear fracture toughness. The 50% mode mixture case fractured at 301 N and had a critical fracture toughness of 630

J/m^2 . This value is significantly higher, and the mode mixture was calculated to be 51%. This is due to slight geometric deficiencies of the test specimen, and possible miss-alignment of the loading tabs. *Figure 23*, particularly at higher load levels, shows that the value for G_{II} is slightly greater than that of G_I . In the 100% mode mixture case, the value for G_I is nominally 0, and crack growth is only dependent upon the Mode II fracture parameters. Crack propagation occurred at 590 N, resulting in a shear fracture toughness of $672 J/m^2$. As the load lever arm length “c” is increased, the propensity for crack growth is also increased, and the crack is grown at much lower loads, however, the slope for shear fracture toughness also increases more rapidly. This concept can be seen in *figure 22*, where a load of 200 N on the specimen in the 22% mode mixture configuration would have extremely high shear fracture toughness.

5.4 Analysis of Analytically Obtained Fracture Parameters:

The above figures and parameters developed in this section are the state of the art method for determining delamination fracture parameters for composite materials. Though reasonably accurate, there are many assumptions made during the analysis of mere load displacement data. Many of these assumptions like the assumption that fiber bridging does not occur, that crack growth is always stable, and that load frame compliance may be corrected with calibration specimens only serve to induce error into an already cumbersome process for data extraction. The following, section 5.5, demonstrates the simplicity of data analysis using DIC; Chapter 7 proves the effective use of DIC to calculate fracture parameters. The accepted analytical analysis

presented in this chapter is repeatedly used to generate values for G_I and G_{II} throughout this course of study.

The terms ASTM G_I and ASTM G_{II} used throughout this research program are synonymous with fracture parameters extracted using analytical methods. Please note that these values may vary throughout this research as each specimen is unique to some degree. Small variations in the geometric properties, particularly crack length have a tremendous impact on the analytical value reported. Additionally the ASTM values change greatly based on what load level is investigated. For comparison purposes, the geometric data used for analytical calculates was adjusted for each experiment based off of the geometry for that specimen.

5.5 Mixed Mode Fracture Experiments Analyzed Using Crack Tip

Displacement:

While the load-displacement data in *figure 17* can be used to determine the mixed-mode fracture conditions globally from the ASTM standard, DIC can be used to obtain a local measure of mode mixture, as well as a myriad of fracture parameters. By using DIC, it is possible to predict the mode mixture of the specimen. This technique is of superior reliability to the analytical methods, as displacement measurements are taken directly from the specimen and compliance correction is not an issue. This eliminates the need to correct data for the compliance of the fixture and load frame used for testing, as well as eliminating numerous sources for potential error in the overall system. The use of DIC to extract data also enables analysis on a much more local scale. This local investigation of the region surrounding the crack tip is much more interesting, as certain components, such as global bending and

displacement no longer effect the displacement measurements at the crack tip. Using DIC, displacement data may be generated specifically in the region surrounding the crack, known as crack tip displacement, as well as the full field displacement fields in the two dimensional plane around the crack tip.

Before extensive time and resources are devoted to full field displacement techniques, a deeper investigation into the crack tip behavior may be of some benefit. Crack tip displacement (CTD) analysis can be used as long as displacement data is accurately obtained along the edge of the crack. This is the COD (Crack Opening Displacement) and CSD (Crack Shear Displacement). The expressions for COD and CSD in the crack tip region for orthotropic bodies was previously developed by Lekhnitskii and Sih [14] are as follows for an orthotropic specimen:

$$\text{COD} = \left[4(2)^{1/4} \frac{(a_{11}a_{22})^{1/4}}{\sqrt{\pi}} \left(\frac{2a_{12} + a_{66}}{2a_{11}} + \sqrt{\frac{a_{22}}{a_{11}}} \right)^{1/4} \right] \sqrt{G_I} \sqrt{r} \quad (5)$$

$$\text{CSD} = \left[4(2)^{1/4} \sqrt{\frac{a_{11}}{\pi}} \left(\frac{2a_{12} + a_{66}}{2a_{11}} + \sqrt{\frac{a_{22}}{a_{11}}} \right)^{1/4} \right] \sqrt{G_{II}} \sqrt{r} \quad (6)$$

The orientation of the CSD and COD can be seen in *figure 25*. This is an image of a typical crack specimen loaded for 22% mode mixture; the high magnification on this image truly enables more refined data analysis. In this image, the scale is approximately 304 pixels/mm. Other notable features are the secondary crack forming right under the crack tip. This is an indication that crack propagation is about to occur with the slightest perturbation of the system.

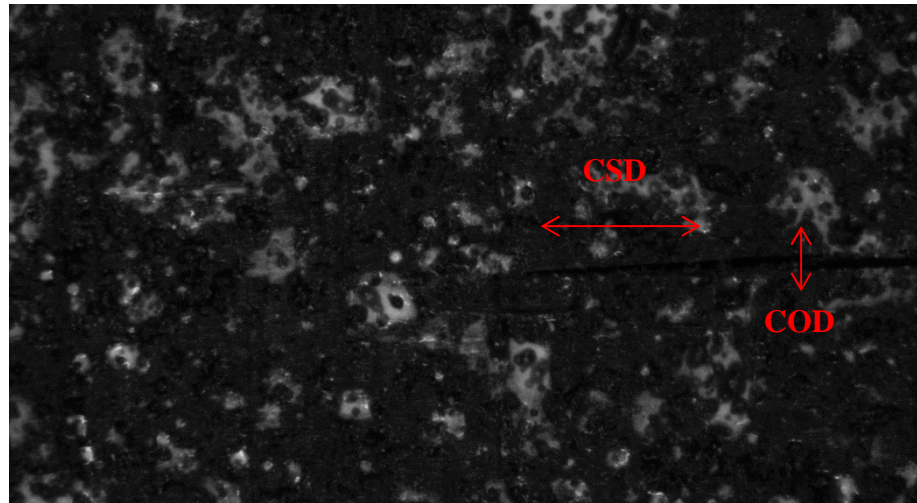


Figure 25. A typical cracked specimen showing orientation of CSD and COD.

This CTD analysis can complement the full-field displacement analysis by providing more refined extraction of G_I and G_{II} . Displacements were measured using DIC, and the commercial DIC software, VIC-2D, from Correlated Solutions (Columbia, SC). Two methods were used to extract displacement data; using the VIC-2D inspection tool crack tip opening, as well as crack shear opening displacements may be measured. Alternatively more reliable, and less noisy means of acquiring the same data results were achieved by observing the full field data, and rather meticulously noting the displacements of the row of pixels directly above and directly below the crack. Taking the difference between the two data points yields the crack opening, or crack shear displacement when noting the u and v displacement fields.

Experimentation was not without difficulty. During Pure Mode II testing and at high magnification, the displacement and deflection of the beam itself becomes so great that the initial field of vision is moved off the camera early on during the testing, making DIC very challenging. It was not until later in this course of study

when an investment was made on a traveling microscope stand which enabled crack growth to be easily tracked, and keep the camera focused on a single, section of the test specimen. This is a necessary step for DIC, as future images must be compared to the reference image where no load, or displacement is applied to the laminate. Also, each test provides unique issues to data collection; tests which exhibited high levels of Mode I loading suffer from rotation issues, wherein the displacements measured by DIC are skewed because of the curvature of the specimen's legs as the opening displacement is increased at the loading tabs. This was corrected by post processing data that exhibits this tendency. High Mode II loading results in increased loads, and appreciable bending of the composite laminate to occur. With this, the sample must be corrected for rotation, and displacement. This too may be corrected in post processing, when fitting measured and extracted DIC data to theoretical solutions.

5.6 Crack Tip Displacement Results From DIC Analysis

Near-field displacements transverse to the crack can be seen in *figure 26* for a 100% mode mixture test. An example of the far-field shear strain can be also be seen in *figure 26*. The extracted CSD and CTD displacements along with their fits to *equations (5)* and *(6)* can be seen in *figure 27*. Results matched the orthotropic equations rather well, and in particular for CSD. Fitting COD required the use of higher order terms, without which a high quality fit was not attainable. This is indicative of the dominance of rotation due to cantilever bending. The lack of K-

dominance in COD near the crack tip may be due to the notch effects from the ASTM standard.

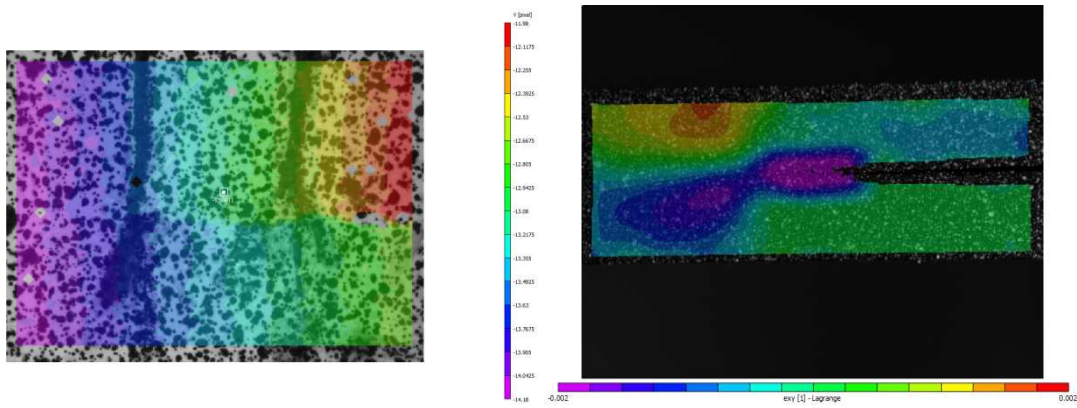


Figure 26: DIC results showing (left) near-field displacements transverse to the crack, and (right) far-field shear strain at the crack tip with various length scales.

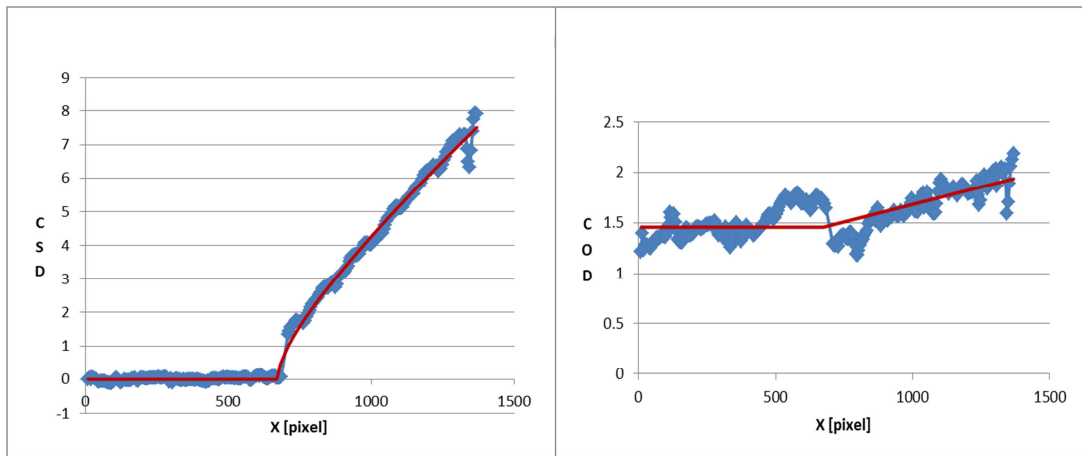
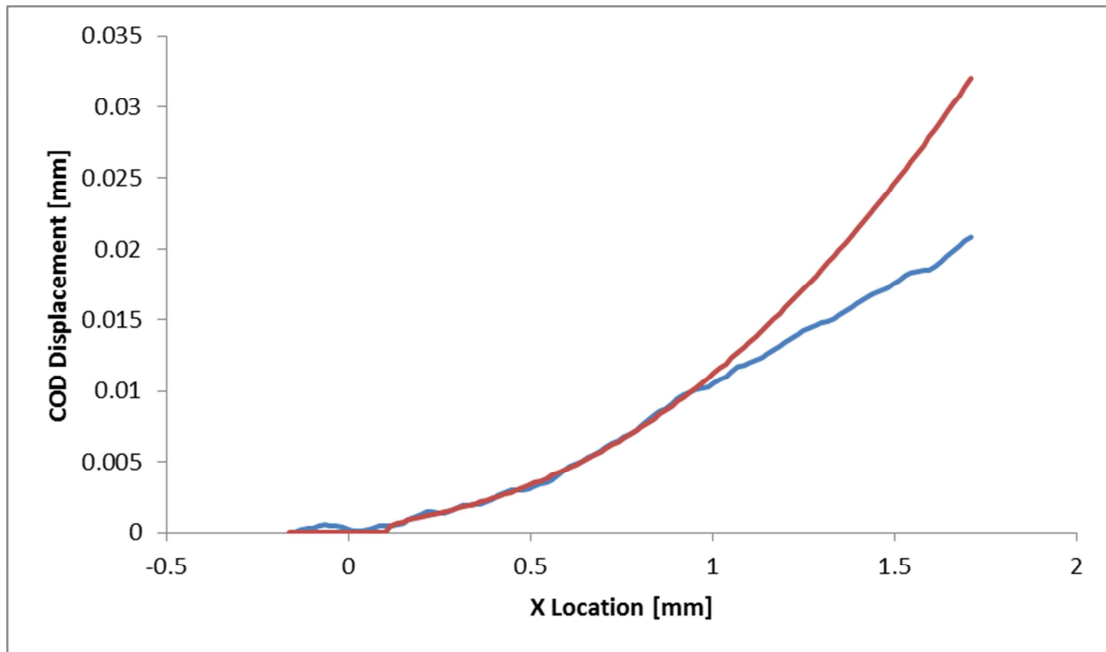


Figure 27. CSD (left) and COD (right) extracted from a 50% Mode II test using DIC and subsequent fits using equations (5) and (6).

The data represented in *figure 27*, particularly for Crack Opening Data is rather noisy, though this would be expected for a 50% mode mixture case, and opening displacements as such are only on the order of a few pixels. This crack tip

displacement analysis is however extremely useful for identifying the location of the crack tip, a task which is not only daunting, but almost impossible to discern visually. Initial results for a 22% mode mixture test can be seen in *figure 28* for the CSD and CTD corresponding to the load near initial crack extension in the load-displacement results in *figure 17*. These results also tend to indicate more rotational displacements in the opening mode, and only a K-dominant trend in the Mode II.



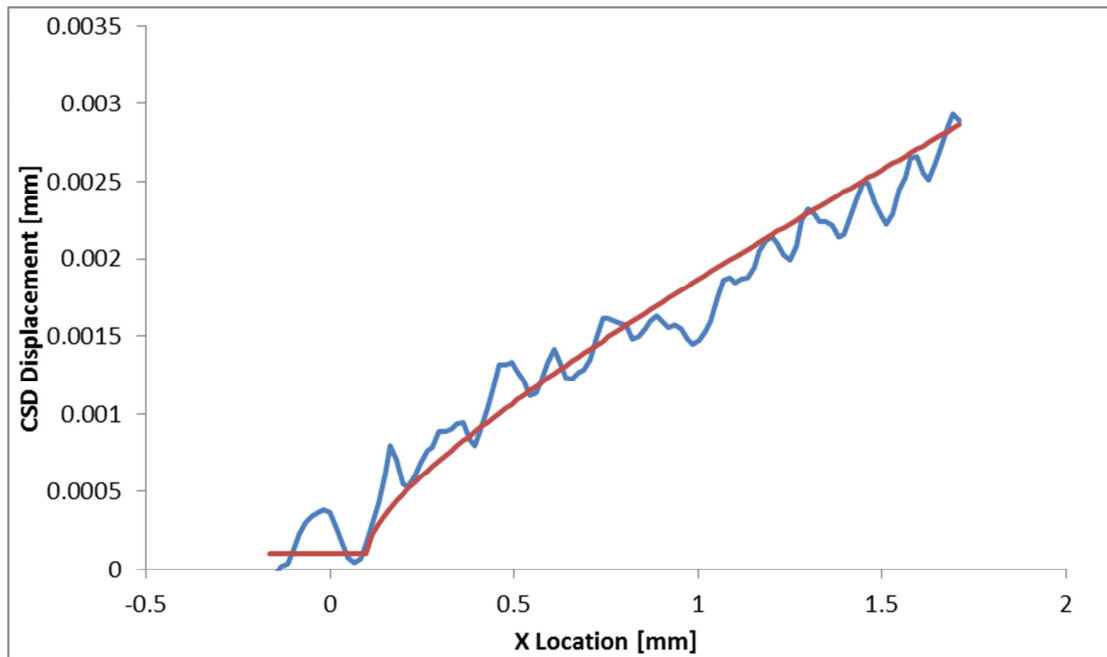


Figure 28: COD (top) and CSD (bottom) extracted from 22% Mode Mixture test using DIC and subsequent fits using equations (5) and (6).

There are several notable features in *figure 28*, primarily, the deviation of the fit and recorded data in the far field. The most immediate reason for this analysis is to calculate fracture parameters, and the far field solution is significantly less important to the analysis. The crack tip displacement equations tend to break down in the far field region, and require significant higher order terms which unduly bias results. In this analysis shown in *figure 28*, the crack opening displacement data beyond 1 mm from the crack is not analyzed for fracture parameters. As a result, a much better fit is obtained in the near field. This cut off point for data analysis can be adjusted as required. When a very small investigation area is used, the result is an enhanced correlation for near tip fracture parameters, and generally improved results.

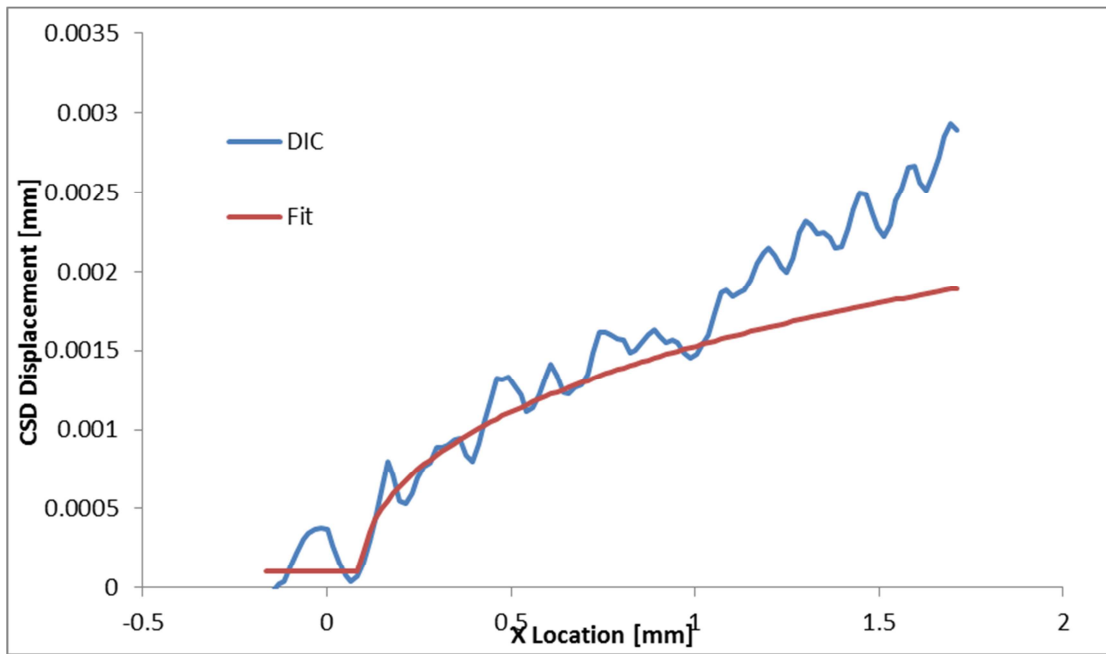
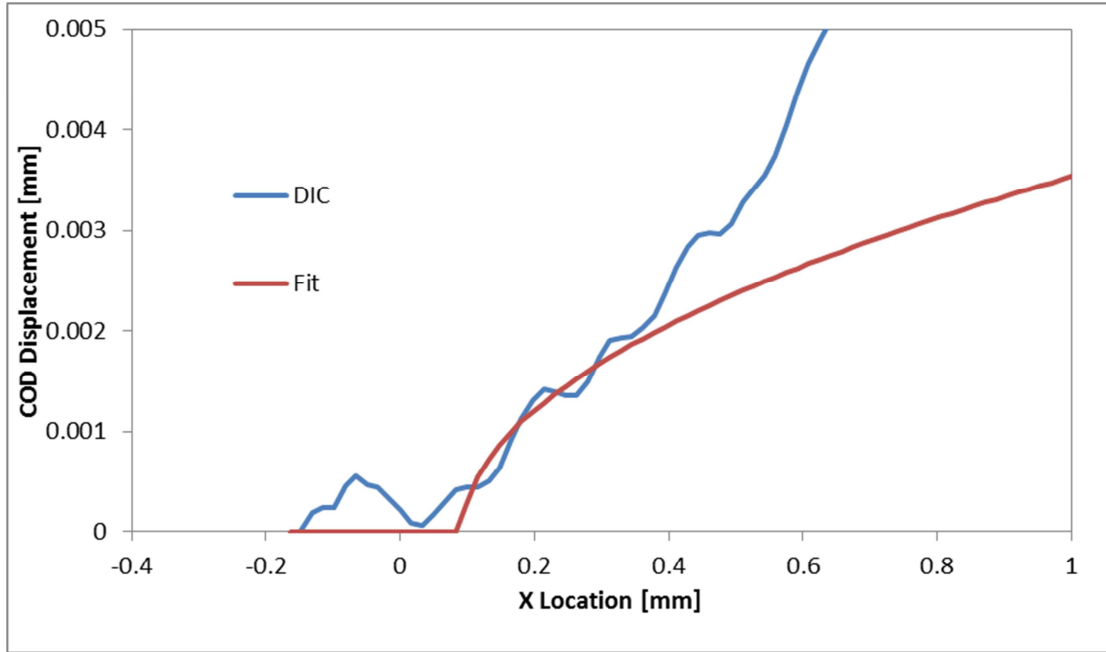


Figure 29: Crack Opening Displacement data and fit for near field solution (Top) and Crack Shear Displacement and fit for near field solution (Bottom).

In *figure 29*, only the near field crack data was used for fitting parameters. As such, only the crack displacement within .25 mm of the crack tip location could bias

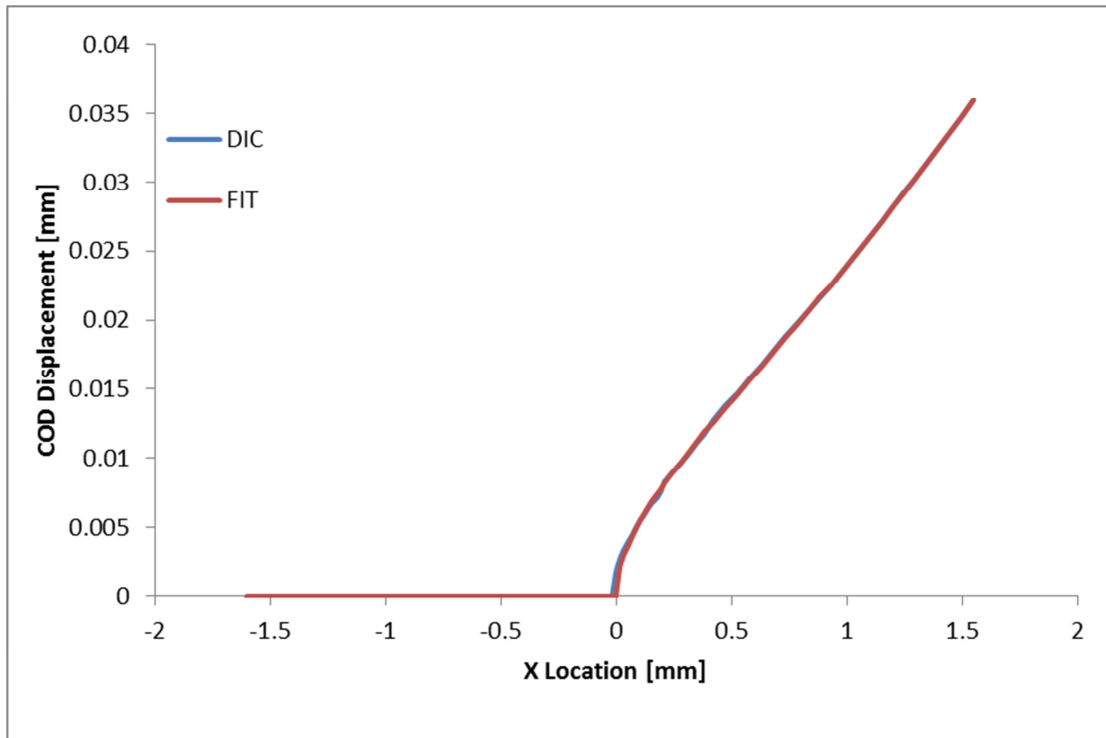
the data. Notice how the far field solution and higher order terms are no longer present when local crack parameters are analyzed as opposed to the far field fit shown in *figure 28*. This analysis results in the added benefit of improved data correlation for fracture parameters, but at the disadvantage of not being able to predict and analyze far field solutions. When using crack tip displacement analysis on composite laminates, the fracture parameters reported are often grossly far from the ASTM reported values. For the close field displacement depicted in *Figure 29*, the value for the Mode I component of shear fracture toughness is reported as $19.695 J/m^2$, with a Mode II component of $14.292 J/m^2$. The fracture parameters reported from the test in *Figure 28* have a value of: $7.394 J/m^2$ for G_I , and a value of $15.811 J/m^2$ for G_{II} . Considering both of these investigations were conducted at the same test, at the same load of 60 N, this analysis can prove just how greatly higher order effects change the resulting fracture parameters of analysis. Neither of these values are even close to the ASTM standard for this test which indicates that the value for G_I , and G_{II} at a load of 60 N, and in a 22% mode mixture set up should be $81.0 J/m^2$, and $20.5 J/m^2$ respectively. The value for Mode II shear component is not too far off of the reported ASTM standard; this can be expected as the CSD fits in *figures 28* and *29*, are rather good. Comparison between the CSD, and COD fits clearly shows that higher order terms are very dominant in crack opening displacement analysis, even when the far field solution is negated as is the case for the crack opening displacement displayed in *figure 29*, the fit quality is still rather poor.

The data in *figures 28* and *29* are in stark contrast to the COD data reported by Lekhnitskii et al [14]. The reason for such a poor fit is the specimen geometry under

loading conditions. During loading, there are significant bending displacements; for crack shear displacement conditions the bending displacements manifest themselves as higher order terms, these terms mathematically are equal and opposite for each leg of the specimen. The result is that for crack shear displacements, the higher order terms cancel each other out, and provide a better fit, consistent with the equation described by equations 5 and 6, as well as the data by Lekhnitskii [14]. For crack opening displacement, these higher order terms are equal but not opposite, and thusly do not cancel out. This results in the necessity of higher order terms to provide a satisfactory fit, but has a profound impact on the fracture parameters found within this analysis.

Another issue with Crack Tip Displacement analysis is the resolution of DIC technique. Notice the amount of noise variation in data for *figure 28*, and *figure 29*. Particularly at the very near tip region, where crack propagation has not yet occurred, a ripple, or increase in displacement may be observed for the measured DIC data. Though the crack tip location is known for tests, displacements in the un-cracked region are assumed to be zero. It cannot be decisively determined whether or not these variations in displacement or noise, a faulty reading in the DIC software, or an actual ripple displacement in the laminate ahead of the crack tip. High magnification tests like this one truly push DIC to the limit of its abilities. Displacements of less than a micron are being used for calculations when the smallest speckle pattern achievable with current techniques is at least 10 microns. This results in a loss of data fidelity, especially at low load levels displacements. *Figure 27* illustrates this rather nicely, as for the crack opening displacement, for a 50% mode mixture loading

condition, is only 2 pixels. This measured displacement data is much less than the noise and variation in the data sampling to begin with. In order to improve results, and accurately determine fracture parameters using crack tip displacement analysis, it is necessary to decrease the size of the speckle pattern, and ensure that this kind of analysis is reserved for high load specimen loading conditions, where measured displacements can be maximized. Failure to comply with these conditions will result in data which has noise that exceeds the range of displacement measurements used for analysis of the laminates fracture parameters. *Figure 30* shows the crack tip displacement data for the same test as shown in *figures 28 and 29*, except this test is at the maximum load of 79 N. It is also corrected for rotations, displacements, and errant data points are removed.



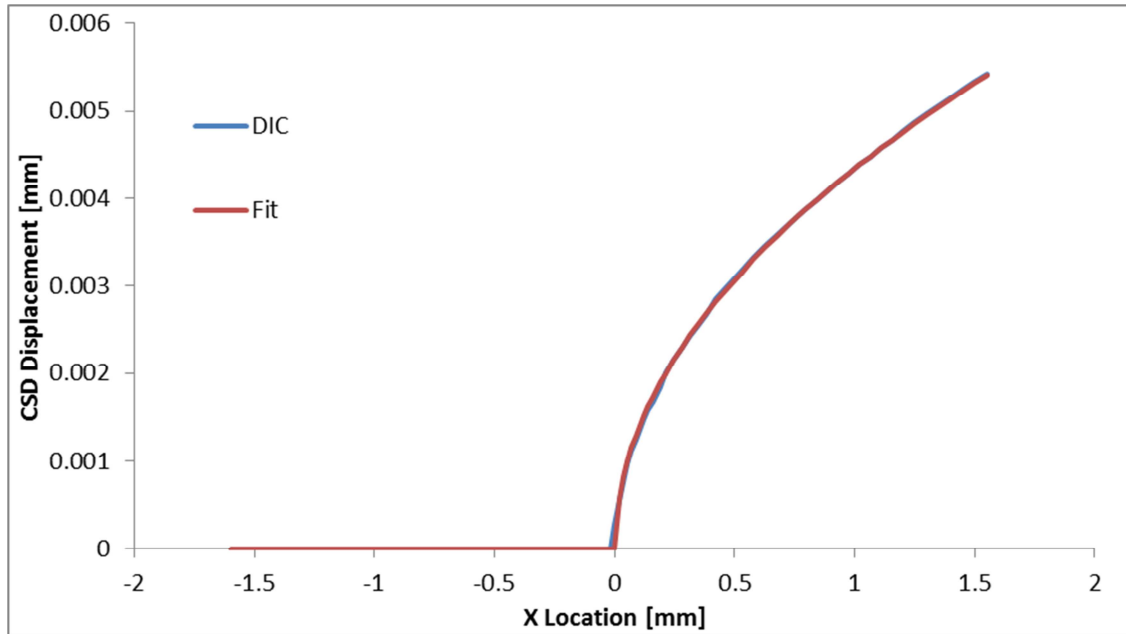


Figure 30: Crack Opening Displacement data and fit for perfect synthetic data at 79 N (Top) and Crack Shear Displacement and fit (Bottom).

For the data presented in *figure 30*, the fracture parameter values of G_I , and G_{II} at a load of 79 N, and in a 22% mode mixture were calculated to be $347.35 J/m^2$, and $99.03 J/m^2$. Though this is still a bit higher than the accepted ASTM values for fracture parameters, it is significantly more accurate than the values predicted in earlier cases using crack tip displacement analysis.

5.7 Crack Tip Displacement Analysis and Conclusions

After initial results were tabulated for crack tip displacement at critical loads in *table 2*, it was clear that there were some significant issues with the crack tip displacement analysis from DIC. *Figure 30* demonstrates how useful, and how easy crack tip displacement fits are for analyzing fracture parameters. However, this is only for the case when data is precise and accurate. DIC data because of the large

singularities at the crack tip, and discontinuity in the already separated regions is neither precise nor accurate for such a small range of data.

CTD analysis only uses 2 single lines of data from the pixels directly above and directly below the crack tip. The software is rarely able to properly determine displacements in the specimen due to the opening of the delaminated region, and manual extraction of the pixels requires excessive effort for the researcher, but still does not solve the issue of singularities in the already cracked region. Additionally resolution errors pertaining to the size of the speckle pattern used for DIC analysis induces error into the measurement process. In order to have a good fit, the displacements must be measured as accurately as possible, and in a manner which can distinguish very discrete changes in position.

Load Level	G_I [J/m ²]	G_{II} [J/m ²]	ASTM G_I [J/m ²]	ASTM G_{II} [J/m ²]
0%	185.6	1.13	405.2	0
22%	254.55	72.41	212.1	58.56
50%	-	-	251.6	259.8
100%	0.0	185.23	0	702.0

Table 2: Strain energy release rate calculated from CTD analysis compared to strain energy release rate calculated from ASTM analysis

Because of the labor intensive CTD analysis, and poor results yielded because of the bad data, little effort was devoted to improving the work developed here. As such further work on CTD analysis was halted in hopes of finding and developing a

more reliable means for extracting fracture parameters from DIC data. The solution was to use the same principles to model deformations but with the full field of data extracted from DIC.

Chapter 6: Fracture Parameters Extracted Using Synthetic Data from FEA Model

6.1 FEA Modeling of Mixed Mode Fracture Fixture

In order to affirm prior work for crack tip displacement, and full field DIC analysis, data was obtained from a FEA model developed by Virakthi and Lee at the University of Maryland [Virakthi, 21], to study fatigue in mixed mode fracture conditions. By comparing the work developed by Virakthi and Lee cohesive zone model with the analysis techniques, and measured displacement data from DIC, there is a unique opportunity to confirm the analysis technique present in this course of study.

The finite element analysis model developed was intended to closely mimic the original test condition, additionally; the same material properties were used for the specimen in the FEA model as were described for the actual experiments in chapter 4. In this case, actual load-displacement data from test specimens was used to describe the deformations of the FEA model. The load configuration applied to the test specimen in the FEA model was developed specifically with the ASTM standard as guidance. *Figure 31* is a depiction of the FEA model used in ABAQUS.

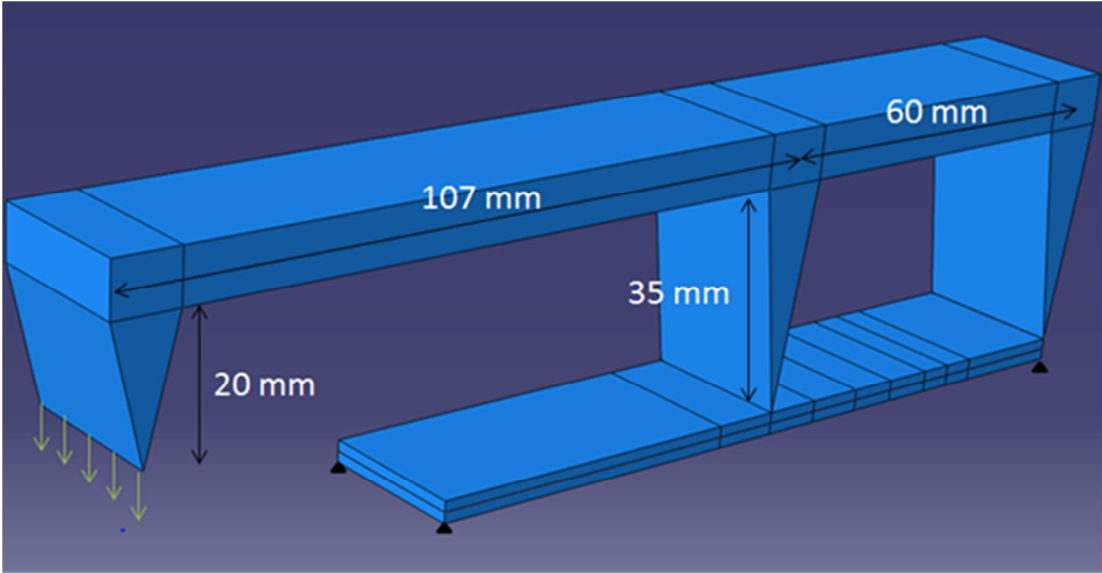


Figure 31: Illustration of the model constructed in ABAQUS [Virakthi, 22]

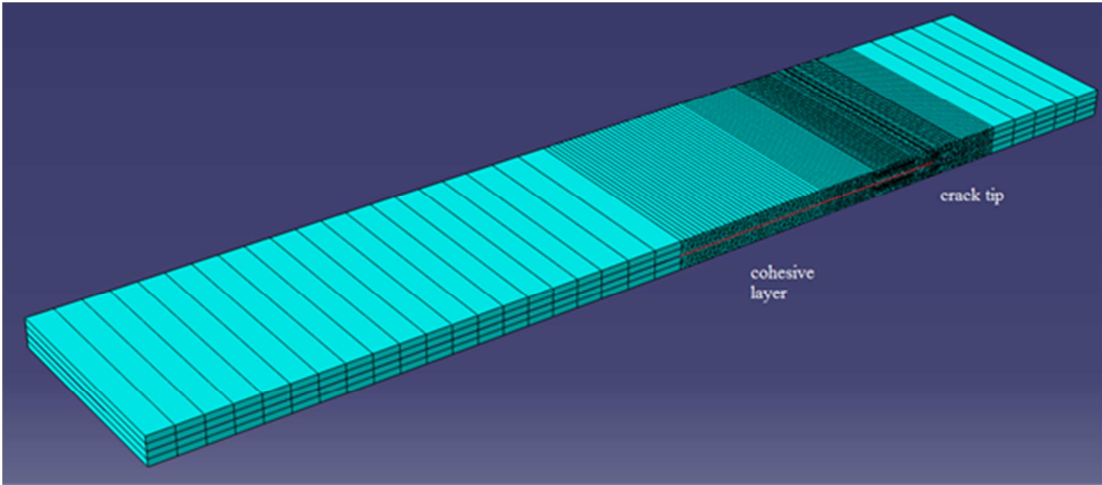


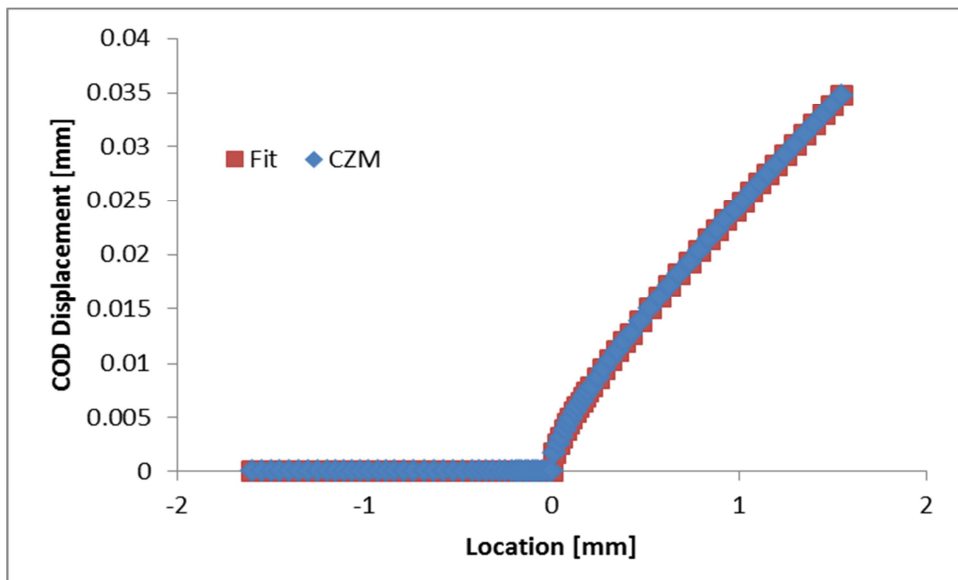
Figure 32: Test specimen model with meshing region, [22].

The FEA data was collected in a similar manner to the actual DIC displacement data, wherein displacements of the material were measurable. The benefit of the FEA model, is that the speckle pattern is no longer a variable, and the COD and CSD displacements are reported extremely accurately, with little or no noise variation in the data. The disadvantage of using FEA synthetic data is that this data is only as good and accurate as the model has been designed to be, and the cohesive zone is not

particularly well understood. The FEA model still must be adjusted to produce the most accurate fracture parameters, however it is still useful for affirming the analytical data fits used for DIC analysis.

6.2 Crack Tip Displacements Analyzed Using Synthetic Data

The same theory used in the previous chapter is now analyzed, but with displacement data extracted through ABAQUS on a FEA model of a mixed mode fracture tested specimen. *Figure 33* shows the measured FEA crack tip displacement data compared to the analytical fit from equations 5 and 6. For the data presented in figure 34, the shear fracture parameters calculated were $G_I = 347.35 \text{ J/m}^2$, and $G_{II} = 99.04 \text{ J/m}^2$.



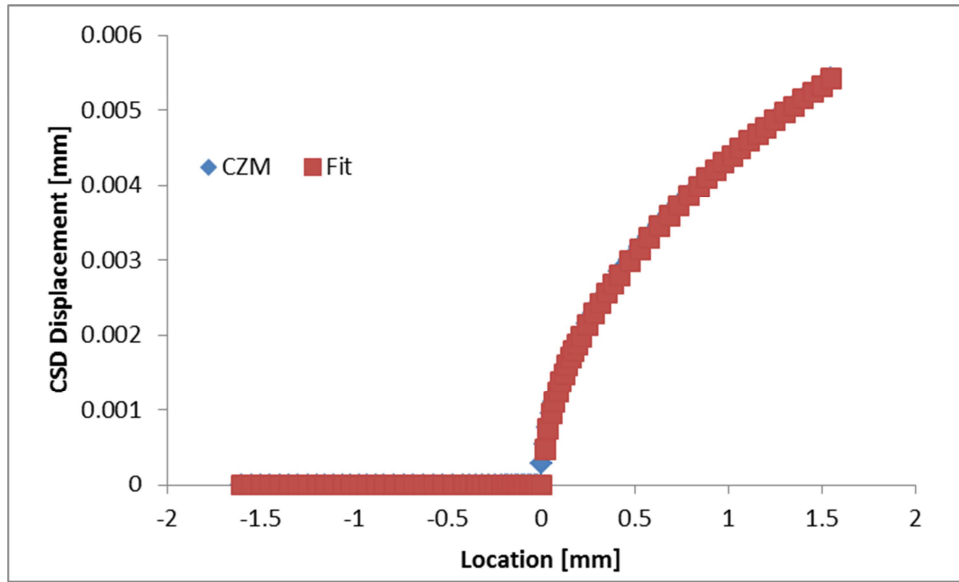
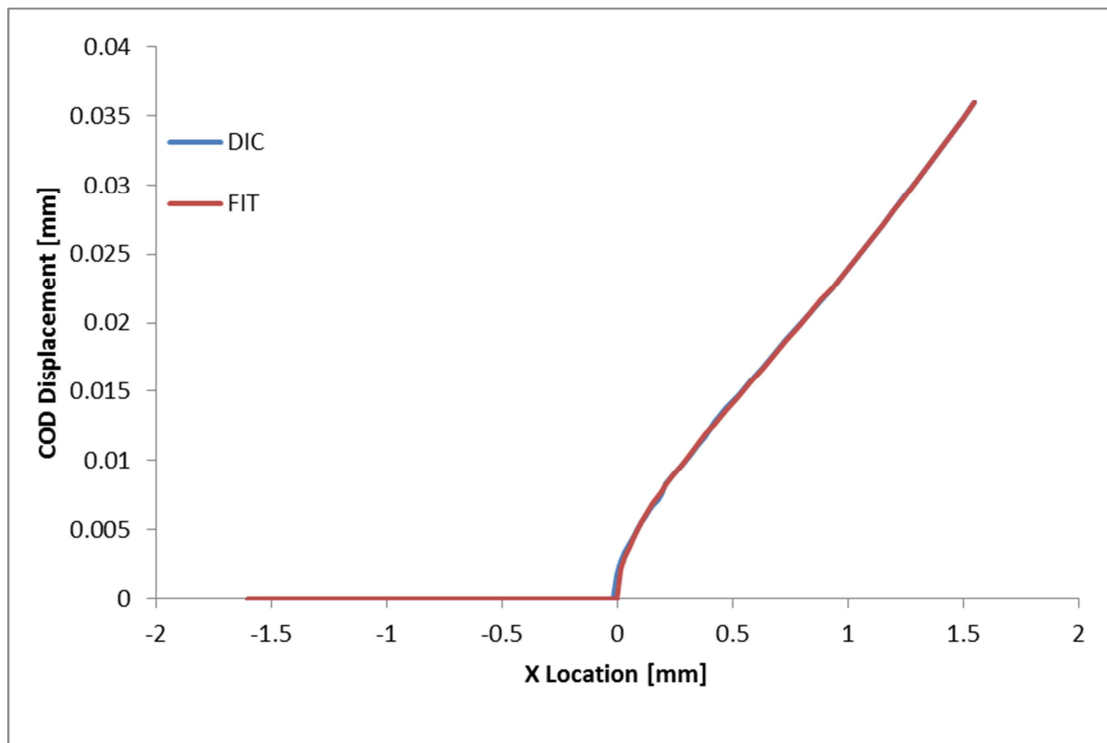


Figure 33: FEA Modeling of crack tip displacement data with analytical fit. For 22% mode mixture case at 28.14 N load.



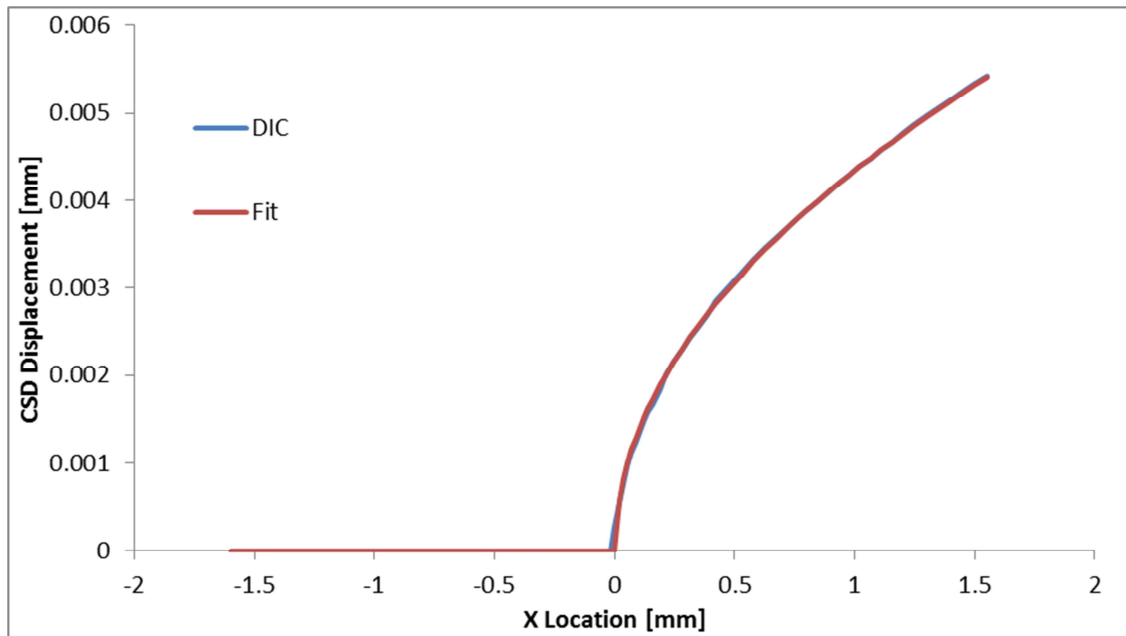


Figure 34: FEA modeling for crack tip displacement analysis for 22% mode mixture case at 79 N load.

Most notably is the severe contrast between the fits for figures with FEA data, and the fits for figures with DIC collected data. The data collected through DIC is obviously more prone to errors, and replete with bizarre and often unexplainable variations in the data. It is hypothesized that this is a result of the poor resolution in the speckle pattern of the data collected through DIC, but it may also be a result of various material effects that are manifest during testing. Using synthetic data, almost perfect fits are attainable. Of particular note is the similarity in shape for the fits for synthetic data, and the measured DIC data. In both cases, the crack opening displacement still exhibits large K dominance in the far field. The use of at least 2 or 3 higher order terms is required for an accurate fit of the data. This raises some questions as to the validity of the assumptions made and data presented by Poursartip

[13], who shows no need for higher order terms, or strange effects in the far field solutions.

Most notably, the use of synthetic data proves the validity of crack tip displacement analysis to some extent, and demonstrates that the analysis chosen is useful, so long as the data collected is reasonable.

6.3 Full Field Displacements Analyzed with Synthetic FEA Data.

The full field solutions for mixed mode bending in composite laminates were also affirmed using cohesive zone modeling data. The actual cohesion zone is still in development, so crack propagation parameters in the FEA model are not yet considered. The FEA data analyzed uses the same equations described in Chapter 3, only this time, they are applied to the entire specimen. Full field DIC adds a level of complexity to the analysis, which now becomes quite time consuming, however, the additional data has a tendency to smooth out, and negate local defects. The result is a more reliable and consistent extraction of fracture parameters. The additional data means defects, and faulty displacement values caused by the resolution of the speckle pattern are no longer an issue.

FEA analysis was conducted on the linear elastic fracture mechanics region leading up to crack propagation. Data was extracted and analyzed for 0%, 22%, 50%, and 100% mode mixture cases at 4 different applied displacements: 1.44 mm and 28.14 N, 2.88 mm and 56.28 N, 4.32 mm and 84.42 N, as well as 5.76 mm and 112.56 N. This is for the 0% and 22% mode Mixture Case. The 50% and 100%

mode mixture case had load displacements comparable to actual load displacements seen during testing.

6.4 Synthetic Data Results Extracted from FEA Modeling:

0% Mode Mixture:

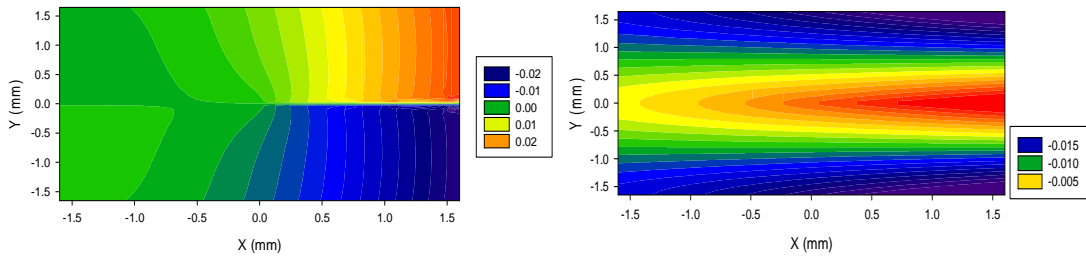


Figure 35a: V and U fields from FEA Modeling at 21.84 N Load, 0% Mixture

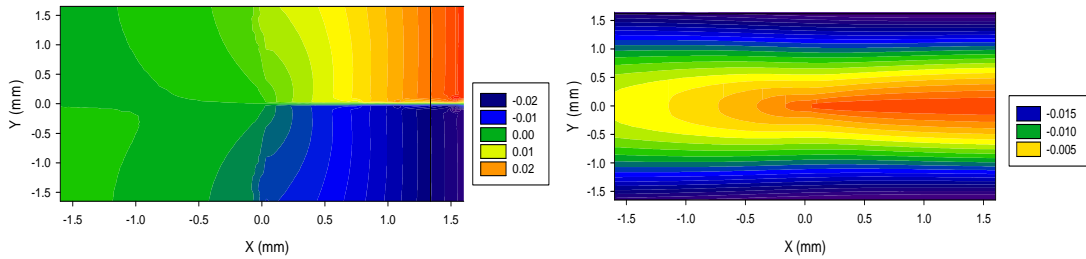


Figure 35b: Analytical Solution for V and U Field at 21.84 N Load, 0% Mixture

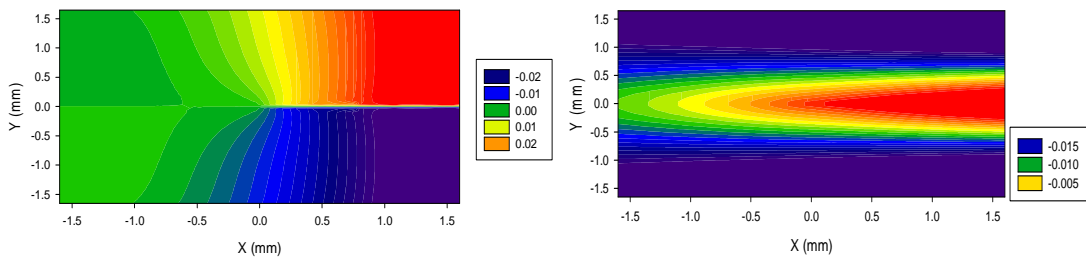


Figure 36a: V and U fields from FEA Modeling at 56.28 N Load, 0% Mixture

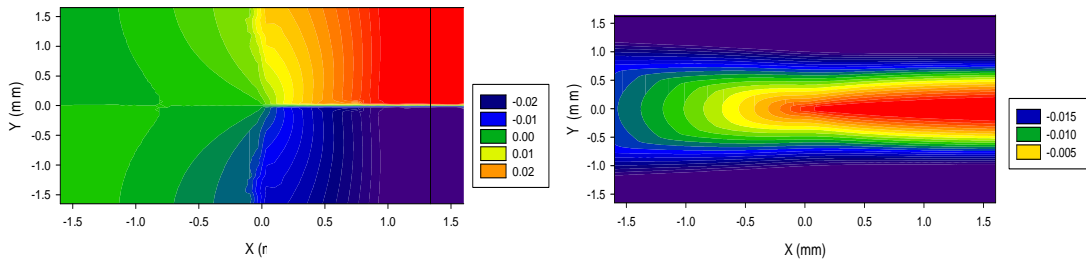


Figure 36b: Analytical Solution for V and U Field at 56.28 N Load, 0% Mixture

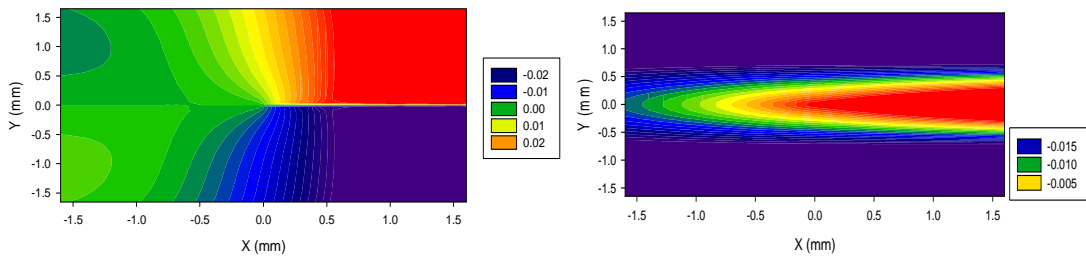


Figure 37a: V and U fields from FEA Modeling at 84.42 N Load, 0% Mixture

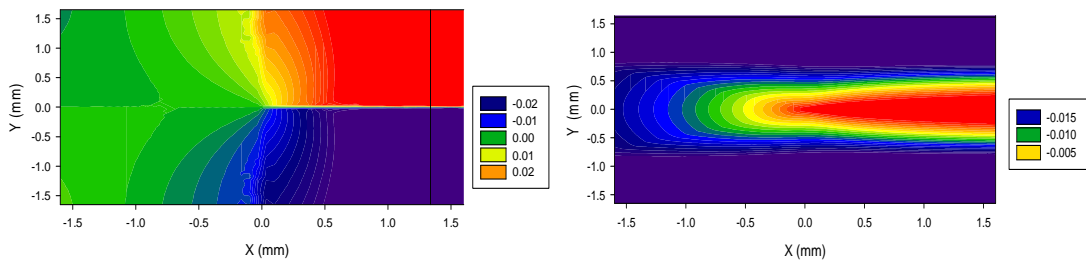


Figure 37b: Analytical Solution for V and U Field at 84.42 N Load, 0% Mixture

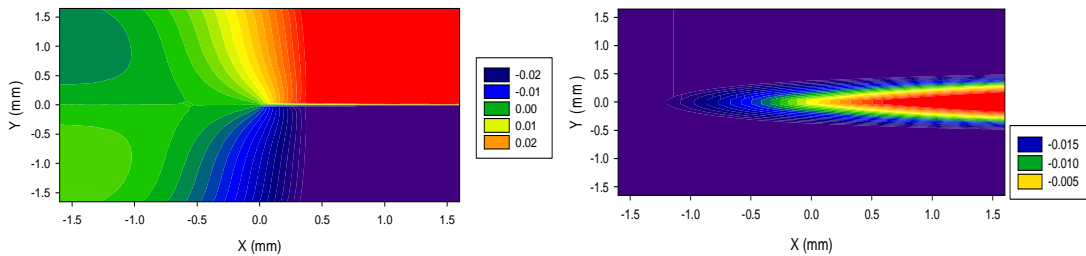


Figure 38a: V and U fields from FEA Modeling at 112.56 N Load, 0% Mixture

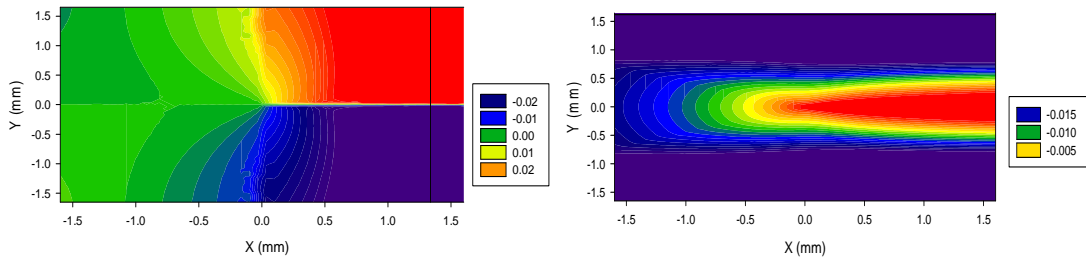


Figure 38b: Analytical Solution for V and U Field at 112.56 N Load, 0% Mixture

22% Mode Mixture:

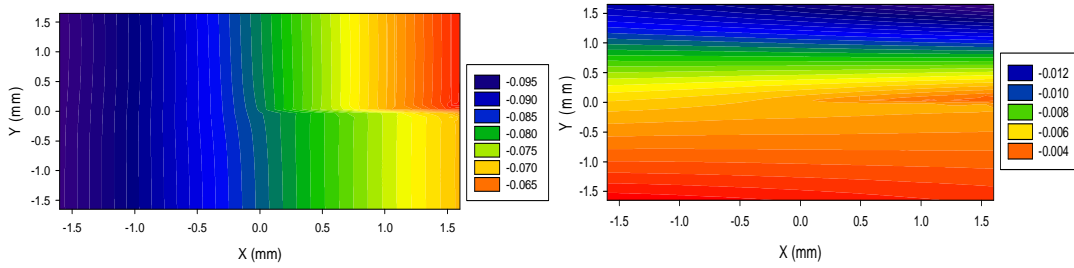


Figure 39a: V and U fields from FEA Modeling at 21.84 N Load, 22% Mixture

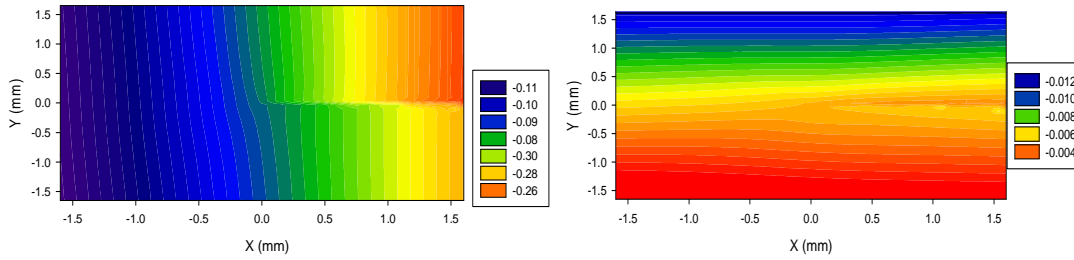


Figure 39b: Analytical Solution for V and U Field at 21.84 N Load, 22% Mixture

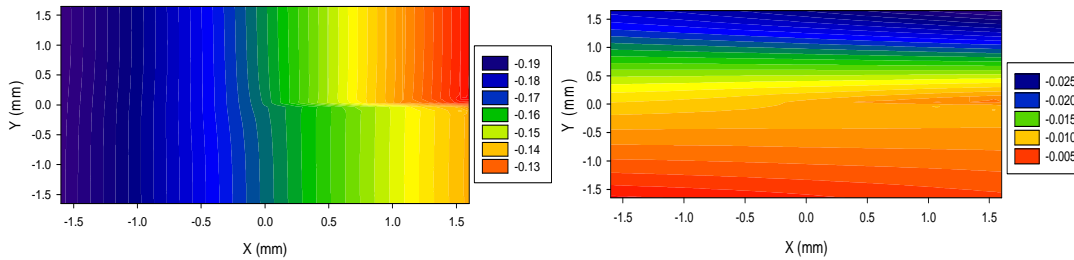


Figure 40a: V and U fields from FEA Modeling at 56.28 N Load, 22% Mixture

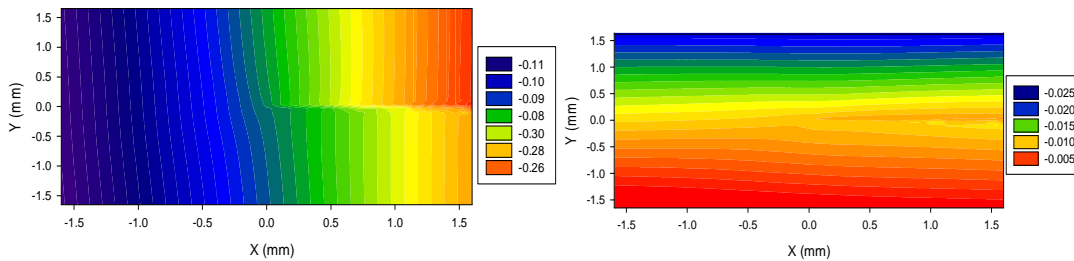


Figure 40b: Analytical Solution for V and U Field at 56.28 N Load, 22% Mixture

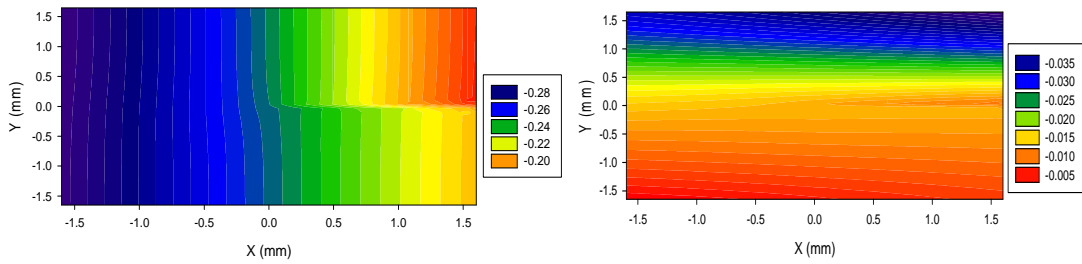


Figure 41a: V and U fields from FEA Modeling at 84.42 N Load, 22% Mixture

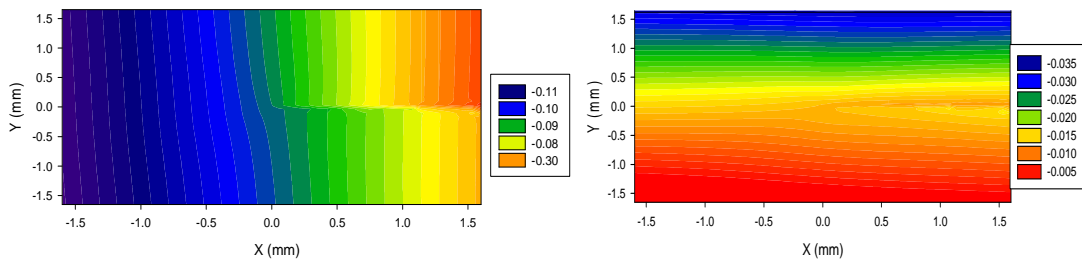


Figure 41b: Analytical Solution for V and U Field at 84.42 N Load, 22% Mixture

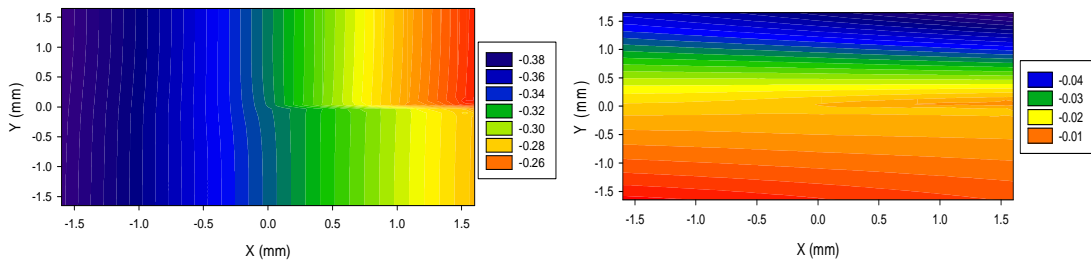


Figure 42a: V and U fields from FEA Modeling at 112.56 N Load, 22% Mixture

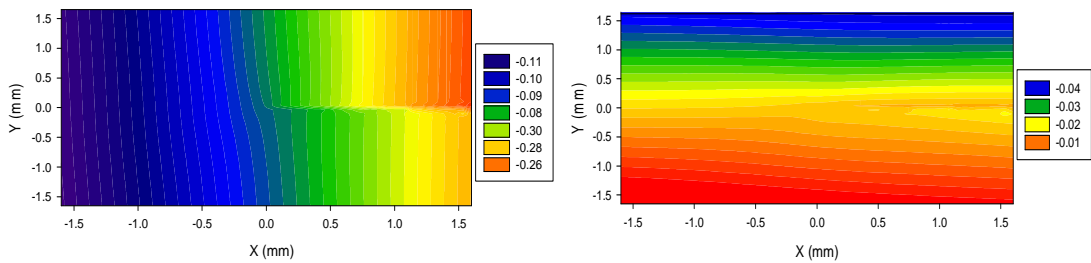


Figure 42b: Analytical Solution for V and U Field at 112.56 N Load, 22% Mixture

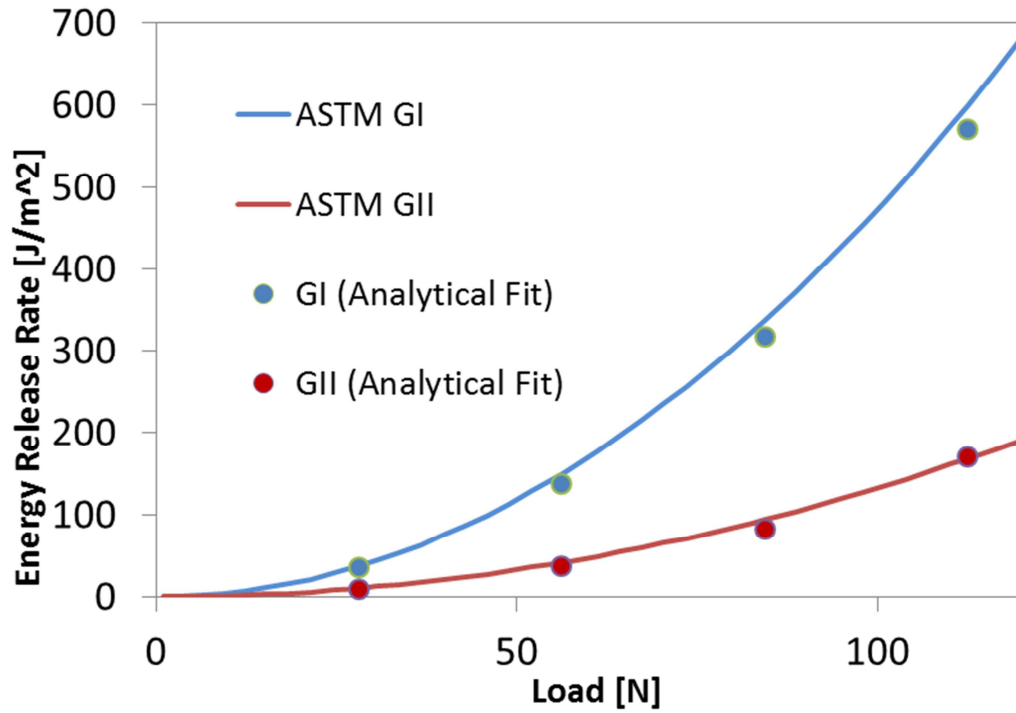


Figure:43 Shear Fracture Toughness extracted from Analytical Full Field Solution compared to ASTM for 22% FEA Test

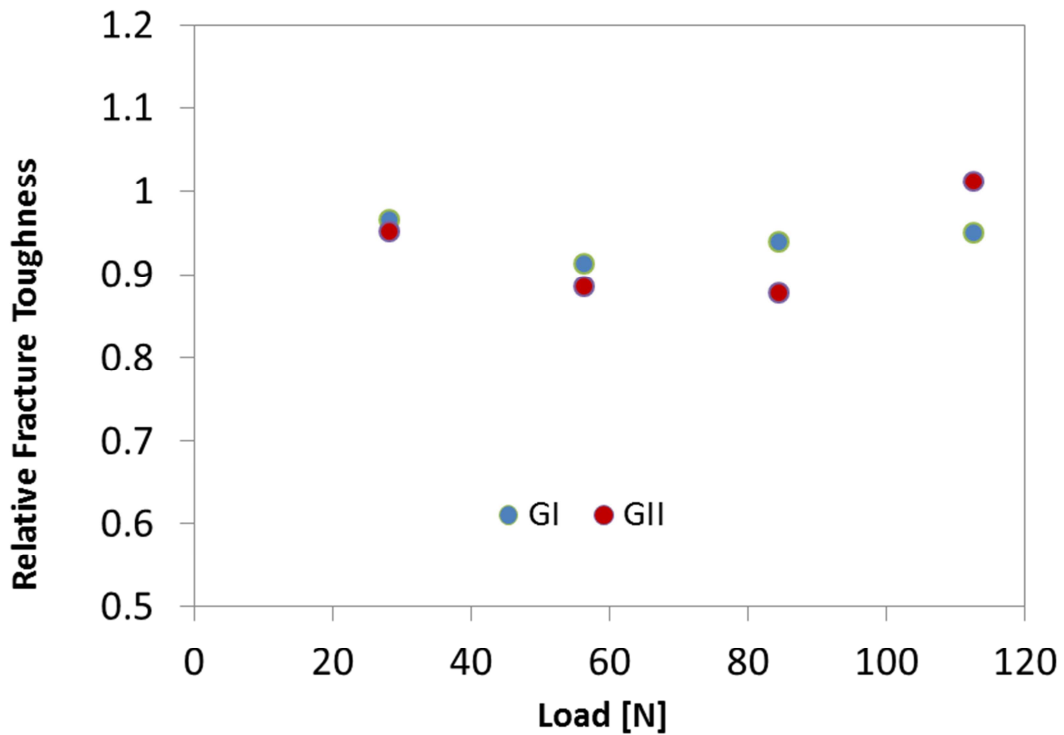


Figure 44: Shear Fracture Toughness extracted from Analytical Full Field Solution compared to AST

50% Mode Mixture:

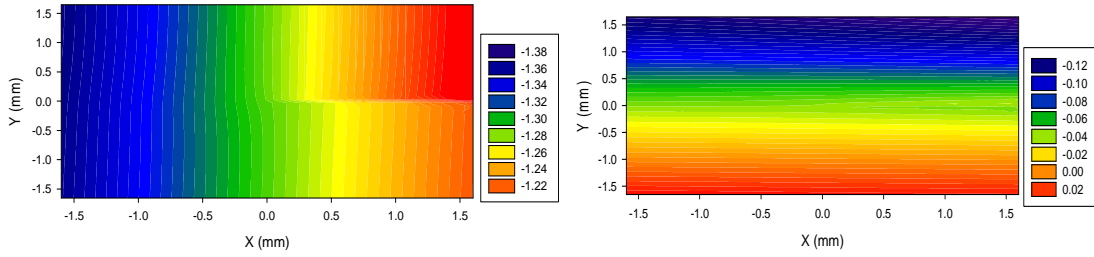


Figure 45a: V and U fields from FEA Modeling at 21.84 N Load, 50% Mixture

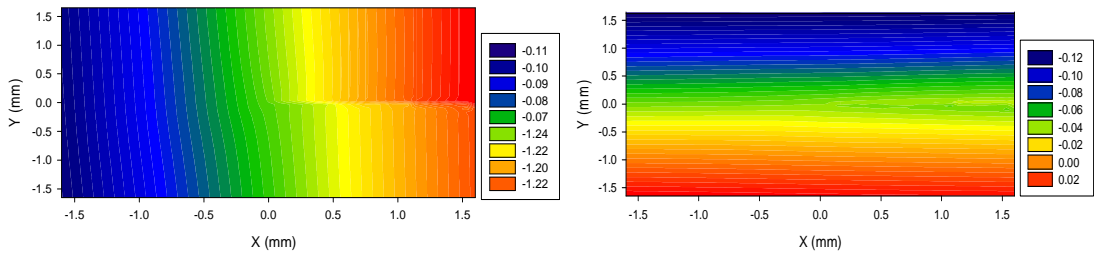


Figure 45b: Analytical Solution for V and U Field at 21.84 N Load, 50% Mixture

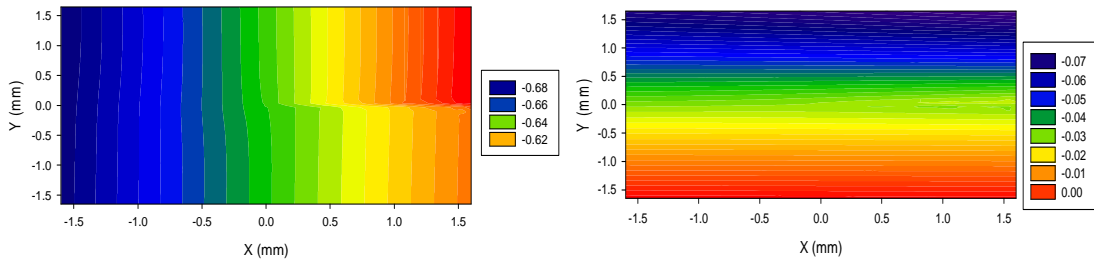


Figure 46a: V and U fields from FEA Modeling at 56.28 N Load, 50% Mixture

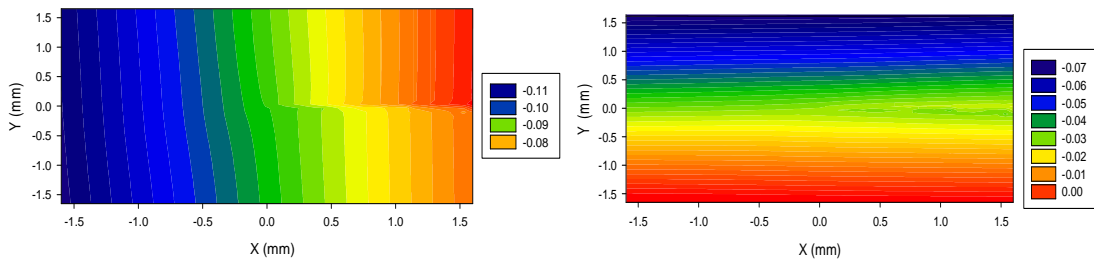


Figure 46b: Analytical Solution for V and U Field at 56.28 N Load, 50% Mixture

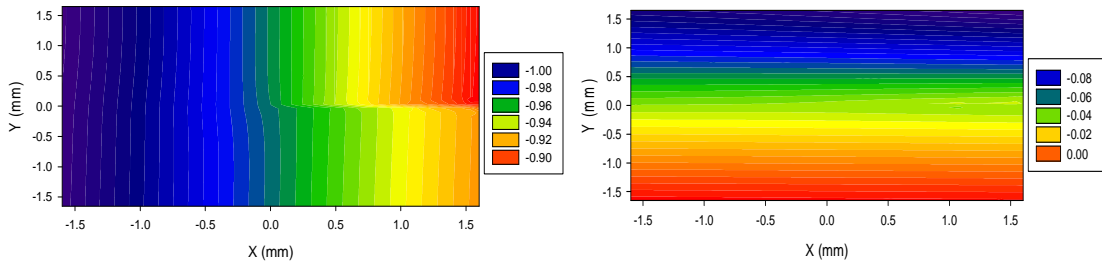


Figure 47a: V and U fields from FEA Modeling at 84.42 N Load, 50% Mixture

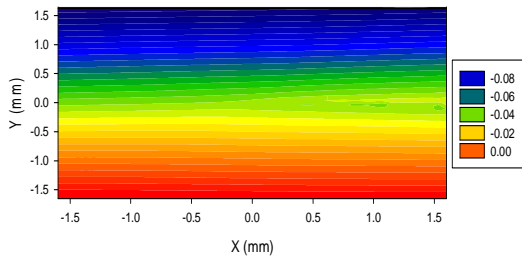
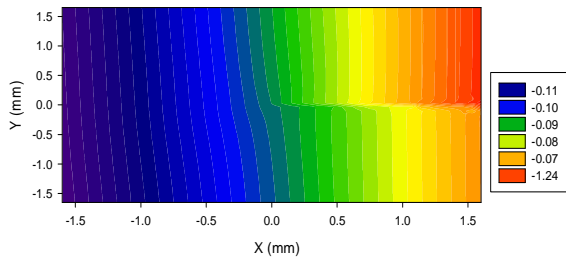


Figure 47b: Analytical Solution for V and U Field at 84.42 N Load, 50% Mixture

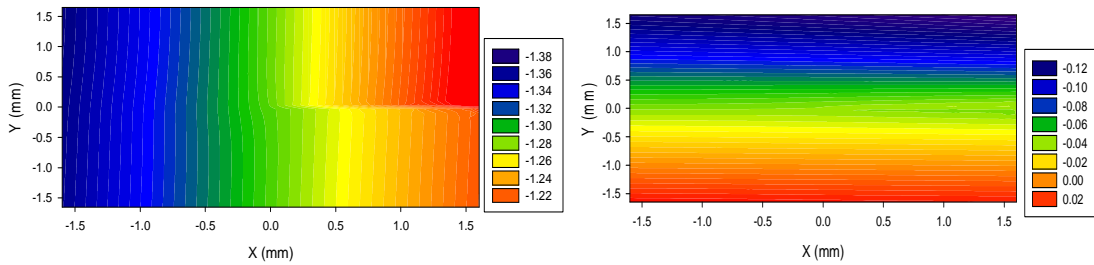


Figure 48a: V and U fields from FEA Modeling at 112.56 N Load, 50% Mixture

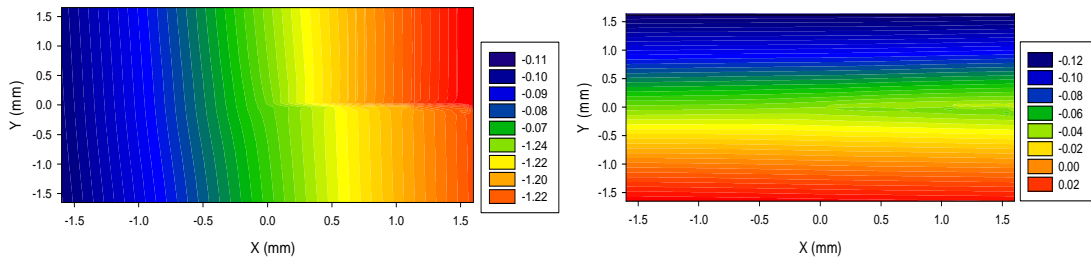


Figure 48b: Analytical Solution for V and U Field at 112.56 N Load, 50% Mixture

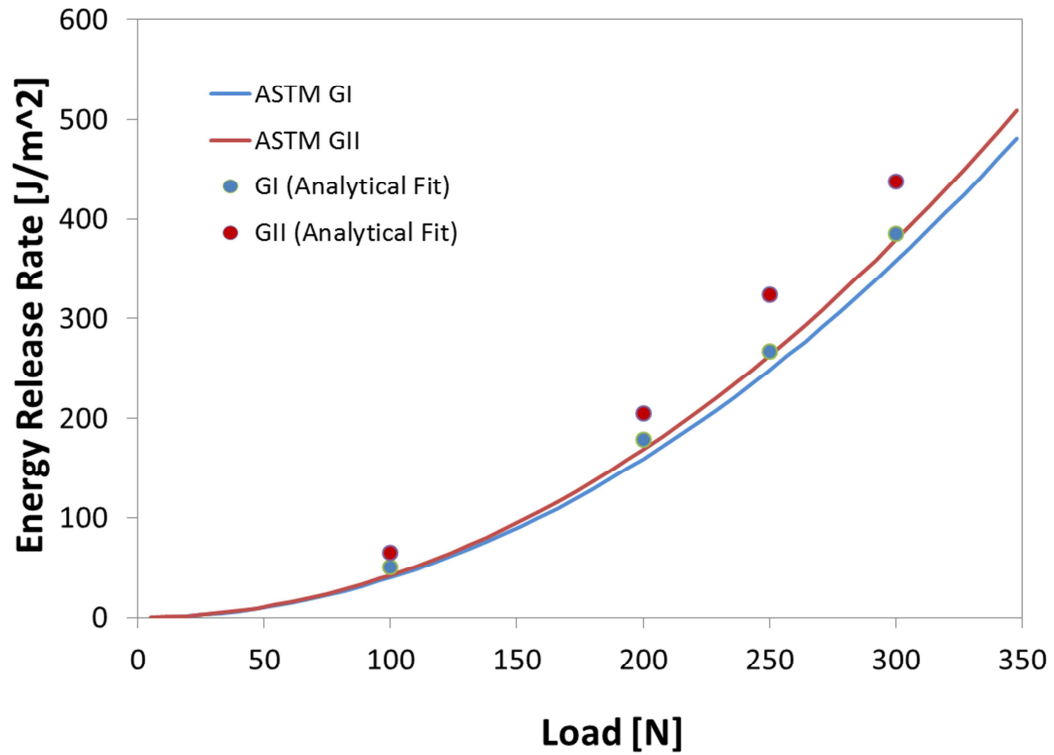


Figure:49 Shear Fracture Toughness extracted from Analytical Full Field Solution compared to ASTM for 50% FEA Test

100% Mode Mixture:

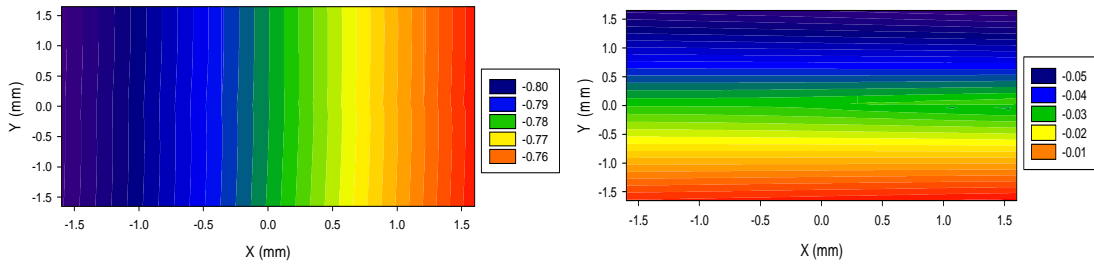


Figure 50a: V and U fields from FEA Modeling at 21.84 N Load, 100% Mixture

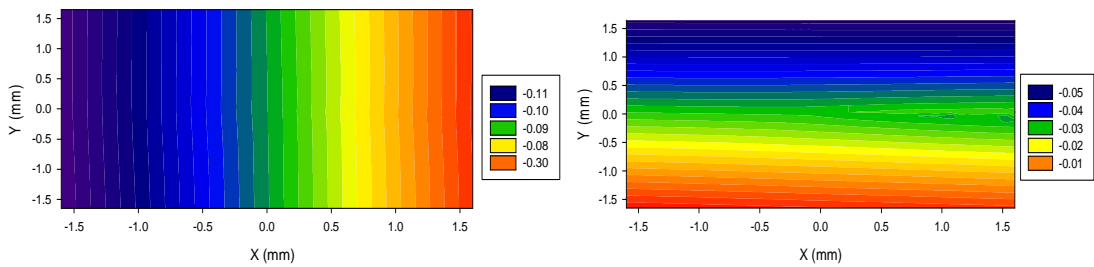


Figure 50b: Analytical Solution for V and U Field at 21.84 N Load, 100% Mixture

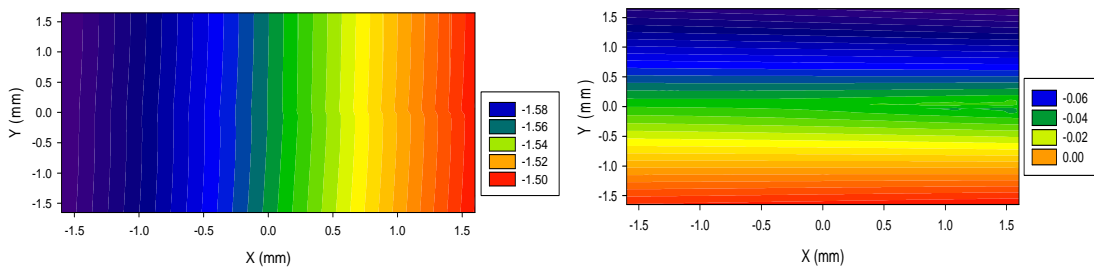


Figure 51a: V and U fields from FEA Modeling at 56.28 N Load, 100% Mixture

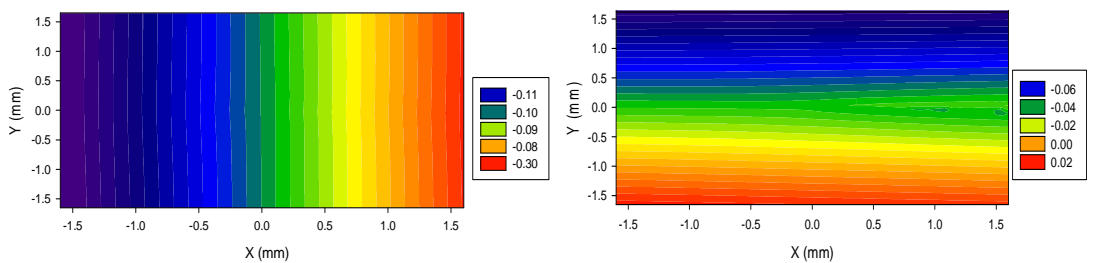


Figure 51b: Analytical Solution for V and U Field at 56.28 N Load, 100% Mixture

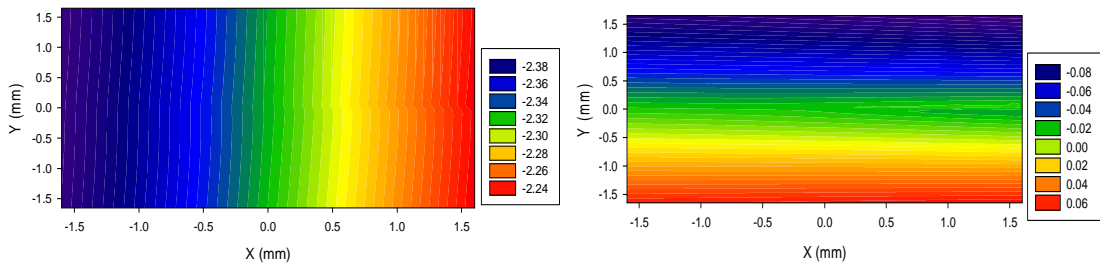


Figure 52a: V and U fields from FEA Modeling at 84.42 N Load, 100% Mixture

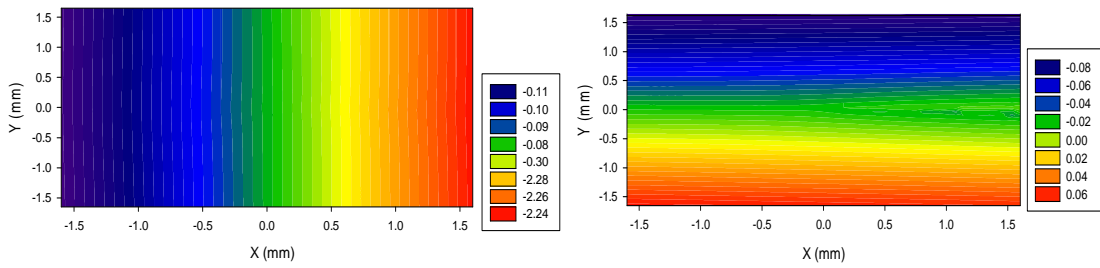


Figure 52b: Analytical Solution for V and U Field at 84.42 N Load, 100% Mixture

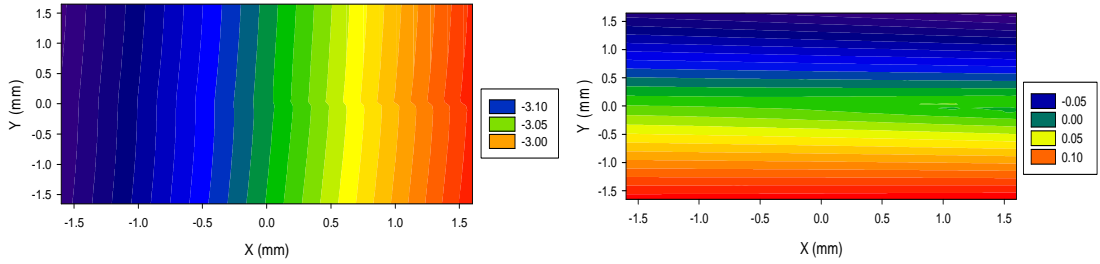


Figure 53a: V and U fields from FEA Modeling at 112.56 N Load, 100% Mixture

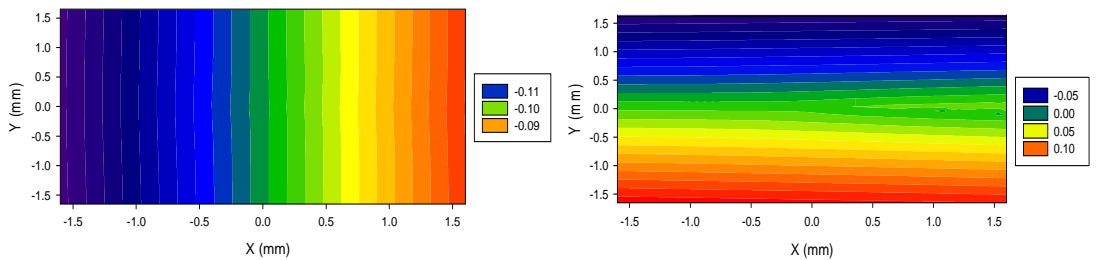


Figure 53b: Analytical Solution for V and U Field at 112.56 N Load, 100% Mixture

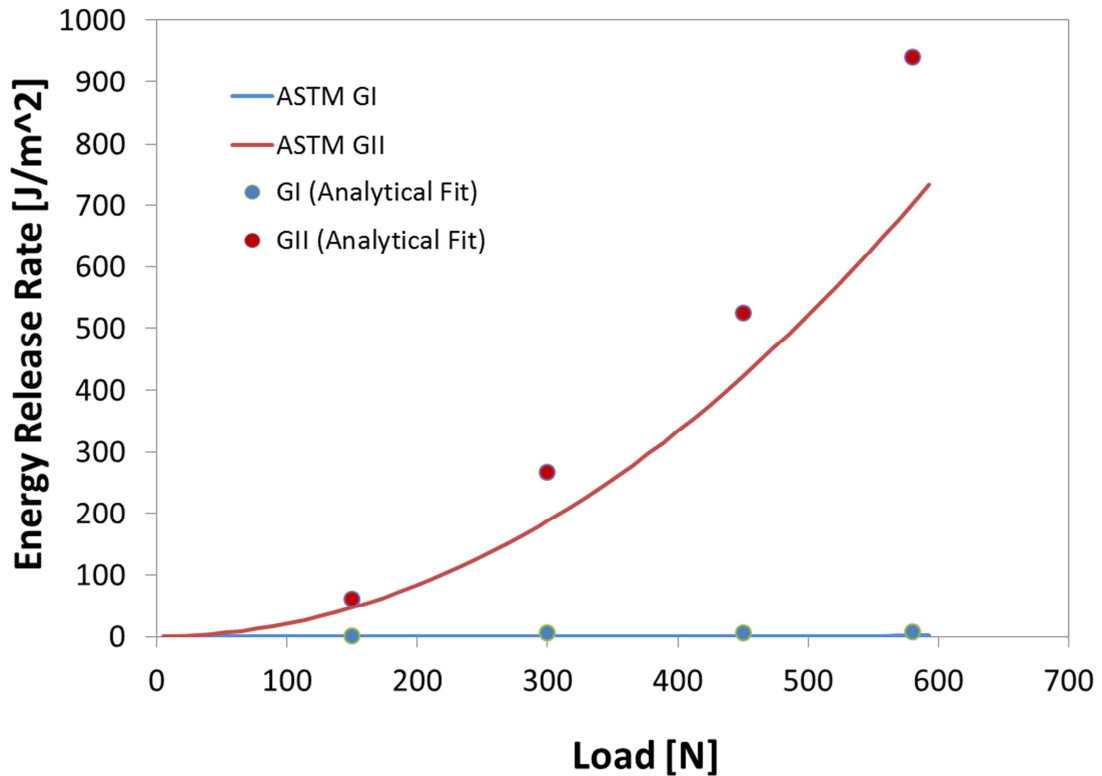


Figure 54: Shear Fracture Toughness extracted from Analytical Full Field Solution compared to ASTM for 100% FEA Test

6.5 Discussion of FEA Results

The finite element analysis model at first was not producing favorable or even usable results when analyzed. Some errors were discovered in the load displacement data being used as inputs into the FEA model, this issue is not resolved and likely accounts for the difference in results comparing the ASTM and FEA model. The model is still in its infant stage and must be calibrated before it can properly describe the cohesive zone between discrete laminate layers. That is why a collaborative effort between the experimentalists and the computational engineers must exist. The true

purpose of using FEA for this course of study was to affirm the possibility of using displacement field analysis to compute fracture parameters. Ideally once the cohesive zone model is completed, analysis may be conducted during crack propagation, which stands currently one of the greatest challenges to measurement, particularly in the case of the unstable high mode II fracture tests. *Table 2* depicts how accurately full field displacement analysis can calculate fracture parameters when provided accurate data. When fitting the fracture parameters to synthetic data from FEA, the optimization is very simple. Usually only one global minimum exists, and there are few local minimum to distort the data analysis. Additionally, there are much fewer terms to account for when fitting synthetic data, crack tip position is known, and is set at 0 mm for both the x and y direction. Rotation is already corrected for in the FEA program, and bending effects are negligible. The result is that only the parameters for G_I , G_{II} and the stress intensity factors K_I and K_{II} must be optimized. Thusly, these fracture parameters are obtained with ease, and with little effort. Interestingly enough, the values are still not perfect, and often times the calculated value for G_I and G_{II} is larger than the ASTM standard. It should be noted that the ASTM standard is by no means perfect, and should not be accepted as the actual (perfect) values for fracture parameters, the ASTM standard is extremely sensitive to the calibration parameters, highly sensitive to the crack length, and very sensitive to the geometric relations of the material. Though extreme care is taken to ensure that these measurements are as accurate and properly measured as possible, there is still some room for error, particularly in crack tip location measurements. The crack tip is measured based off of the visual interpretation of where the opening is in relation to

the loading pins. The crack tip actually extends beyond the visually detectable edge of the crack by some distance on the order of one mm. This is enough to effect the ASTM fracture parameters by as much as 5%. The ASTM standard also does not take into account defects in the material or fiber bridging and other unique carbon fiber damage mechanisms. The full field fits are not perfect, but with the presence of good data with little noise, and with no resolution issues, a reasonable value for fracture parameters may be obtained.

22% Mode Mixture						
Load Level	G_I [J/m ²]	G_{II} [J/m ²]	ASTM G_I [J/m ²]	ASTM G_{II} [J/m ²]	Difference G_I [%]	Difference G_{II} [%]
28.37 N	24.21	7.20	25.97	7.19	-6.78	0.14
55.73 N	94.38	28.30	100.3	27.76	-5.90	1.95
86.14 N	220.43	79.14	239.5	66.31	-7.96	19.35
113.5 N	379.50	97.22	415.8	115.1	-8.73	-15.53
50% Mode Mixture						
Load Level	G_I [J/m ²]	G_{II} [J/m ²]	ASTM G_I [J/m ²]	ASTM G_{II} [J/m ²]	Difference G_I [%]	Difference G_{II} [%]
100 N	50.23	64.74	39.75	42.074	26.36	53.87
200 N	178.64	205.03	159.00	168.31	12.35	21.82
250 N	267.36	324.91	248.41	262.93	7.63	23.57
300 N	385.12	438.20	357.70	378.61	7.67	15.74
100% Mode Mixture						
Load Level	G_I [J/m ²]	G_{II} [J/m ²]	ASTM G_I [J/m ²]	ASTM G_{II} [J/m ²]	Difference G_I [%]	Difference G_{II} [%]
150 N	1.004	61.50	0.067	46.94	-	31.02
300 N	6.70	267.24	0.269	187.8	-	42.30
450 N	6.33	524.83	0.605	422.5	-	24.22
580 N	7.96	940.26	1.010	701.8	-	33.98

Table3: Fracture parameters for synthetic data from FEA model compared to ASTM standard.

The issue of the disagreement between the load displacement curves generated between FEA analysis and experimental analysis can only be explained by one thing. There is obviously a mischaracterization of the material properties used for this

analysis. Specifically the accepted value for Young’s modulus in the fiber direction must be too high. Reducing the accepted value for E_{1f} would result in larger opening displacements at smaller loads, and produce results even more consistent with the FEA model. This issue is still unresolved, and the previously accepted value for fiber modulus will still be used. The load displacement data for the 22% case as well as the 0% mode mixture case matched reasonably well to the load displacement data from the FEA model, and matched poorly for the 50% and 100% mode mixture cases. This may explain why the fracture parameters extracted from FEA analysis is much closer to the ASTM for the low mode mixture cases.

Case	FEA Load-Displacement Slope	Experimental Load-Displacement Slope	Slope % Difference
0%	159 N/mm	38.86 N/m,	309.16 %
22%	19.54 N/mm	13.55 N/mm	44.20 %
50%	60.67 N/mm	36.93 N/mm	64.28 %
100%	130.28 N/mm	82.29 N/mm	58.31 %

Table 4: Difference in slope of load displacement curve for FEA model, and experimental data

The synthetic FEA data has nearly perfect fits for the CTD data, and the 22% case. The fit is also very good for the 50% mode mixture experiments and the 100% mode mixture results. The analysis for the 0% mode mixture was the least acceptable. This is likely a result of immaturity in the FEA model. The model is developed explicitly to model fracture using the Wyoming Test Fixture Mixed Mode Bending Test. 0% mode mixture testing requires an entirely different fixture and FEA model. Attempts were made to adjust the current model for pure mode I testing,

however these attempts were not good enough, as the 0% mode mixture data was not within acceptable levels of deviation.

The failure to extract exact fracture parameters is a result of difficulties in extracting reaction loads in the FEA model. With a prescribed displacement the load at the point of load application for the WTF is an output. This model struggles to accurately model the macroscopic response of composite laminates in this condition. *Table 3* shows the slopes of the linear region of the load displacement curves for both actual experiments and FEA models. The discrepancy here is an indication that the accepted value for fiber modulus is wrong, or the FEA model's macroscopic response is incorrect.

Overall the high correlation between the FEA data, and the ASTM analytical data indicates that DIC is a successful means of extracting fracture parameters. The use of DIC has been affirmed for both crack tip displacement analysis, and full field displacement analysis for ideal "perfect" data with a known crack tip location. The experience and process used to analyze FEA data was repeated for DIC data with much success.

Chapter 7: Full Field Fracture Analysis Using DIC

7.1 Full Field Displacement analysis of Mixed Mode Fracture Fixture

Significant errors were noted in the analysis of composite specimens when analyzing them using crack tip displacement analysis. Even though this theory was affirmed using synthetic data from a cohesive zone model of the mixed mode bending fracture specimen in Chapter 6, it is noted that data measurement and displacement extraction is the primary issue limiting proper fracture parameter extraction when analyzing data using crack tip displacement theory. Comparing *figures 53 and 54* clearly shows how noisy data extracted with DIC can be. These variations only increase the error in fracture parameter extraction, and particularly in the case for crack tip displacement analysis, the limited number of data points results in a greater sensitivity to resolution errors.

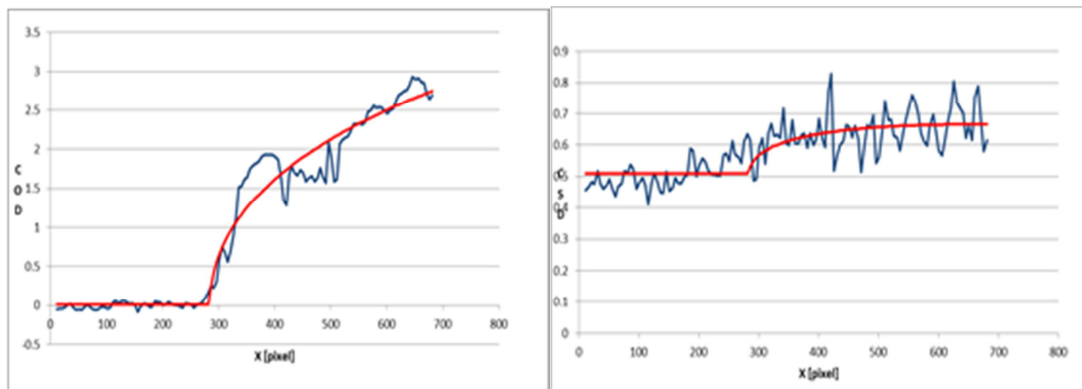


Figure 55: Crack Tip displacement fits at 76 N load for 22% Mode Mixture Test

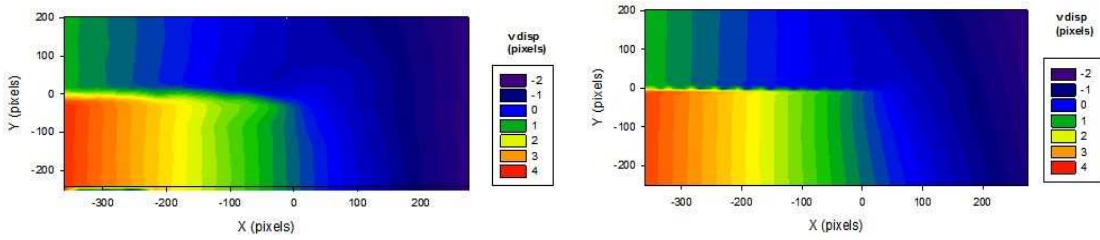


Figure 56a. DIC and Analytical solution for full field displacements transverse to crack at 76 N load for 22% Mode Mixture Test.

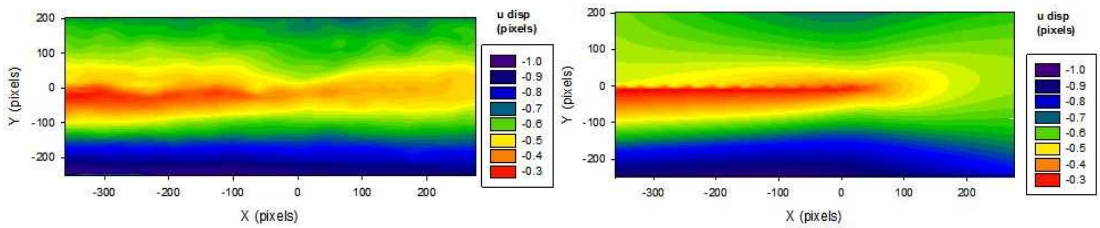


Figure 56b. DIC and Analytical solution for full field displacements in direction of crack at 76 N load for 22% Mode Mixture Test.

The idea behind using full field displacement analysis is that increasing the number of data points to be analyzed with the fitting program will reduce the fracture parameters sensitivity to defects in the collected data. Often times the contours from the extracted data, as may be seen in *figure 56a* and *figure 56b*, shows signs of poor data resolution with wavy lines, seemingly out of place bumps, edge defects, and lost or missing data at some points. The raw data may be prescreened to remove excess and fallacious data, however the contours are represented in excel with files with over 100,000 data points. Manual deletion of erroneous data points would be a futile exercise. The use of Full field data analysis was envisioned to negate many of the issues associated with crack tip displacement theory and generally improve the veracity of the fracture parameters reported from DIC data extraction.

When observed, the crack opening displacement depicted in *figure 53* and *figure 54a*, it is quite obvious that the DIC data measured is a bit noisy, though noticeably less so for the full field analysis. Once again, these faults in the raw data are a result of the resolution of the speckle pattern and are an unavoidable issue for all DIC tests. However, the use of full field analysis negates some of this effect and can extract more accurate fracture parameters despite the presence of noise in the data. Full field analysis is also better equipped to extract fracture parameters with the presence of certain phenomena like fiber bridging. The crack tip displacement data for the above test yields fracture parameters of: G_I of 200.6 J/m², G_{II} of 37.03 J/m², and a Mode Mixture of 15%. The Full field DIC solution depicted in *figure 54* returned fracture parameters of: G_I of 15.113 J/m², G_{II} of 3.848 J/m², with a mode mixture of 21%.

Even though the values for full field test are nowhere near the accepted ASTM fracture parameters of: $G_I = 317$ J/m², and $G_{II} = 87.4$ J/m² for this particular test configuration. This is a result in flawed data collection. Prior to the use of a translating microscope stage, the microscope was only adjusted by manually positioning the camera. This means that stable image detection and crack tip tracking was not a possibility. Because of the large crack tip location displacements involved with fracture testing in the mixed mode bending test fixture, the microscope was readjusted to put the crack tip in the center of the focus at a load of 70 N, and this image was then used as the reference image as opposed to the required 0 load condition needed for proper analysis. The resulting displacements reported for the test specimen in *figure 54* is only the displacements between 70 N load, and a 76 N

load. Though it is well known that this practice results in poor data, and unrealistic fracture parameters, the quality of the fit is very good and proves the viability of full field DIC analysis if conducted properly.

The complete expansion of the crack tip displacement field for full field analysis of an orthotropic material is developed by Liu et al. [23], Shukla et al. [24] and used by Mogadpali [16] for analyzing stress intensity factors. The detailed derivation of the full field equations may be found in reference [24]. The transversely isotropic elastic constants referred to in the following equations as a_{ij} are defined for unidirectional carbon fiber used in this course of study are listed in equations (15) and (16). When an orthotropic material aligned in the direction of the crack subject to opening mode loading, strain components can be assumed to be [16, 23, 24]:

$$\begin{aligned} \varepsilon_{xx} = & \frac{\alpha - \beta}{2\alpha} \{a_{12} - a_{11}(\alpha + \beta)^2\} ReZ_1 + \frac{\alpha + \beta}{2\alpha} \{a_{12} - a_{11}(\beta - \alpha)^2\} ReZ_2 \\ & + \frac{\beta}{2\alpha} \{a_{11}(\alpha + \beta)^2 - a_{12}\} ReY_1 + \frac{\beta}{2\alpha} \{a_{12} - a_{11}(\beta - \alpha)^2\} ReY_2 \quad (21) \end{aligned}$$

$$\begin{aligned} \varepsilon_{yy} = & \frac{\alpha - \beta}{2\alpha} \{a_{22} - a_{12}(\alpha + \beta)^2\} ReZ_1 + \frac{\alpha + \beta}{2\alpha} \{a_{22} - a_{12}(\beta - \alpha)^2\} ReZ_2 \\ & + \frac{\beta}{2\alpha} \{a_{12}(\alpha + \beta)^2 - a_{22}\} ReY_1 + \frac{\beta}{2\alpha} \{a_{22} - a_{12}(\beta - \alpha)^2\} ReY_2 \quad (22) \end{aligned}$$

$$\gamma_{xy} = \frac{a_{66}}{2\alpha} (\alpha^2 - \beta^2) \{ImZ_1 - ImZ_2\} - \frac{a_{66}\beta}{2\alpha} \{(\beta + \alpha)ImY_1 - (\beta - \alpha)ImY_2\} \quad (23)$$

For the above equations, α and β are not the same as in the ASTM analysis:

$$2\beta^2 = \frac{a_{66} + a_{12}}{2a_{11}} + \sqrt{\frac{a_{22}}{a_{11}}}; \quad 2\alpha^2 = \frac{a_{66} + a_{12}}{2a_{11}} - \sqrt{\frac{a_{22}}{a_{11}}}$$

For a finite plate with an edge crack, the complex functions Z_1 , Z_2 , Y_1 , and Y_2 are represented as follows: [16, 24]

$$Z_1(z_1) = \sum_{n=0}^N A_n Z_1^{n-1/2} \quad \text{and} \quad Z_2(z_2) = \sum_{n=0}^N A_n Z_2^{n-1/2} \quad (24)$$

$$Y_1(z_1) = \sum_{m=0}^M B_m Z_1^m \quad \text{and} \quad Y_2(z_2) = \sum_{m=0}^M B_m Z_2^m \quad (25)$$

Where:

$$z_1 = x + i(\beta + \alpha)y = r_1 e^{i\theta}; \quad z_2 = x + i(\beta - \alpha)y = r_2 e^{i\theta}; \quad i = \sqrt{-1}$$

In this complex analysis, the x and y coordinate system has its origin set to coincide with the crack tip with the x axis aligned in the direction of the crack. In equation (24) and (25), N and M are the number of terms required for an accurate fit.

[16] The strains are related to the u and v field displacements through the following relations: [16]

$$\varepsilon_{xx} = \frac{\partial u}{\partial x}; \quad \varepsilon_{yy} = \frac{\partial v}{\partial y}; \quad \gamma_{xy} = \frac{\partial u}{\partial y} + \frac{\partial v}{\partial x} \quad (26)$$

The integration of equation (21) with respect to x, and equation (22) with respect to y ultimately yields the full field displacement components for u and v. [16, 23, 24]

$$\begin{aligned}
u &= \frac{\alpha - \beta}{2\alpha} \{a_{12} - a_{11}(\alpha + \beta)^2\} \text{Re}\bar{Z}_1 + \frac{\alpha + \beta}{2\alpha} \{a_{12} - a_{11}(\beta - \alpha)^2\} \text{Re}\bar{Z}_2 \\
&+ \frac{\beta}{2\alpha} \{a_{11}(\alpha + \beta)^2 - a_{12}\} \text{Re}\bar{Y}_1 + \frac{\beta}{2\alpha} \{a_{12} - a_{11}(\beta - \alpha)^2\} \text{Re}\bar{Y}_2 \\
&+ g(y)
\end{aligned} \tag{27}$$

$$\begin{aligned}
v &= \frac{\alpha - \beta}{2\alpha} \{a_{22} - a_{12}(\alpha + \beta)^2\} \frac{\text{Im}\bar{Z}_1}{\beta + \alpha} + \frac{\alpha + \beta}{2\alpha} \{a_{22} - a_{12}(\beta - \alpha)^2\} \frac{\text{Im}\bar{Z}_2}{\beta - \alpha} \\
&+ \frac{\beta}{2\alpha} \{a_{12}(\alpha + \beta)^2 - a_{22}\} \frac{\text{Im}\bar{Y}_1}{\beta + \alpha} + \frac{\beta}{2\alpha} \{a_{22} - a_{12}(\beta - \alpha)^2\} \frac{\text{Im}\bar{Y}_2}{\beta - \alpha} \\
&+ f(x)
\end{aligned} \tag{28}$$

$$\bar{Z}_1(z_1) = \sum_{n=0}^N \frac{2}{2n+1} A_n Z_1^{n+1/2} \quad \text{and} \quad \bar{Z}_2(z_2) = \sum_{n=0}^N \frac{2}{2n+1} A_n Z_2^{n+1/2} \tag{29}$$

$$\bar{Y}_1(z_1) = \sum_{m=0}^M \frac{1}{m+1} B_m Z_1^{m+1} \quad \text{and} \quad \bar{Y}_2(z_2) = \sum_{m=0}^M \frac{1}{m+1} B_m Z_2^{m+1} \tag{30}$$

These afore listed equations (27) and (28) include unknown factors of integration $g(y)$ and $f(x)$ which are the rigid body translation in the x and y direction, as well as the rigid body rotation in the x-y plane. [16] These values are zero when analyzing the synthetic FEA data described in *Chapter 6*, but are unknown in the full field analysis described later in this chapter.

7.2 Refined Full Field Analysis

With several weeks of work, the fitting code was refined to account for rotations, displacements, and corrected to list pixel location based on its relative location to the crack tip. The same analysis was conducted for various mode mixtures at different loads. The displacement data is modified from the output to be corrected for rotations and translation, the x and y location of the crack tip is estimated, as well as the fracture parameters. Once a good estimate is obtained, the solve feature of Microsoft excel can be used to systematically adjust fracture parameters until the mean squares sum of the fit and recorded displacement is at a minimum, and the best fit for the data is obtained. *Figure 55* is the real time graphic used in Excel to gauge the proximity of the fit to an actual minimum value.

Equations (27) and (28) are slightly modified for use in the fitting program to become:

$$\begin{aligned}
 u = u_o + \sqrt{G_I}c_1\sqrt{r} & \left(k * \cos\left(\frac{\theta}{2}\right) - .5 * \cos(-1.5 * \theta) - .5 * \cos\left(\frac{\theta}{2}\right) \right) \\
 & + \sqrt{G_{II}}c_2\sqrt{r} \left(k * \sin\left(\frac{\theta}{2}\right) - .5 \sin(-1.5 * \theta) - .5 * \sin\left(\frac{\theta}{2}\right) \right) \\
 & + c_3 r * \cos(\theta)(k + 1) + c_4 r * \sin(\theta)(k + 1) \quad (31)
 \end{aligned}$$

$$\begin{aligned}
 v = v_o + \sqrt{G_I}c_1\sqrt{r} & \left(k * \sin\left(\frac{\theta}{2}\right) + .5 * \sin(-1.5 * \theta) + .5 * \sin\left(\frac{\theta}{2}\right) \right) \\
 & + \sqrt{G_{II}}c_2\sqrt{r} \left(-k * \cos\left(\frac{\theta}{2}\right) - .5 \cos(-1.5 * \theta) + 1.5 * \cos\left(\frac{\theta}{2}\right) \right) \\
 & + c_3 r * \sin(\theta)(k - 3) + c_4 r * \cos(\theta)(-k - 1) \quad (32)
 \end{aligned}$$

Where,

$$c_1 = 4(2)^{\frac{1}{4}} \frac{(a_{11}a_{22})^{1/4}}{(k+1)\sqrt{\pi}} \left(\frac{2a_{12} + a_{66}}{2a_{11}} + \sqrt{\frac{a_{22}}{a_{11}}} \right)^{\frac{1}{4}}$$

$$c_2 = 4(2)^{\frac{1}{4}} \sqrt{\frac{a_{11}}{\pi}} \left(\frac{2a_{12} + a_{66}}{2a_{11}} + \sqrt{\frac{a_{22}}{a_{11}}} \right)^{\frac{1}{4}}$$

and

$$r = \sqrt{x^2 + y^2}$$

The fitting program uses raw data input from the Digital Image Correlation test results, material properties found in equation (16), fracture parameters, and slightly modified versions of equations (27) and (28) to fit the raw displacement data to the equations (31) and (32).

All of this analysis is done in units of pixels, and only at the end of the analysis, when the fracture parameters are reported, are they adjusted for the actual magnification level. For these tests, the magnification level was set to 304 pixels/mm

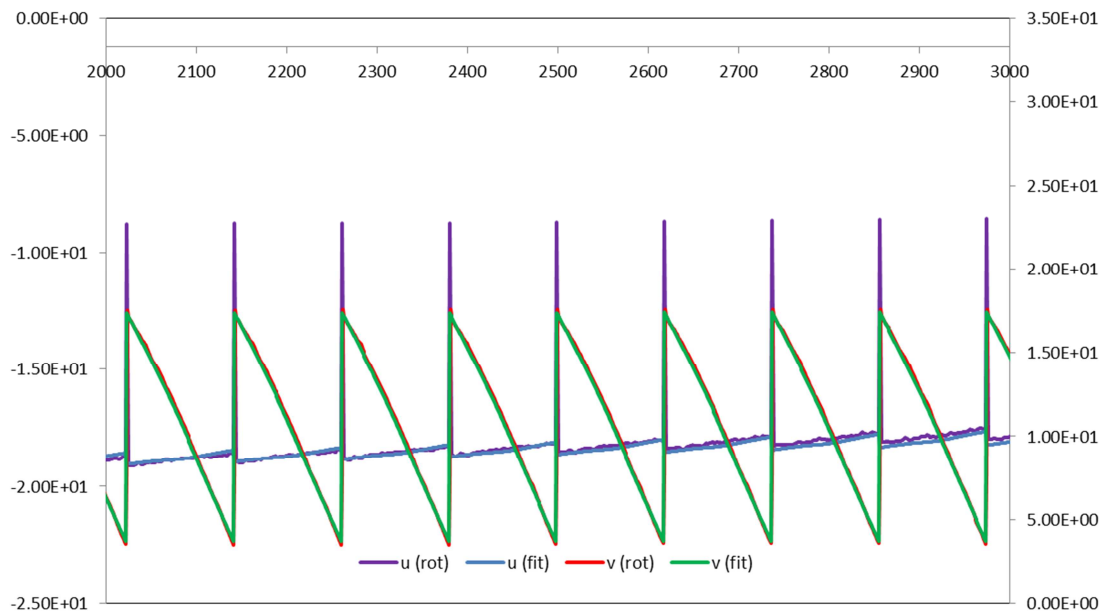


Figure 57: Full Field measured DIC displacement, and Fit functions for a “good” quality fit of 22% mode mixture fracture test.

The fitting function for full field analysis has several free parameters which must be solved for. The most obvious parameters which are used in the analysis are: G_I , the Mode I fracture toughness, G_{II} , the Mode II fracture toughness, K_I , the Mode I stress intensity factor, K_{II} , the Mode II stress intensity factor. There are also parameters built into the code for determining the crack top location in both the x direction and the y direction, as well as the u and v field displacements relative to the crack tip location. These values are all set to 0 for the synthetic data, however, for extracted DIC data the precise pixel location for the crack tip is not known, and must be calculated. There is a parameter for the data rotation, the crack rotation, the front strain, the bending, the higher order bending term, the pixel of the neutral axis, and the linear variation in u. The following outlines the process for fitting raw DIC data to the full field displacement functions, and extracting fracture parameters. The data used will be for a 50% mode mixture case with a load of 270 N.

The first step is to insert the X and Y coordinate system into the spreadsheet. These values are in pixels. The crack tip location is then subtracted from the corresponding X or Y location value. This yields the location relative to the crack tip, and is effective for normalizing the data to a reference point. This is then modified by multiplying the relative crack tip location by the cosine of the data rotation parameter. This rotates the coordinate system accordingly. The next step is to input the u and v displacement fields into the fitting function. A similar process is used

with the same parameters to transform and rotate the displacement field data. The u and v displacement field data is compared to the u and v displacement fit data with a least squares sum. The fitted displacement data is adjusted by varying the aforementioned fracture parameters until a global minimum is reached, and the difference between the measured and fitted displacements is as small as possible. Special functions are built into the code to limit the number of data points which affect the fit. By adjusting the number of pixels relative to the crack tip which are used in the least squares sum, far field effects may be negated, as such the fracture parameters do vary when this term is adjusted.

In order to obtain a quality fit, parameters should be initially set to 0. In putting raw displacement data, after adjusting the coordinate system to return values relative to the crack tip location resulted in the following contours:

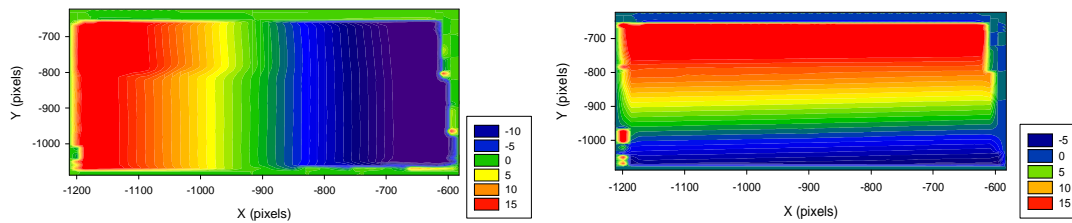


Figure 58: Full Field measured DIC displacements in v and u field for 50% test at 270 N load.

Notice the outer ring of bad data in *figure 58*. This is a good indication that the outer most data points should be excluded in this analysis. Also, note the approximate location of the crack tip as may be seen in the v field for *figure 58*. It is slightly higher than would be anticipated. The first run in the solver program returned a G_I value of $112 J/m^2$ and a G_{II} value of $12739 J/m^2$. This is obviously incorrect, and

attributed to the fact that the x, y location of the crack tip selected by the fitting function was (-614.9, -577.2). The contour for this erroneous test is not included as the results were non-sensible. This value is understandably incorrect, as the crack location should be positive. Because of this grossly incorrect data the fit contours are not shown. The numerous local minimum values demonstrate the importance of using seeding to bait the program into the correct answer. The actual crack tip location is approximately (350, 180), and the values for G_I and G_{II} should be around $150 J/m^2$. As such, seeding these approximate values into the computer may assist the function in finding a true global minimum and optimal fit for the data.

With seeded data, the fit became much more reasonable in *figure 60*:

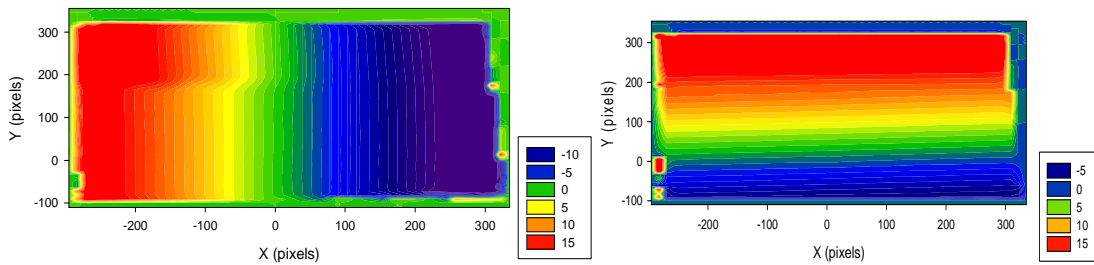


Figure 59: Full Field DIC displacements in v and u field for 50% test at 270 N load.

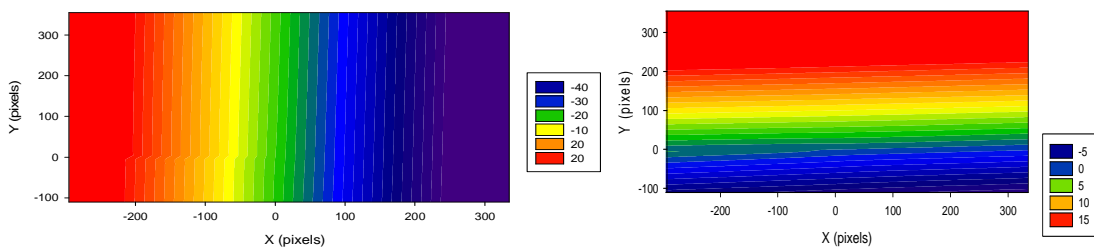


Figure 60: Fitted displacements in v and u field for 50% test after data seeding.

This fit is significantly better, but still not close enough. The fitting program returned a G_I value of $10.97 J/m^2$ and a G_{II} value of $68.98 J/m^2$. This is

obviously incorrect, and attributed to the fact that the x, y location of the crack tip selected by the fitting function was (339,363). This data is much more accurate than the original run, but still far from a close fit. The lack of rotation terms continues to cause a false value for crack tip location to be returned from the fit. It is necessary to include a term for bending with properly seeded results. By including crack tip rotation, and data rotation, the fit is improved:

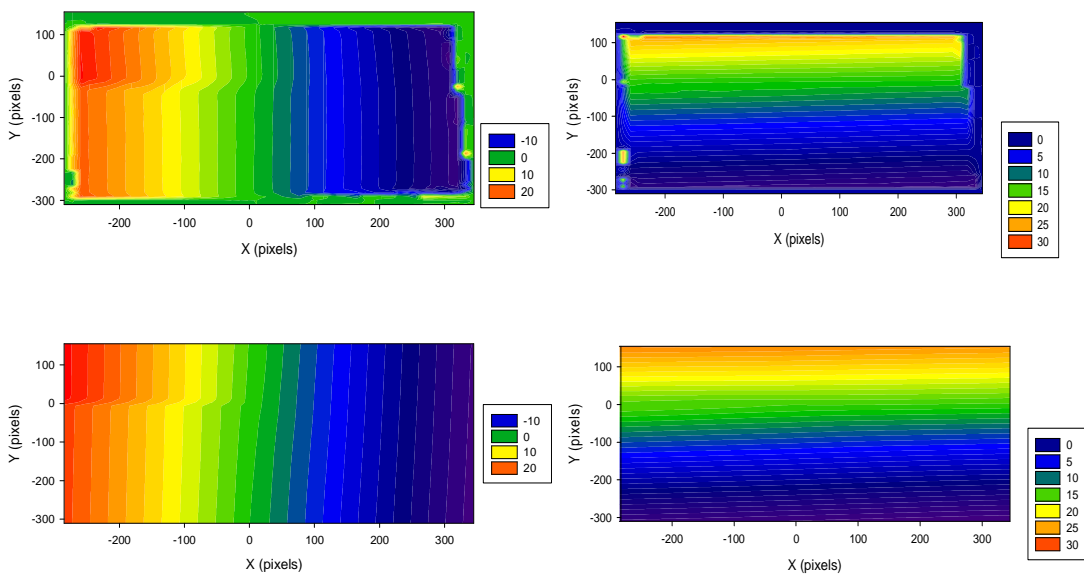


Figure 61: DIC and fitted displacements for v and u field for 50% test after data seeding and addition of crack rotation parameters.

Though this improved data analysis yields better results, and the fracture parameters are closer to the appropriate values, the mode mixture reported is now poor. The fitting program returned a G_I value of $216.59 J/m^2$ and a G_{II} value of $82.81 J/m^2$. Adding v field bending displacements into the fitting function may work to adjust these parameters. Additionally the area of investigation will be reduced so as to eliminate any far field displacement data from effecting the fit. After several iterations of the fitting function, it had honed in on the crack tip location of (350.166,

178.000) pixels. Once an accurate crack location is established, those parameters may be removed from the fitting function and are effectively locked in place. Further iterations may be run to establish other parameters along with the use of appropriate seeding to ensure accuracy. After several iterations, the fitting program returned a G_I , value of 145.046 J/m^2 and a G_{II} value of 128.5189 J/m^2 . This corresponds well to the accepted values for fracture parameters, however, the residual sum is still 18621. A more accurate analysis may be conducted by reducing the size of the investigation area from 150 pixels around the crack tip to 100 pixels around the crack tip. This removes any bias from the far field, solution, and decreases the need for higher order terms. A reduction in the investigation area yields even more accurate values of: $G_I = 132.14 \text{ J/m}^2$ and a $G_{II} = 142.21 \text{ J/m}^2$. Eventually, the analysis is refined enough to yield the optimal solution, and best values for strain energy release rate are determined with $G_I = 140.82 \text{ J/m}^2$ and a $G_{II} = 144.57 \text{ J/m}^2$. And the following displacement fields:

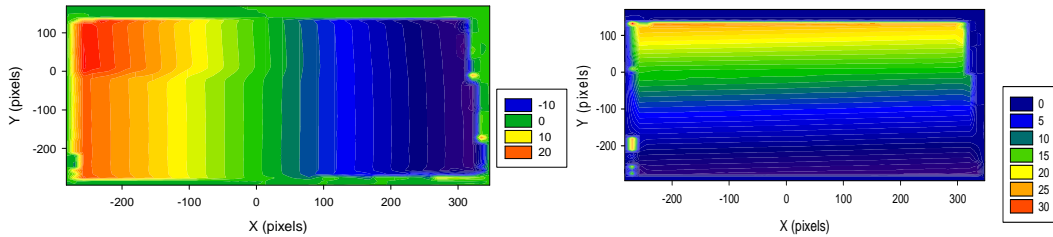


Figure 62a: DIC displacements in v and u field for 50% test.

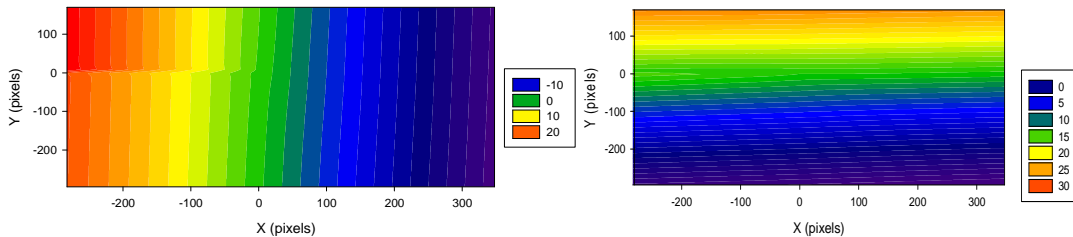


Figure 62b: Final optimal fit for displacements in v and u field for 50% test.

7.3 Full Field Analysis for 0% Mode Mixture DIC Data

The pure Mode 1 fracture test is unique from all other tests in many respects. The 0% Mode Mixture tests are all conducted with an entirely different test apparatus, the double cantilever beam test (DCB). The advantage of this testing procedure is that there is no strain component of the fracture testing, as such crack propagation is extremely slow and stable. *Figure 63* shows the load displacement data for a standard DCB test. Only once all shear dominant fracture is removed from the specimen does it behave with better stability, and crack growth becomes slow and controlled.

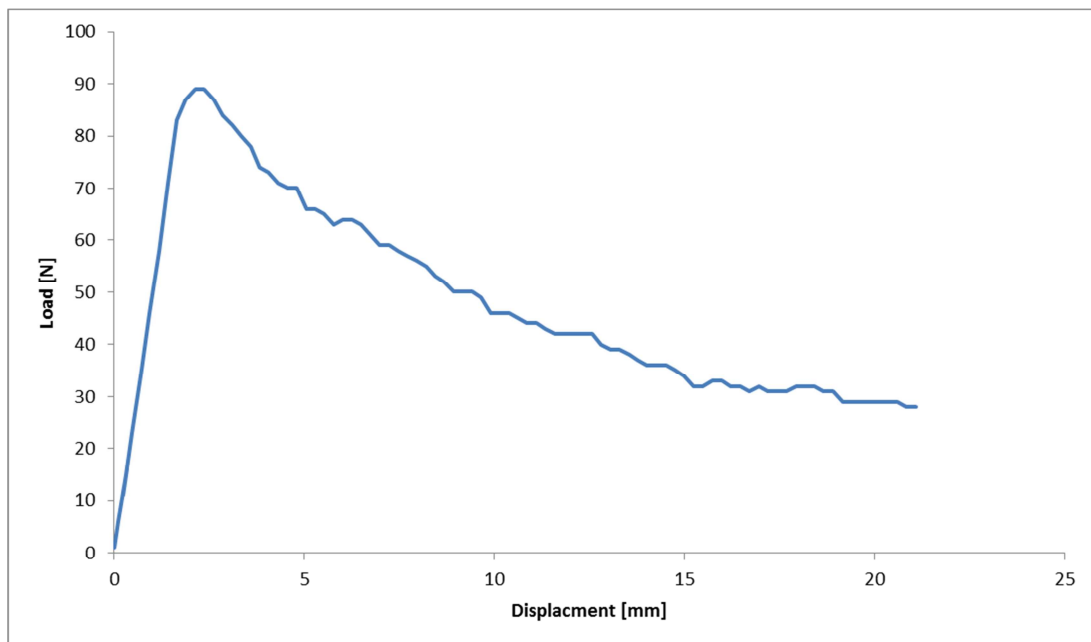


Figure 63: Load displacement curve for 0% Mode Mixture fracture test (DCB)

Figure 64 also demonstrates the slow controlled crack propagation characteristic of high mode I testing. This data for crack length was recorded by marking 1 mm increments on the test specimen and filming the far field opening

displacement. The test images were then correlated to the load displacement curve, and change in crack length with respect to displacement was noted. This is an essential step for calculating the strain energy release rate using analytical solutions.

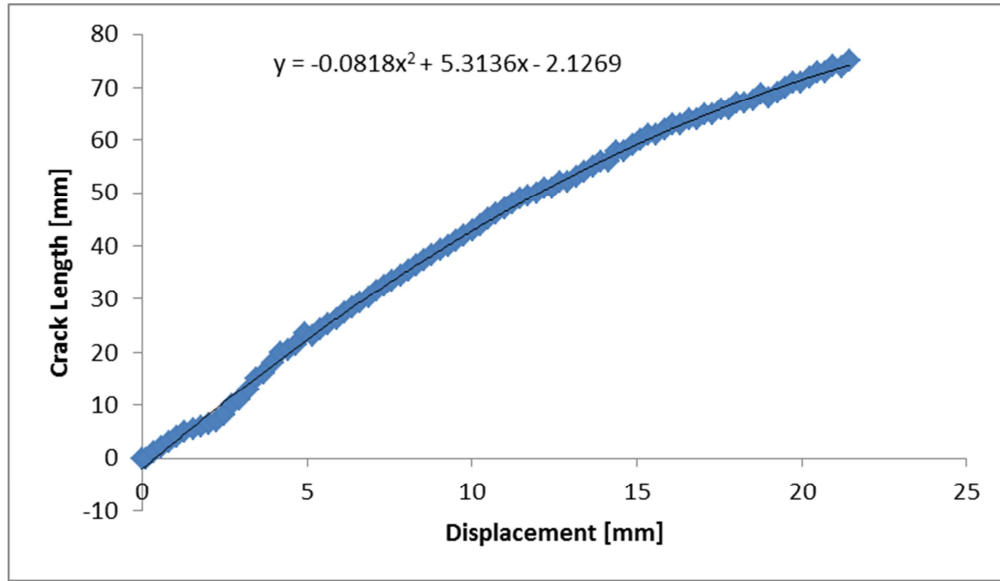


Figure 64: Crack length with respect to displacement during DCB test

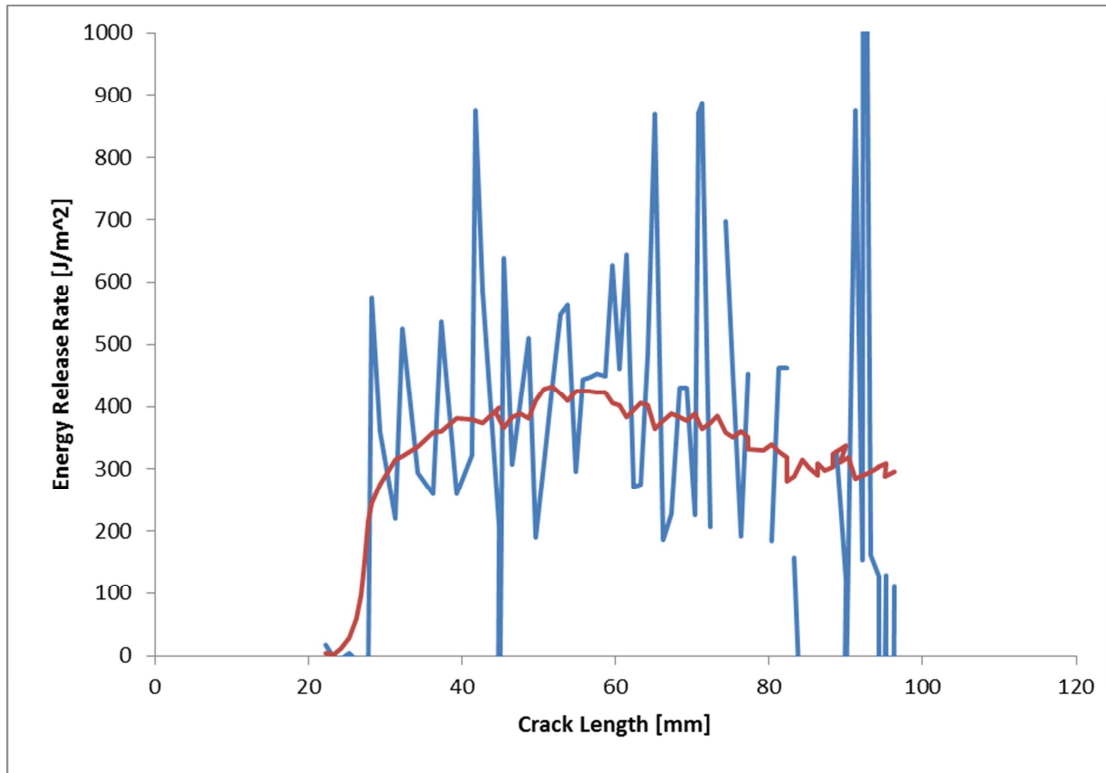


Figure 65: Strain energy release rate G_I with respect to crack length for 0% DCB test.

The fracture parameters displayed in *figure 65* were all calculated using *equations 7, 8, and 9* detailed in Chapter 3. The blue curve fluctuates rapidly, and the energy release rate can be taken as the average value. The red curve represents *equation 9*, and a much more consistent value for energy release rate. The critical value for crack propagation is approximately 405 J/m^2 . This value is consistent through the entire test.

DIC with the 0% mode mixture tests was a bit more complicated than expected. The fitting function had a propensity to diverge with fracture parameters growing to out of control values. This was mitigated by carefully seeding the appropriate solution in the fitting function. Though the values presented here are far from ideal, they were some of the closest values attainable for the at 0% mode mixture test configuration.

Load Level	G_I [J/m^2]	G_{II} [J/m^2]	ASTM G_I [J/m^2]	ASTM G_{II} [J/m^2]
40 N	97.04	2.65	209.81	0
48N	588.13	0	421.35	0
50 N	1480.26	4.4	428.04	0

Table 5: Fracture parameters for DIC data compared to ASTM standard, 0% Mode Mixture before crack growth.

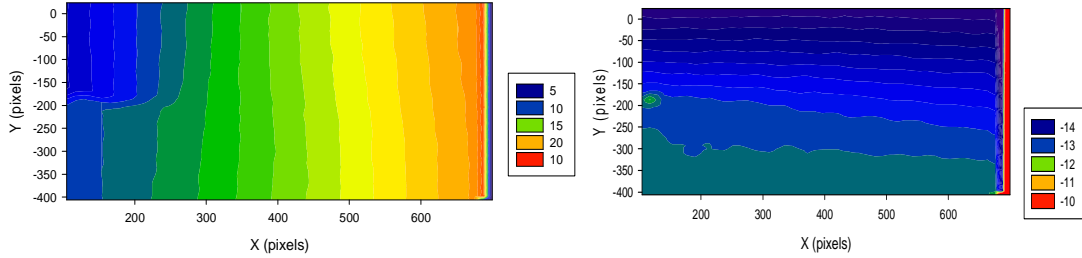


Figure 66a: V and U fields from DIC at 40 N Load, 0% Mixture

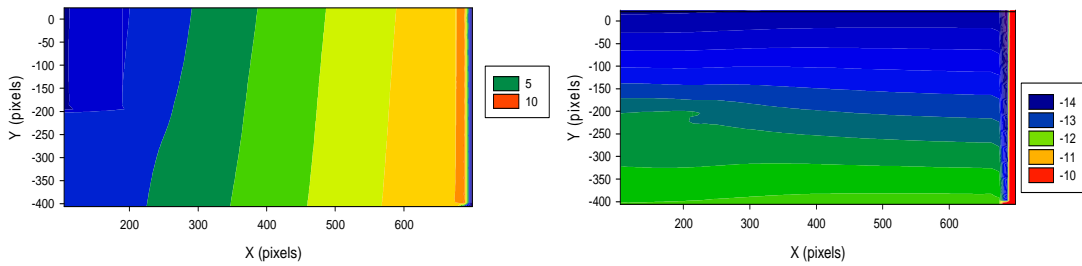


Figure 66b: Analytical Solution for V and U Field at 40 N Load, 0% Mixture

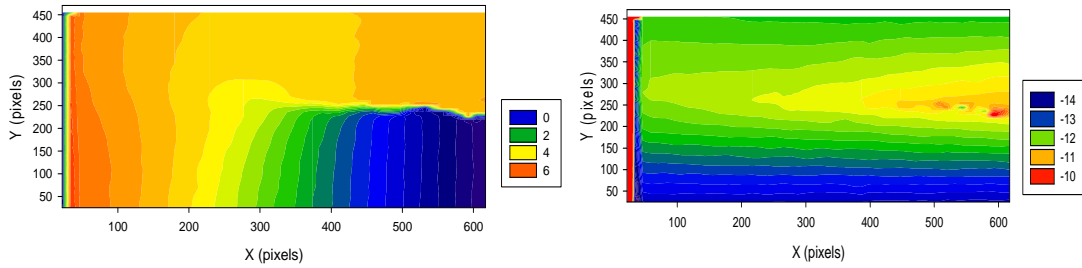


Figure 67a: V and U fields from DIC at 50 N Load, 0% Mixture

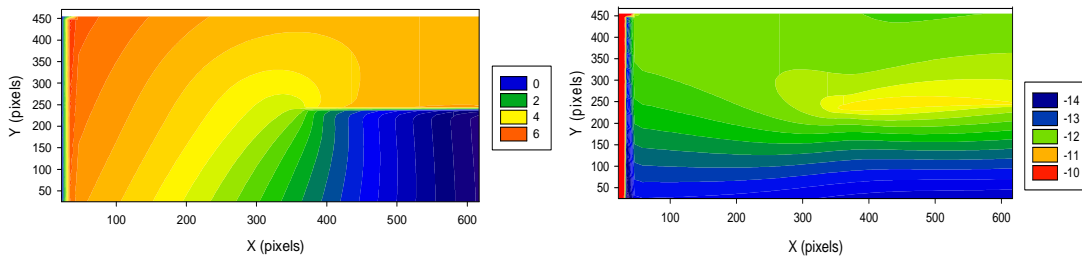


Figure 67b: Analytical Solution for V and U Field at 50 N Load, 0% Mixture

The fits shown in *figure 66* and *figure 67* are not good because there was bad data again. This is the single greatest challenge to effective use of DIC. One solution to this could potentially be conducting full-field DIC on a small area around the crack tip. This is because for large deformations, some of the regions in the underformed (reference) image go out of the field of view in the deformed image used for DIC analysis. Another method for improving data would be to exclude the data near the crack tip. This data is inherently bad because of the discontinuity in the deformations. This “bad” data appears in the contours above in *figure 66* as the purple or red outline.

These fits still indicate a high G_I value $1480.26 J/m^2$, not convincing that this analysis is applicable to the DCB test as well as the mixed mode tests. Regardless of the data’s fit, there are still a lot of higher order term effects present for the 0% mode mixture data. Additionally, the crack tip is pretty close to the left side of the image. Ideally, having the crack tip located close to the center of the analysis enables more accurate extraction of fracture parameters, as there is more data in the immediate area of interest. The analysis in *figure 67* is conducted with mostly data in the already cracked region where singularities, discontinuities, and higher order terms dominate the analysis. That is why the analysis conducted in *figure 66* demonstrates a much more accurate and believable value for G_I of $97.04 J/m^2$. In mode I dominate tests, the crack growth is propagated at extremely low loads, and the stability inherent in mode I crack growth means it is very hard to detect. This analysis occurs after the crack has grown, further biasing the analysis, and explaining why the crack tip is at the very edge of the analyzed image.

7.4 Full field Analysis for 22% Mode Mixture DIC Data

Test 23 was conducted with a unidirectional carbon fiber composite laminate. The lever arm length was adjusted to provide 22% mode mixture. The images taken at various load and displacement levels were then compared to the ASTM fracture parameters. Only several load levels were observed, as crack growth was premature for what is typically observed in 22% mode mixture tests. The test was then continued after initial crack growth occurred, and more strain energy release rates were extracted from the afore described fitting scheme to establish values for strain energy release rate both before initial crack growth, and after crack propagation occurred. The bulk of the analysis in this course of study was conducted for specimens with this loading configuration at 22% mode mixture.

Load Level	G_I [J/m ²]	G_{II} [J/m ²]	ASTM G_I [J/m ²]	ASTM G_{II} [J/m ²]
60 N	126.85	31.7124	122.4	33.78
70 N	198.20	56.376	166.6	45.98
79 N	285.41	77.83	212.1	58.56

Table 6: Fracture parameters for DIC data compared to ASTM standard, 22% Mode Mixture before crack growth.

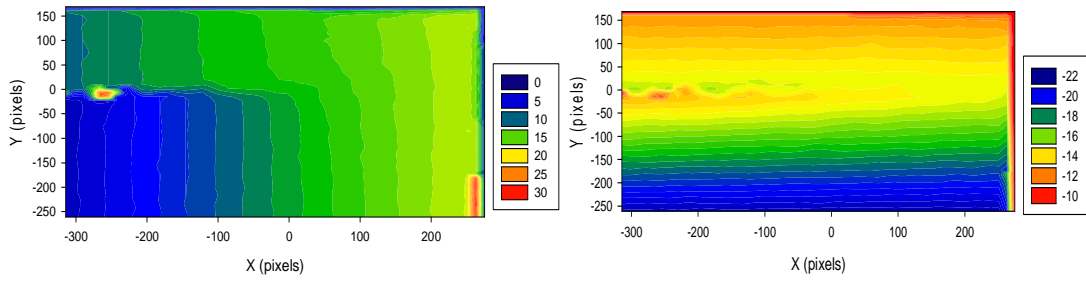


Figure 68a: V and U fields from DIC at 60 N Load, 22% Mixture

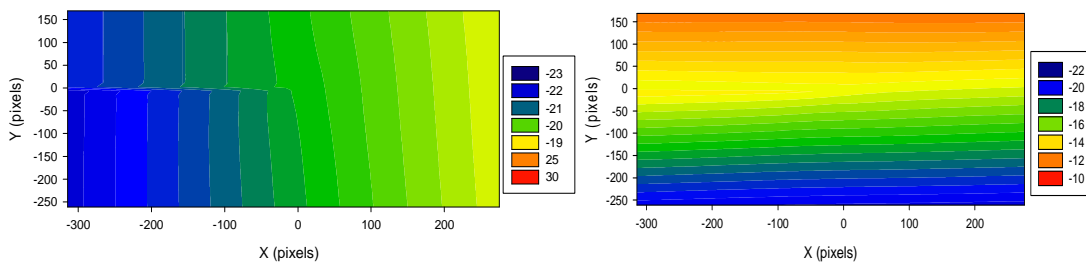


Figure 68b: Analytical Solution for V and U Field at 60 N Load, 22% Mixture

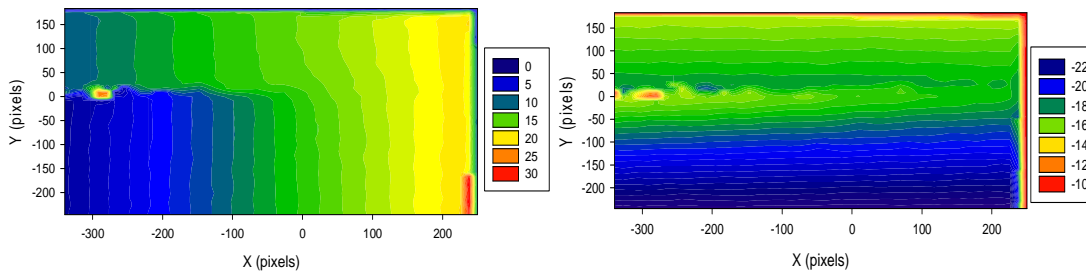


Figure 69a: V and U fields from DIC at 70 N Load, 22% Mixture

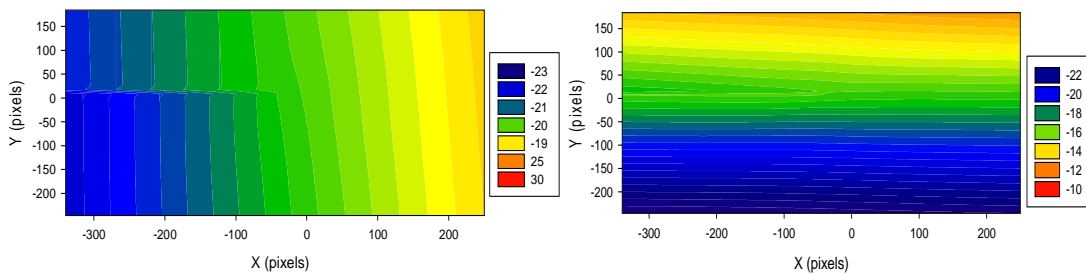


Figure 69b: Analytical Solution for V and U Field at 70 N Load, 22% Mixture

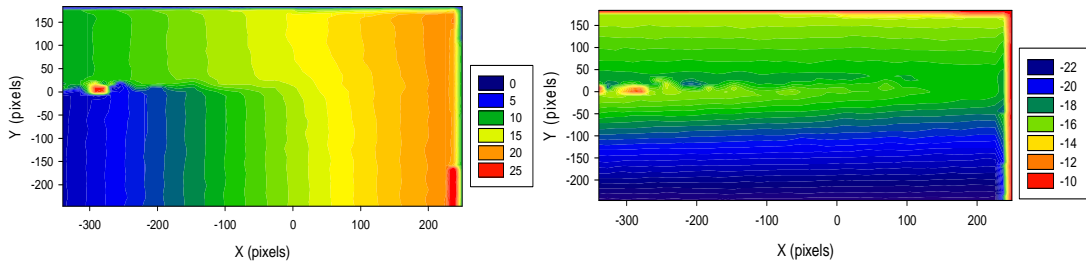


Figure 70a: V and U fields from FEA Modeling at 79N Load, 22% Mixture

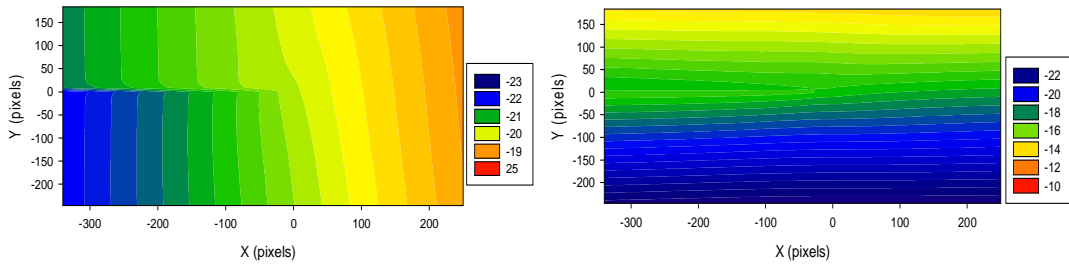


Figure 70b: Analytical Solution for V and U Field at 79 N Load, 22% Mixture

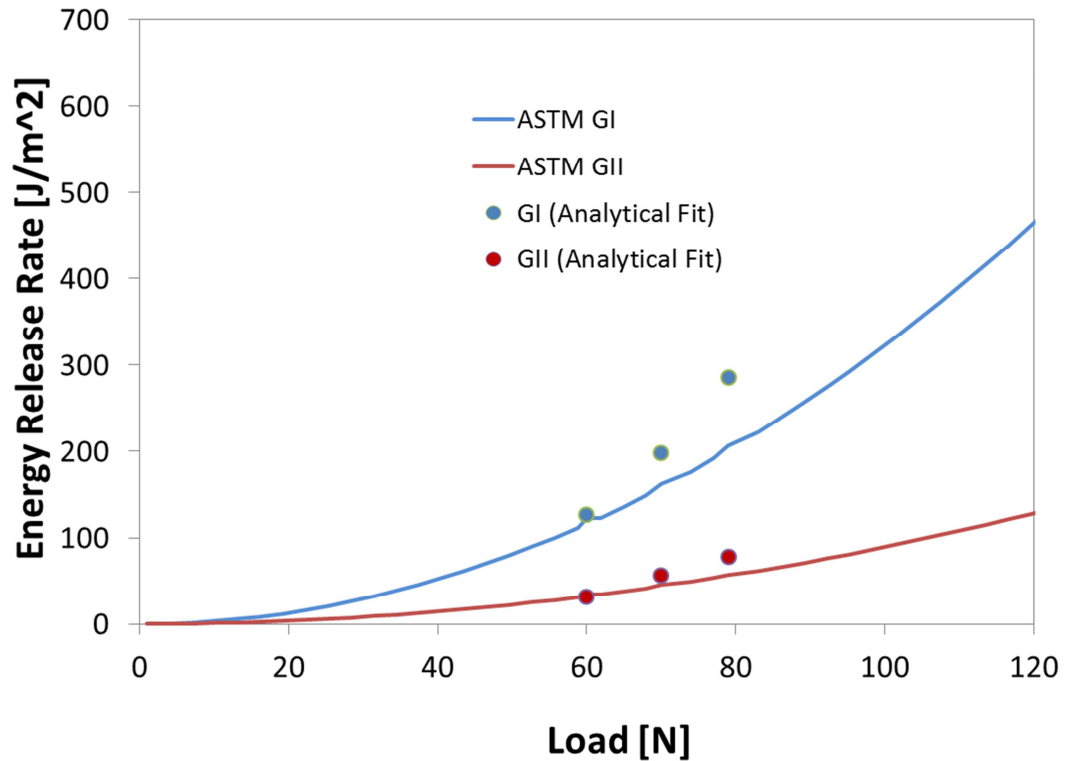


Figure 71: Fracture Parameters calculated from DIC data compared with ASTM Standard for LEFM region of 22% mode mixture fracture test

The strain energy release rates reported from DIC generally tend to be greater than the expected ASTM values. This is the case for both initial crack propagation as well as the post initial crack growth region. The full field analysis was conducted a second time on data extracted after initial load shedding occurred, which yielded very similar results.

7.5 Full field Analysis for 22% Mode Mixture DIC Data After Crack

Propagation:

Load Level	G_I [J/m ²]	G_{II} [J/m ²]	ASTM G_I [J/m ²]	ASTM G_{II} [J/m ²]
40 N	148.87	43.16	114.6	32.95
50 N	225.51	71.3529	176.0	50.64

59 N	349.48	88.09	251.4	72.73
------	--------	-------	-------	-------

Table 7: Fracture parameters for DIC data compared to ASTM standard, 22% Mode Mixture post initial crack growth.

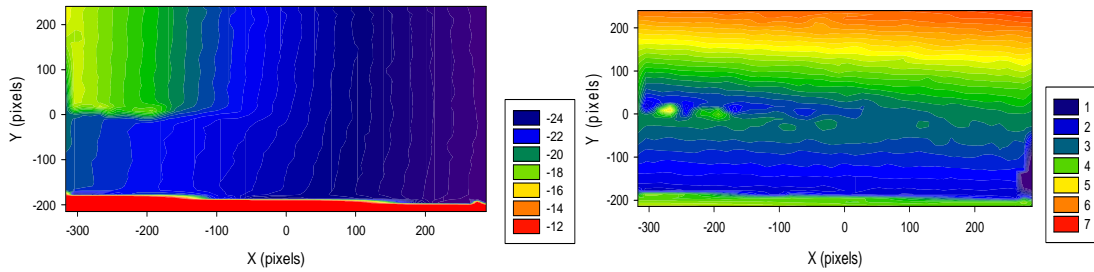


Figure 72a: V and U fields from DIC at 40 N Load, 22% Mixture

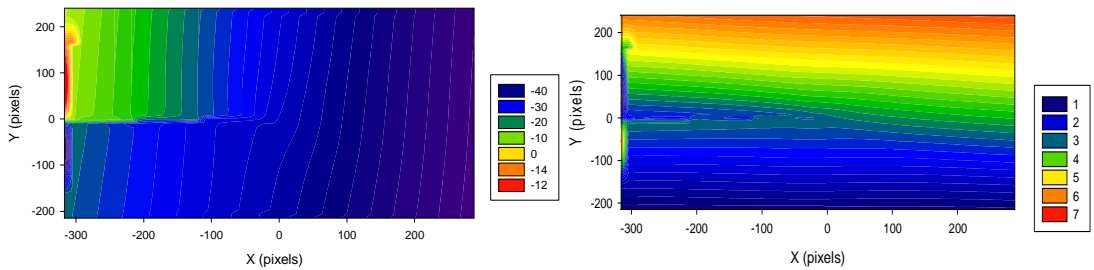


Figure 72b: Analytical Solution for V and U Field at 40 N Load, 22% Mixture

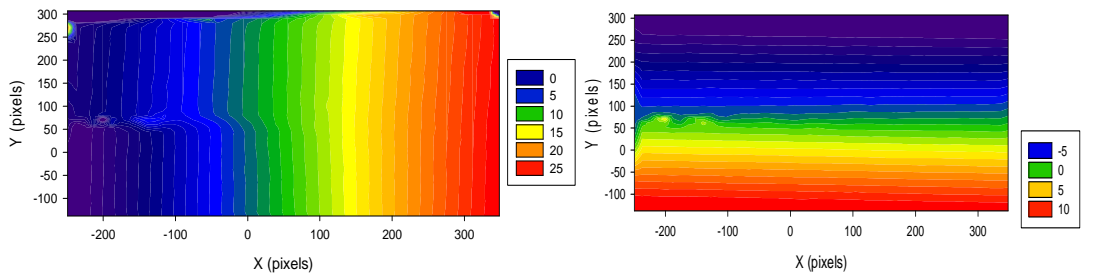


Figure 73a: V and U fields from DIC at 50 N Load, 22% Mixture

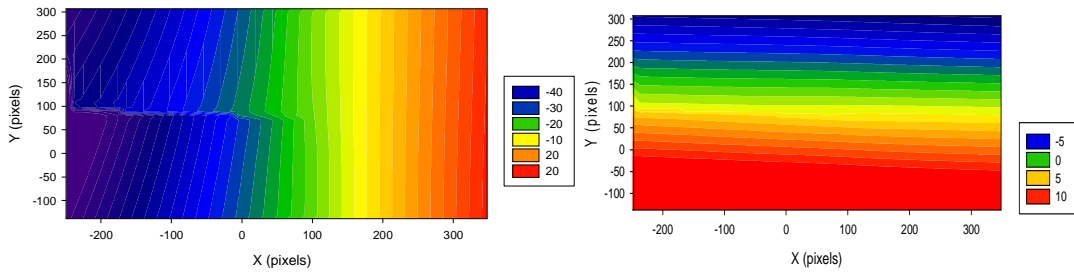


Figure 73b: Analytical Solution for V and U Field at 50 N Load, 22% Mixture

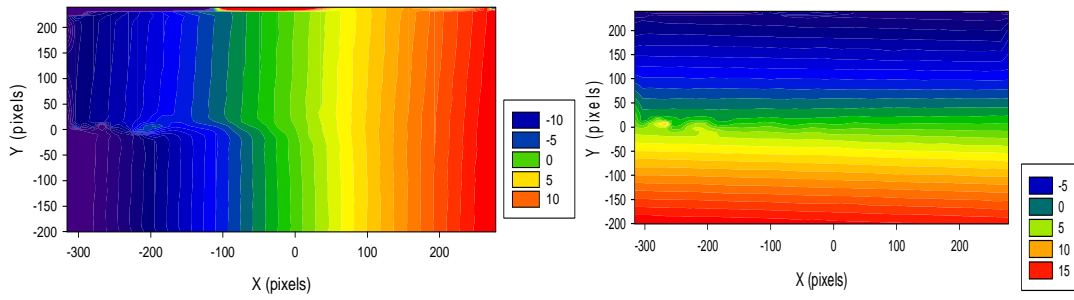


Figure 74a: V and U fields from DIC at 59 N Load, 22% Mixture

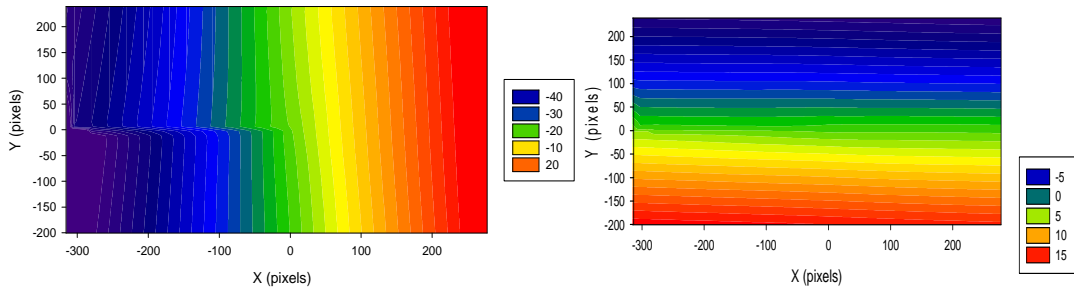


Figure 74b: Analytical Solution for V and U Field at 59 N Load, 22% Mixture

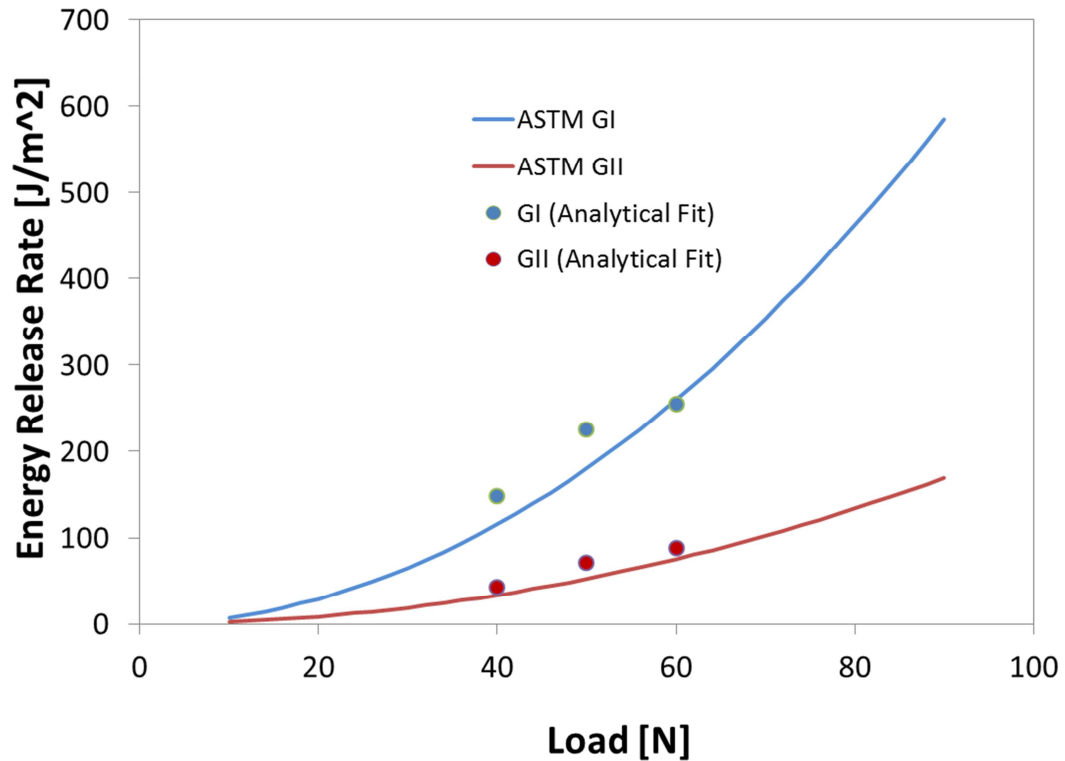


Figure 75: Fracture Parameters calculated from DIC data compared with ASTM Standard after initial crack propagation of 22% mode mixture fracture test

By comparing *figure 63* and *figure 59* it can be seen that the strain energy release rate remains relatively constant at critical loads when crack growth occurs. The resulting plastic deformation when crack growth does occur results in a change in the geometric properties of the test specimen. The ASTM standard may then be adjusted for the new geometry of crack length, and the load displacement slope. A composite curve comparing the strain energy release rate as a function of load for a full test, including regions after crack growth is shown in *figure 64*. The green arrows indicate the trend for the curves as the crack grows. Fracture toughness should remain constant throughout a test, and this is noticeable as the peaks of the curves are generally at the same y values. It should be noted that *figure 64* is largely

estimated as no exact values for crack length were measured during the test. Real time crack length measurements during the test are extremely difficult to measure with accuracy when there is any unstable mode II crack growth present in the test, as such the shape of this figure is largely based off of estimated values.

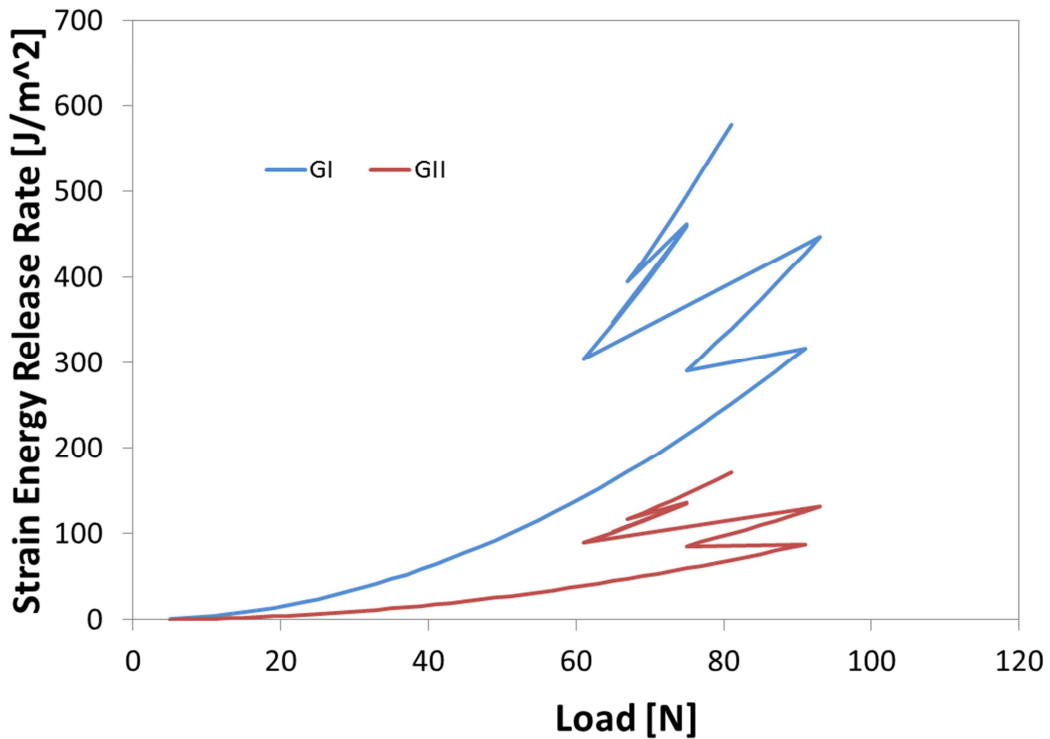


Figure 76: Strain energy release rate with increasing load and crack length for a 22% mode mixture test. (Test 17)

Figure 77 models the strain energy release rate as a function of crack length.

Theoretically the strain energy release rate should remain constant for increasing crack length. The inaccuracy of this data can be attributed to the large number of assumptions required for its generation.

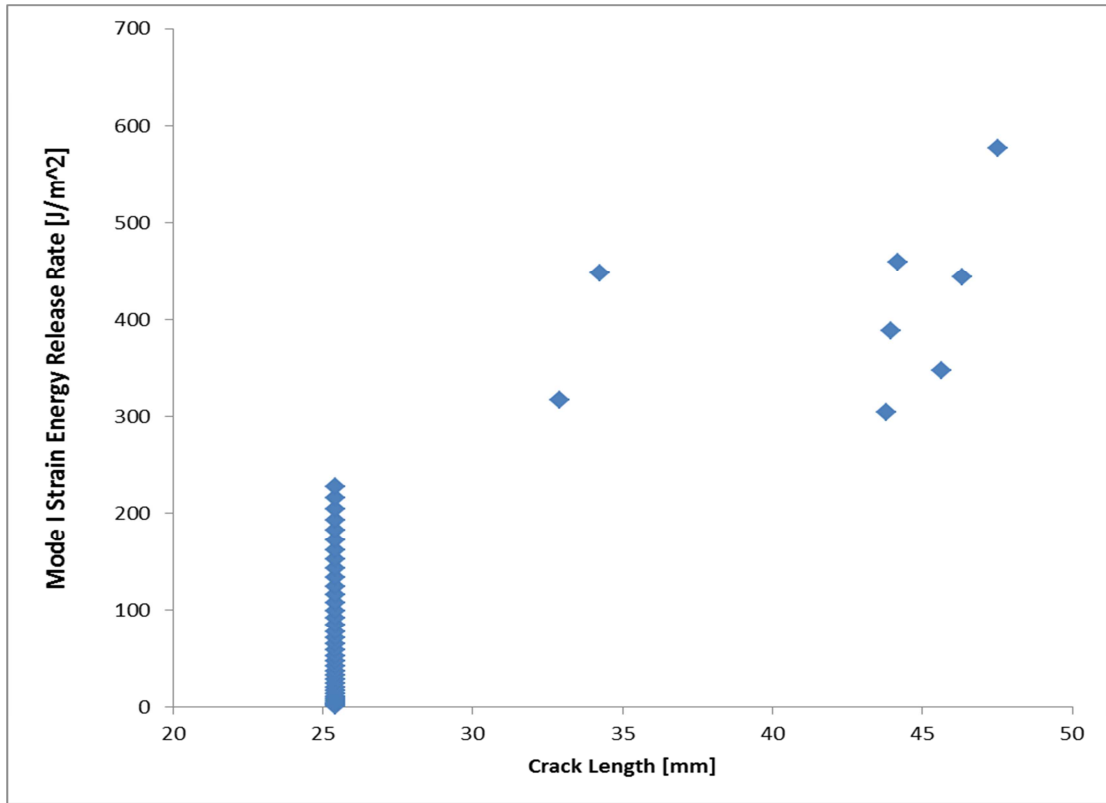
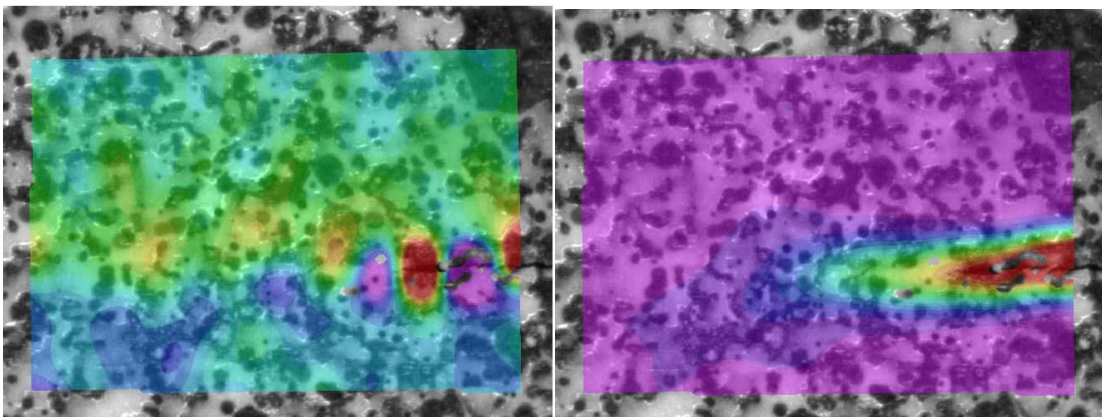


Figure 77: Strain energy release rate with increasing crack length for a 22% mode mixture test. (Test 17)

The program used to correlate images, vic 2D is also capable of exporting a significant number of other parameters. Along with displacement data, the program may be used to analyze strain during the test. The strain contours in the xx, yy, and xy orientation are shown in *figure 78*.



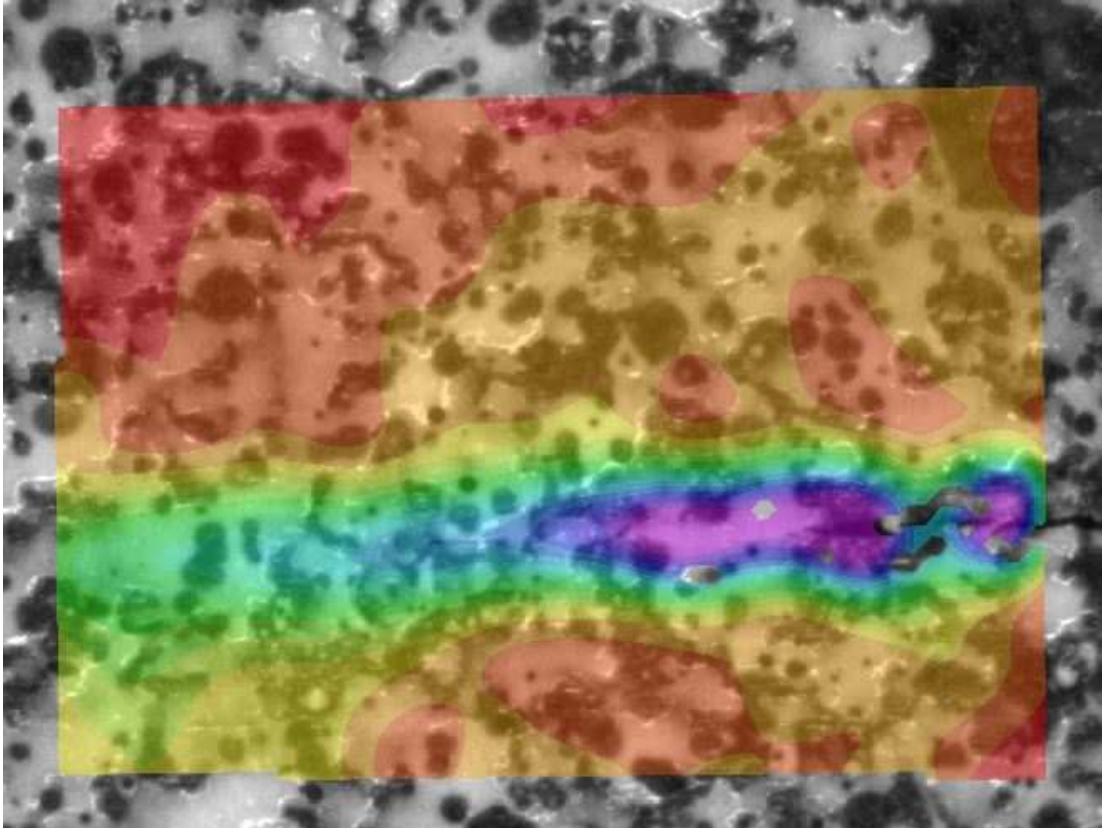


Figure 78: Strain in xx (left) yy (right) and xy orientation (bottom)

These strain fields may also be used for the extraction of fracture parameters, but that analysis has not yet been conducted.

One possible cause for the discrepancy between results returned from DIC and the ASTM standard, is the presence of fiber bridging. The ASTM standard goes through great lengths to ensure that it is not an issue in the test by using delamination inserts, slow crack growth, and only unidirectional laminates. These conditions are rarely experienced in industry and in real life, and the future work for this project would include investigations into materials which do not conform to the ASTM standard. Even with all of the risk mitigation factors established by test protocol and the ASTM standard, fiber bridging still occurs. *Figure 79* shows fiber bridging as it occurs in the same test specimen analyzed above for 22% mode mixture.

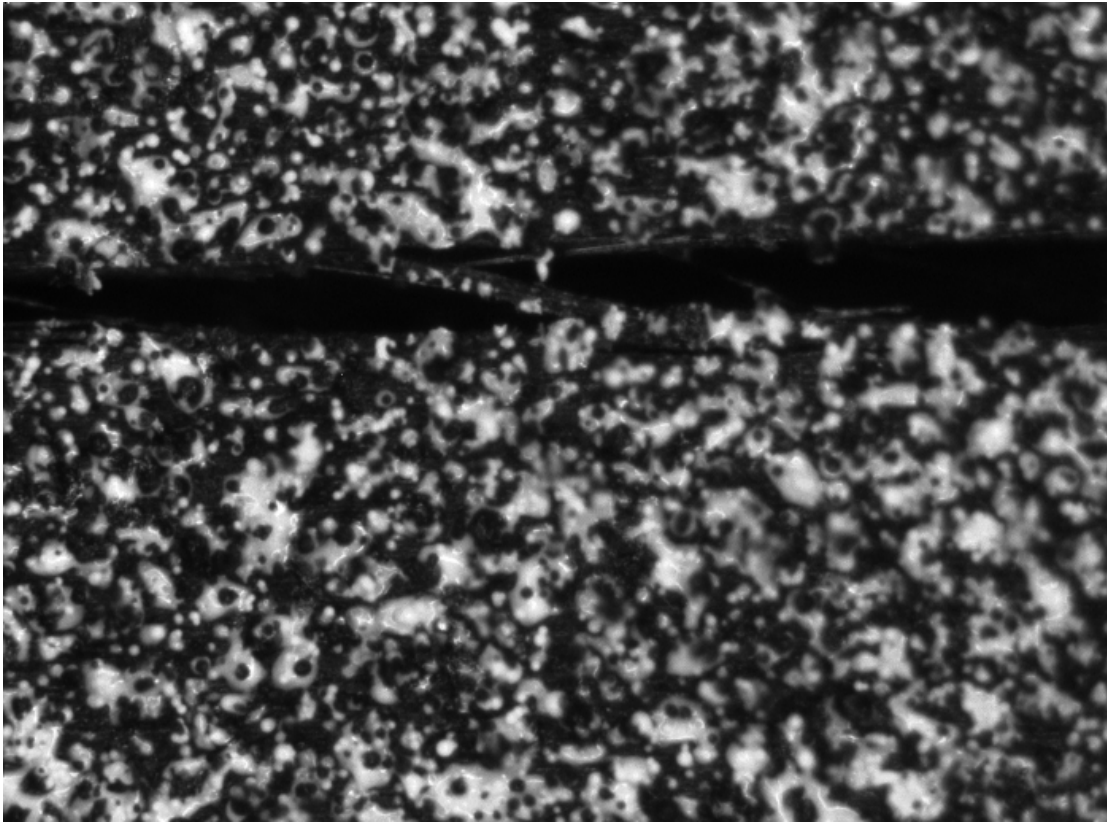


Figure 79: Fiber bridging in a 22% mode mixture test analyzed for DIC.

Fiber bridging is the process wherein individual or groups of fibers remain connected from one side of the delamination to the other side. They may extend across the entire width of the sample and induce what is essentially a second crack above or below the original delamination plane, or they may only be several fibers wide. Though they often break shortly after forming, fiber bridges can greatly influence the fracture properties of any test specimen. It was extremely fortuitous that this fiber bridge occurred precisely on the outer plane where digital imaging and microscopy is permissible. Fully destroying the specimens to investigate the crack plane also shows numerous small and loose fibers aligned perpendicular to their original orientation. This is an indication that fiber bridging has occurred during the test. Future work

would focus on characterizing fiber bridging by attempting to induce this effect and obtaining DIC data for it. It can be stated however, that fiber bridging does effect the DIC data for the 0% and 22% mode mixture cases.

7.6 Full Field Analysis for 50% Mode Mixture DIC Data:

The 50% mode mixture fracture analysis using DIC turned up much less fruitful than the 22% case. Because this case is now dominated by shear type fracture modes, the crack growth is much more unstable. Opening displacements are minimal, and the nature of the fixture induces larger bending displacements and rotations in the test sample. As such, the analysis becomes significantly more complicated, and the fitting function requires the use of numerous higher order terms and rotational corrections. This may be seen in *figure 62*, as the optimal fit for 50% mode mixture data at high load.

Load Level	G_I [J/m ²]	G_{II} [J/m ²]	ASTM G_I [J/m ²]	ASTM G_{II} [J/m ²]
200 N	85.59	148.79	135.52	142.65
270 N	140.82	144.57	247.02	259.91
299 N	252.26	223.69	307.93	323.12

Table 8: Fracture parameters for DIC data compared to ASTM standard, 50% Mode Mixture.

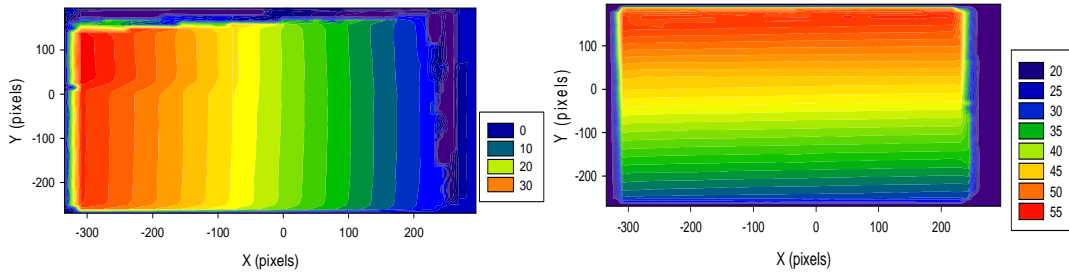


Figure 80a: V and U fields from DIC at 200 N Load, 50% Mixture

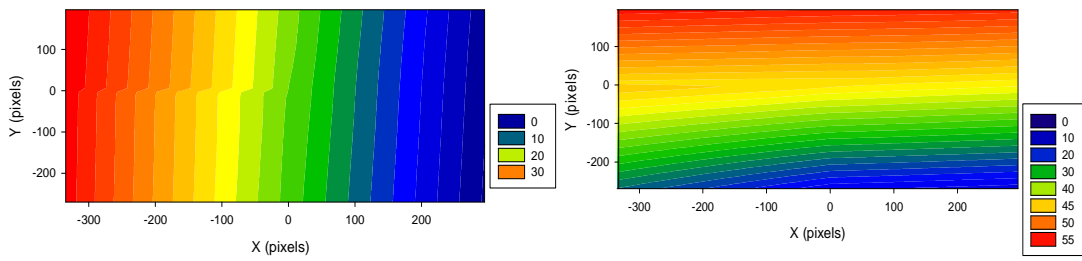


Figure 80b: Analytical Solution for V and U Field at 200 N Load, 50% Mixture

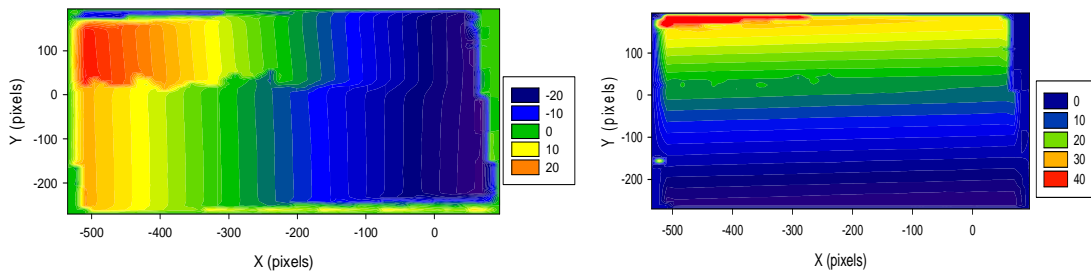


Figure 81a: V and U fields from DIC at 299 N Load, 50% Mixture

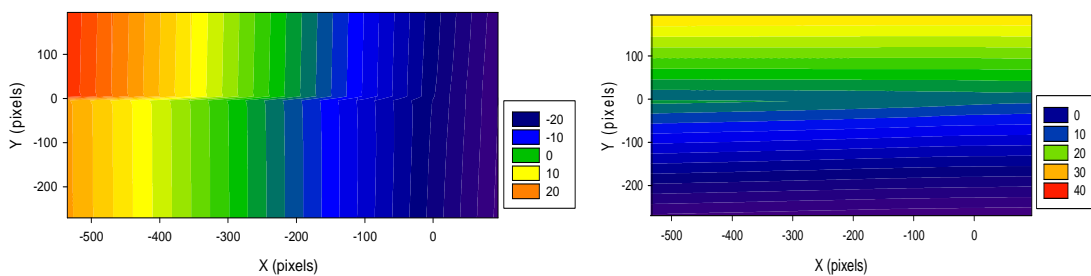


Figure 81b: Analytical Solution for V and U Field at 299 N Load, 50% Mixture

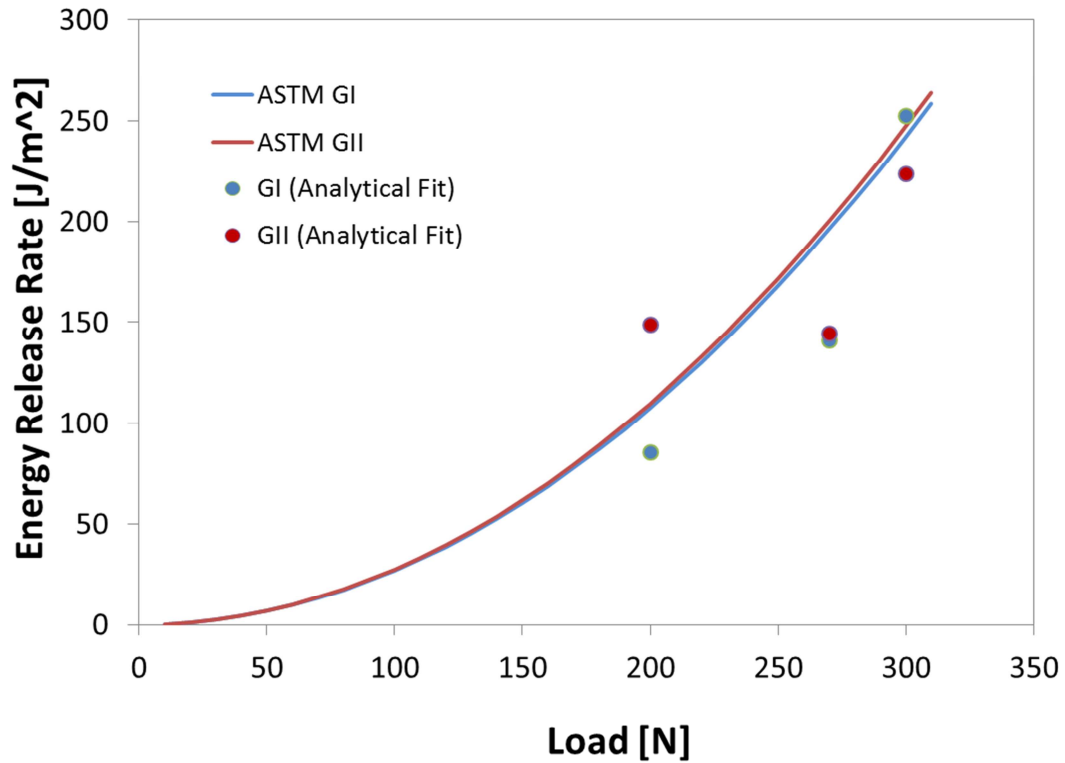


Figure 82: Fracture Parameters calculated from DIC data compared with ASTM Standard after initial crack propagation of 50% mode mixture fracture test

7.7 Full field Analysis for 100% Mode Mixture DIC Data:

The 100% mode mixture case, much like the 0% mode mixture case did not yield the most favorable results. They were however, close enough to show the same trends and general shape of the load displacement curve for a fracture test. Like the other tests, the fracture parameters calculated were typically greater than the fracture values predicted by the ASTM standard.

Load Level	G_I [J/m ²]	G_{II} [J/m ²]	ASTM G_I [J/m ²]	ASTM G_{II} [J/m ²]
300 N	0	214.26	0	173.6

330 N	0	308.04	.23	210.1
350 N	0	352.36	.30	236.3
370 N	0	355.94	.38	264.1
380 N	0	355.89	.40	278.6
460	0	399.655	.58	408.3

Table 9: Fracture parameters for DIC data compared to ASTM standard, 100% Mode Mixture.

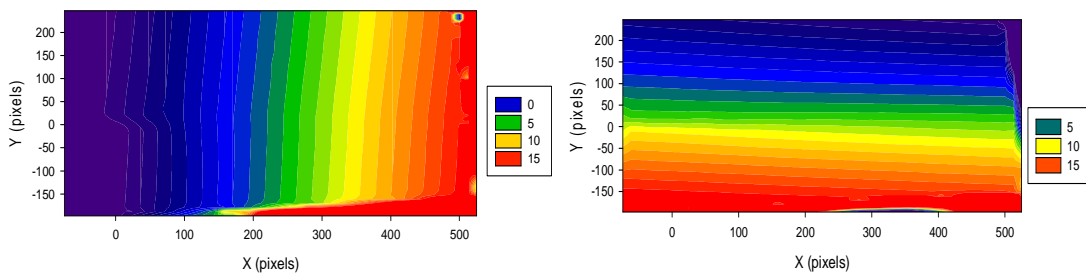


Figure 83a: V and U fields from DIC at 300 N Load, 100% Mixture

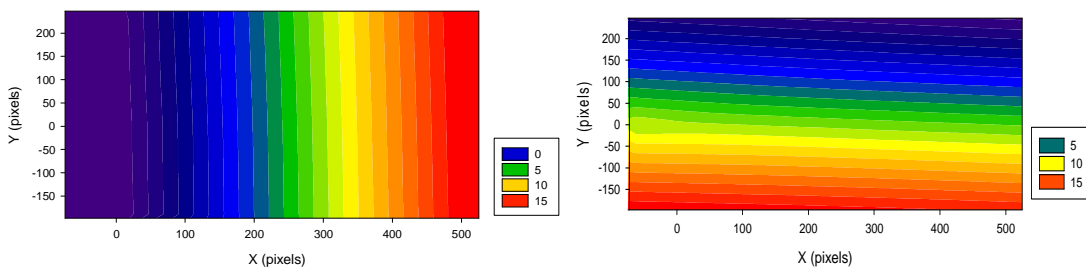


Figure 83b: Analytical Solution for V and U Field at 300 N Load, 100% Mixture

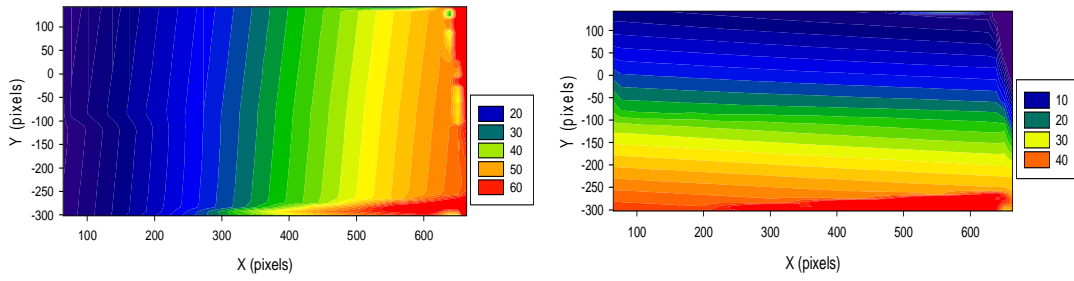


Figure 84a: V and U fields from DIC at 350 N Load, 100% Mixture

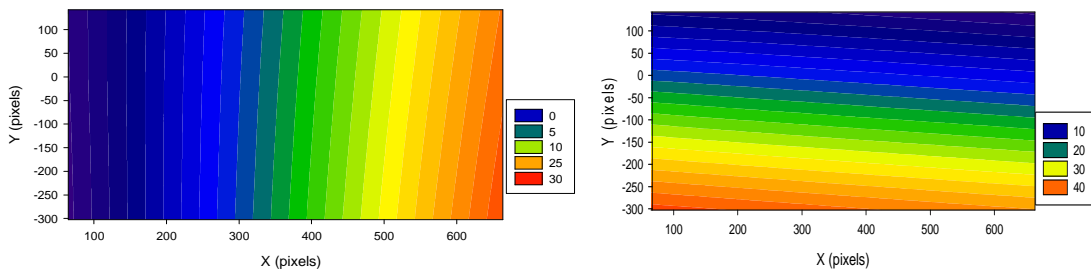


Figure 84b: Analytical Solution for V and U Field at 350 N Load, 100% Mixture

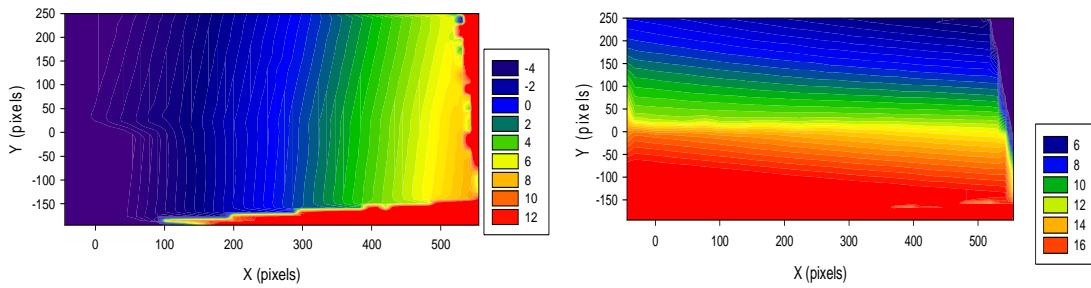


Figure 85a: V and U fields from DIC at 380 N Load, 100% Mixture

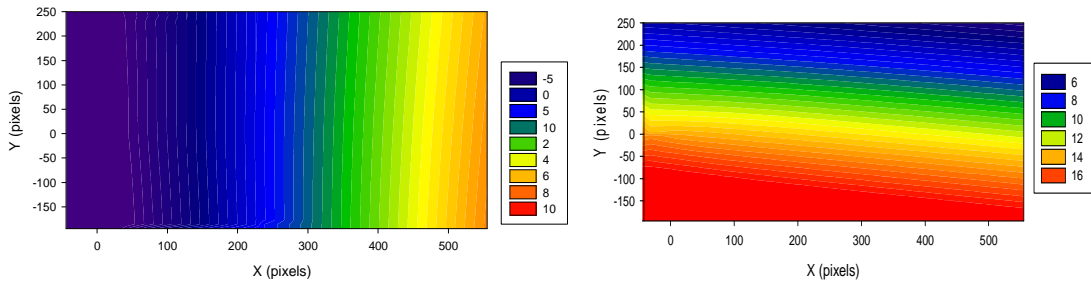


Figure 85b: Analytical Solution for V and U Field at 380 N Load, 100% Mixture

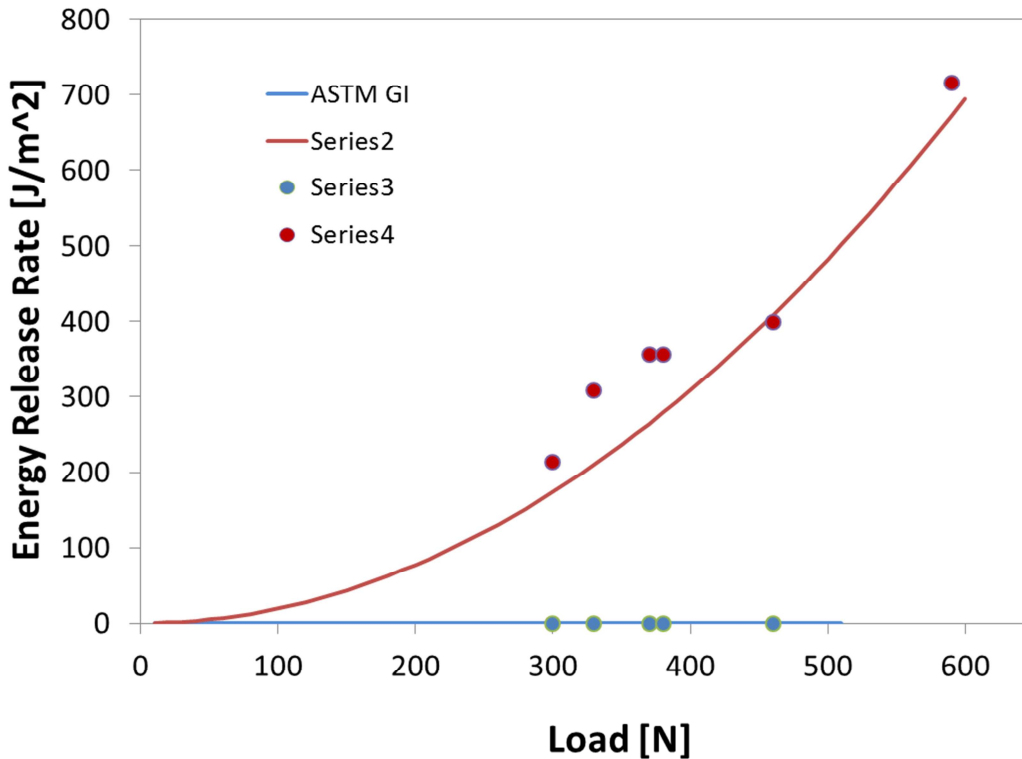


Figure 86: Fracture Parameters calculated from DIC data compared with ASTM Standard after initial crack propagation of 100% mode mixture fracture test

The greatest challenge in fitting the 100% mode mixture data, and one of the greatest reasons for the high amount of error displayed in *figure 84* is the significant amount of rotation induced by beam bending and deflection during the test. Because high mode II testing occurs at very high loads, the beam sees a large amount of bending deformation. *Figure 85* shows the strain fields present in the analysis of the 100% mode mixture case. The orientation of the crack tip from the horizontal may be observed as well in this figure. These large amounts of rotation make analysis particularly difficult to converge on the most accurate solution as this adds many more terms for the fit.

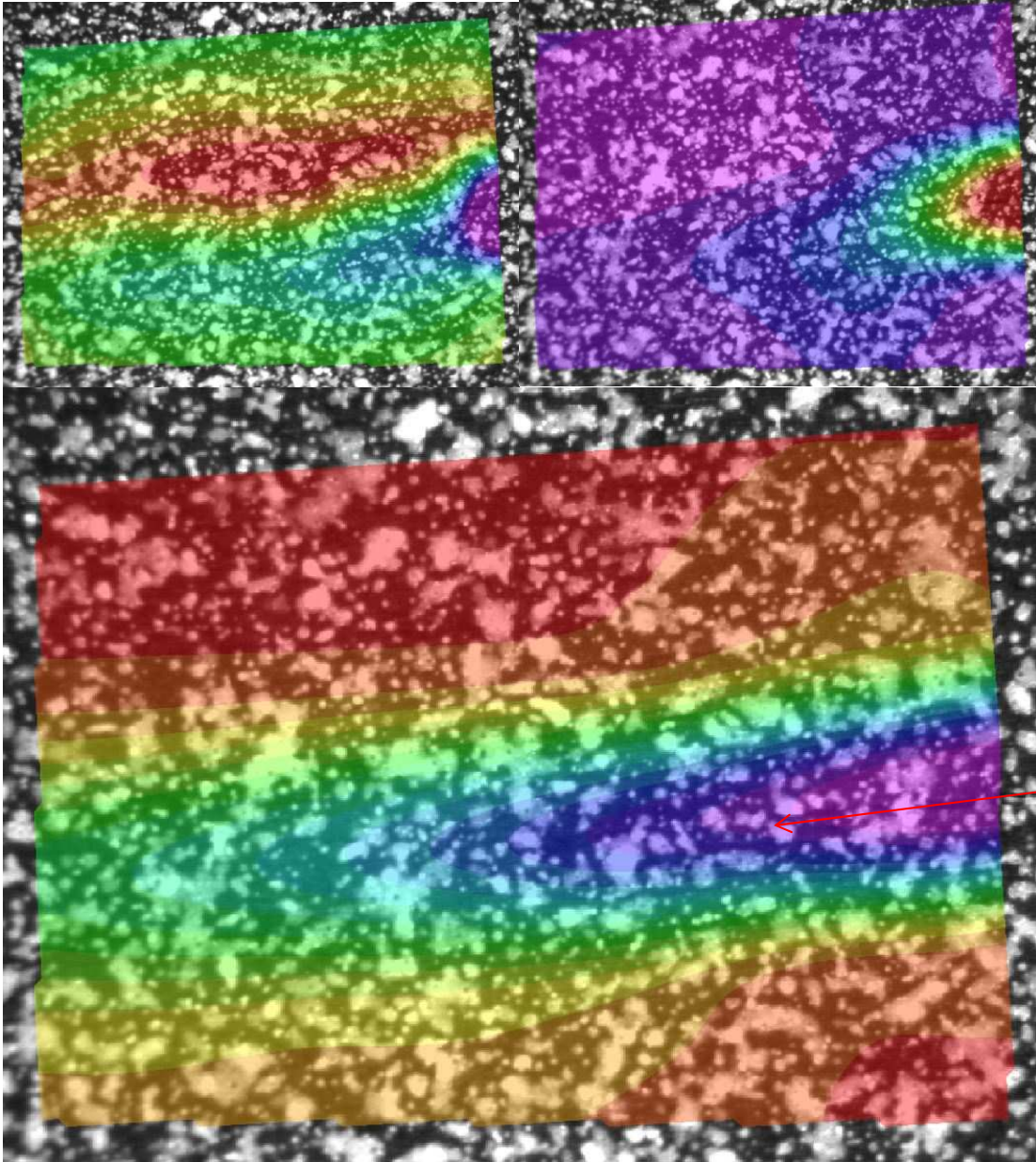


Figure 87: Strain in xx (left) yy (right) and xy orientation (bottom)

The strain field shown here in *figure 87* for the 100% mode II case is much more pronounced than the strain field in *figure 78* for the 22% mode mixture test. This is because of the significantly larger loads experienced by a 100% mode mixture case. The thin red arrow represents the location and angle of the crack tip. This test was originally conducted with a crack tip horizontal to the bottom edge of the image.

The large amounts of deflection and bending are visible here. Additionally, *figure 87* shows how far beyond the crack tip the strains reach. In this image, the cracks edge is nearly at the transition from the dark blue to light blue contour. Though the crack tip ends there, the stresses are present far beyond the edge of the image.

7.8 Analysis of Fracture Parameters Extracted from Full Field DIC

Displacement Data:

22% Mode Mixture						
Load Level	G_I [J/m ²]	G_{II} [J/m ²]	ASTM G_I [J/m ²]	ASTM G_{II} [J/m ²]	Difference G_I [%]	Difference G_{II} [%]
60 N	126.85	31.7124	122.4	33.78	3.64	6.12
70 N	198.2	56.376	166.6	45.98	18.97	22.61
79 N	285.41	77.83	212.1	58.56	34.56	32.91
22% Mode Mixture, Post Crack Growth						
Load Level	G_I [J/m ²]	G_{II} [J/m ²]	ASTM G_I [J/m ²]	ASTM G_{II} [J/m ²]	Difference G_I [%]	Difference G_{II} [%]
40 N	148.87	43.16	114.6	32.95	29.90	30.99
50 N	225.51	71.3529	176	50.64	28.13	40.90
59 N	349.48	88.09	251.4	72.73	39.01	21.12
50% Mode Mixture						
Load Level	G_I [J/m ²]	G_{II} [J/m ²]	ASTM G_I [J/m ²]	ASTM G_{II} [J/m ²]	Difference G_I [%]	Difference G_{II} [%]
200 N	85.59	148.79	135.52	142.65	36.84	4.30
270 N	140.82	144.57	247.02	259.91	42.99	44.38
299 N	252.26	223.69	307.93	323.12	18.08	30.77
100% Mode Mixture						
Load Level	G_I [J/m ²]	G_{II} [J/m ²]	ASTM G_I [J/m ²]	ASTM G_{II} [J/m ²]	Difference G_I [%]	Difference G_{II} [%]
300 N	0	214.26	0	173.6	-	23.42
370 N	0	355.94	0.38	264.1	-	34.77
380 N	0	355.89	0.4	278.6	-	27.74
460	0	399.655	0.58	408.3	-	2.12

Table 10: Fracture parameters from DIC data compared to ASTM Analysis

The fracture parameters extracted from full field analysis of DIC displacement data is extremely good. Most variations within the data is within acceptable levels of error, and is likely once again a result of noise in the data. The data presented for fracture parameters extracted from DIC is extremely valuable. This is the first time anyone has been able to characterize fracture parameters for delaminated carbon fiber laminate structures utilizing DIC. Additionally, this analysis yields an even more useful parameter for industry. In the process of the using the fitting function, the closest fit value for crack tip location is returned. Using this analysis it is possible to determine the exact location and size of a crack tip simply by applying a fine speckle pattern and taking two images, one a zero load, and another with applied load. The deformation contours shown throughout this chapter clearly indicate the location of the crack tip once properly assessed.

Even though there is still room for enhanced data collection, there is substantial evidence to support the successful application of DIC as a means to extract fracture parameters for composite laminates. This will enable future analysis and determination of fracture properties for composite orientations, and test configurations for which no analytical solution currently exists. DIC can be applied to not only synthetic displacement data, but also experimental data at numerous testing configurations.

Chapter 8: Scientific and Technical Contributions

8.1 New Test Protocol for Obtaining Mixed Mode Energy Release Rates using a Wyoming Test Fixture and DIC

A new test protocol has been developed for testing laminated composite specimens using the Wyoming test fixture for mixed mode loading and DIC for measuring the near tip crack field displacements. Details for the protocol are reported at the end of Chapter 4 for the test procedure and Chapter 5 for the data analysis.

8.2 Measurement of Mixed Mode Energy Release Rates

For the first time, a comparison of mixed mode energy release rates obtained from a Wyoming test fixture has been made using fits of an analytical solution to (a) synthetic FEA data and (b) DIC data. The following is a comprehensive summary of the values for G_I and G_{II} extracted with the different data processing methods. Please note that some methods are not capable of producing specific results for G_I , and G_{II} , but rather a single value for G in which case the individual values for G_I and G_{II} are estimated using the value for shear fracture toughness as well as the mode mixture. All values reported are the critical value when crack propagation is present. All values reflect an average value for instances when multiple tests were conducted.

0% mode mixture:

Method	G_I	G_{II}	G_C	Mode Mixture
---------------	-------	----------	-------	---------------------

<i>ASTM Standard</i>	405.2 J/m ²	0 J/m ²	405.2 J/m ²	0%
<i>Load-Displacement Analytical</i>	411.535 J/m ²	0 J/m ²	411.535 J/m ²	*estimated*
<i>Crack Tip Displacement [DIC]</i>	185.7 J/m ²	0 J/m ²	185 J/m ²	0%
<i>Full Field Analysis [DIC]</i>	588.13 J/m ²	0 J/m ²	588.13 J/m ²	0%

Table 11: Summary of fracture parameters for 0% Mode Mixture

22% mode mixture:

Method	G_I [J/m ²]	G_{II} [J/m ²]	G_c [J/m ²]	Mode Mixture
<i>ASTM Standard</i>	212.1	58.56	270.66	21.6%
<i>Load-Displacement Analytical</i>	132.0	36.2	168.2	22%
<i>Crack Tip Displacement [DIC]</i>	254.55	72.41	326.97	22.1%
<i>FEA Synthetic Data</i>	220.43	79.14	299.57	26.4%
<i>Full Field Analysis [DIC]</i>	285.41	77.83	363.24	21.4%

Table 12: Summary of fracture parameters for 22% Mode Mixture

50% mode mixture:

Method	G_I [J/m ²]	G_{II} [J/m ²]	G_c [J/m ²]	Mode Mixture
<i>ASTM Standard</i>	251.6	259.8	511.4	50.8%
<i>Load-Displacement Analytical</i>	268.4	279.4	547.8	*estimated*
<i>Crack Tip Displacement [DIC]</i>	-	-	-	-
<i>Full Field Analysis [DIC]</i>	252.26	223.69	475.96	47.0%

Table 13: Summary of fracture parameters for 50% Mode Mixture

100% mode mixture:

Method	G_I	G_{II}	G_c	Mode Mixture
<i>ASTM Standard</i>	1.1	702.0	703.1	99.8%
<i>Load-Displacement Analytical</i>	0.0	710.5	710.5	*estimated*
<i>Crack Tip Displacement [DIC]</i>	0.0	185	185	100%
<i>Full Field Analysis [DIC]</i>	0.0	715.15	715.15	100%

Table 14: Summary of fracture parameters for 100% Mode Mixture

Even with the slight variations in energy release rate calculated for the different fracture parameters, the values are all within reasonable proximity to the expected ASTM standard. Even for the outlying data points, the trends are all followed rather closely. The most notable trend is for fracture parameters extracted from DIC to be greater than the ASTM standard. It can be conclusively stated that use of DIC is a viable technique for fracture parameter extraction from real time data acquisition.

The advantages of DIC over traditional load displacement methods of data extraction are limitless. There is no need for calibration specimens, no need for compliance correction, no uncertainty from material properties, and no assumptions required for the use of DIC. There simply needs to be a reference image at zero load a good high resolution speckle pattern, and another image at the deformed load condition under investigation. Once again, the greatest challenge to conducting DIC and successfully extracting fracture parameters is the resolution of the data used. Better data would induce less error, and thus improve the quality of the fit and

enhance the accuracy of the fracture parameters extracted. Another option for enhanced data collection would be to increase magnification. The increased magnification focused on the precise crack tip would help to eliminate bad data and remove far field effects which bias the fracture parameters which are calculated from this data. The only obstacle to enhanced magnification is the speckle pattern itself. One of the first areas needing improvement for DIC is a more refined and controlled means of applying a speckle pattern to the data.

Overall DIC has proven to be a successful means of determining fracture parameters from composite laminate structures loaded in mode I, mode II, and mixed mode bending. This analysis has been confirmed with numerous methods, including crack tip displacement analysis, full field analysis, and finite element analysis modeling. The data supports that the equations used to determine fracture parameters are both viable and accurate.

8.3 Measurement of Mixed Mode Crack Growth using New Test Protocol

The data provided in section 7.5 is the first characterization of the crack growth region to date. This data will be used by other researchers at the University of Maryland to develop a Cohesive Zone Model, (CZM) model as part of the FEA model already used in this study. The goal is to develop a CZM model capable of predicting crack growth in fatigued laminated composite structures loaded in mixed mode bending. This is not possible however without actual experimental data to calibrate the model, and uncover discrepancies in the analysis

8.4 Development of Accurate Fitting Function for Fracture Parameters

The program used to extract fracture parameters for crack tip displacements and full field displacements can easily accept new DIC data. The fitting function has been proven accurate with both perfect synthetic data from FEA analysis, and experimental data from DIC. This fitting scheme may now be applied to composite laminates with different and unique lay-up patterns which currently have no analytical method for extracting fracture data. This course of study has pioneered a new means for engineers to rapidly determine crack locations and extract fracture parameters for a wide range of potential laminate configurations.

Chapter 9: Future Work

9.1 Characterization of Fiber Bridging and its Effect on Fracture

Parameters

The first amount of future work is to continue analysis of unidirectional carbon fiber laminates in high mode I testing. By intentionally inducing fiber bridging, it may be possible to analyze the fiber bridging process as it occurs using DIC. Several trial tests may need to be run before fiber bridging occurs on a surface where imaging is permissible, but the analysis yielded if possible will be fruitful. The characterization of fiber bridging will lead to a more accurate method for analyzing fracture parameters in composite materials.

9.2 Characterization and Testing of Multidirectional Laminate Structures

Another area of particular interest is the analysis of composites with different laminate orientation. Towards the end of this course of study, different laminate configurations were manufactured with the intention of testing them in mixed mode bending. Unfortunately, this was never completed. The current ASTM standard is for unidirectional composites only, and the analysis breaks down for different laminate configuration. Bi-axial specimens, specimen weaves, and different laminate configurations are much more common to industry and real life industrial applications than the unidirectional ones used in this course of study. DIC combined with the techniques pioneered here in this report can finally be the answer to successful and

accurate characterization of fracture parameters for difficult and unique specimen geometries.

9.3 Fatigue Fracture Testing of Composite Laminates

DIC could also be used to conduct analysis on the post initial crack region as was the case for the 22% and 0% load configurations. The unstable and rapid crack propagation of the mode II dominate load configurations prevents this analysis. Attempts to even moderately slow crack growth were unfruitful. The only solution remaining for slowing crack growth would be to use fatigue testing as a growth mechanism. Fatigue analysis of carbon fiber composite delamination could be very beneficial analysis.

References

- [1] MIDN Puishys, Joe., “Damage Tolerance of Laser Irradiated Composite Sandwich Structures,” Directed Energy Professional Society Symposium, November, United States Naval Academy 2011.
- [2] Nikbakht, M. and Choupani, N., “Fracture Toughness Characterization of Carbon-Epoxy Composite Using Arcan Specimen,” World Academy of Science, Engineering and Technology, Vol. 41, pp. 738-744, 2008.
- [3] Scale, E. Pete. “A Brief History of Composites in the U.S. – The Dream and the Success,” JOM 48, pp. 45-48, 1996
- [4] Baral, N., “High Modulus Carbon Fiber Composites: Correlation between Transverse Tensile and Mode I Interlaminar Fracture Properties,” Materials Letters, Vol 62, Issues 6-7, pp. 1096-1099, 2008.
- [5] C.M. Medford, “An Investigation into the Effect on Residual Strength of Composite Materials Following Irradiation by a High Energy Laser” United States Naval Academy 2011.
- [6] Adams, Donald F. and Carlsson, Leif A. and Pipes, R. Byron., “Experimental Characterization of Advanced Composite Materials,” Third Ed. Boca Raton, FL: CRC Press, pp. 185-210, 2003.
- [7] Carlsson, Leif A. and Pipes, R, Byron., “Experimental Characterization of Advanced Composite Materials,” Englewood Cliffs, NJ: Prentice-Hall, Inc, pp.157-191, 1987.
- [8] Robinson, R. (n.d.). Cracking dams. Retrieved from <http://simscience.org/cracks/advanced/math1.html>

- [9] Haslach, Henry W. and Armstrong, Ronald W., "Deformable Bodies and Their Material Behavior," Danvers, MA: John Wiley & Sons, Inc, pp. 383-425, 2004.
- [10] Bruck, Hugh. "Introduction to Fracture Mechanics: Energy Release Rate." ENME808Y. University Of Maryland. 22 2012. Lecture
- [11] Bruck, Hugh. "Crack Tip Stress Fields and the Stress Intensity Factor." ENME808Y. University Of Maryland. 25 2012. Lecture
- [12] Priel, E. and Bussiba, A. and Gilad, I. and Yosibash, Z., "Mixed mode failure criteria for brittle elastic V-notched structures." International journal of fracture 144: 247-265, 2007.
- [13] Poursartip, A. and Gambone, S. and Ferguson, S. and Fernlund, G., "In-Situ SEM Measurements of Crack Tip Displacements in Composite Laminates To Determine Local G in Mode I and II," Engineering Fracture Mechanics, Vol. 60, No. 2, pp. 173-185, 1998.
- [14] Sih, G. C., Paris, P. C. and Irwin, G. R., "On cracks in rectilinearly anisotropic bodies." International Journal of Fracture Mechanics, pp. 189-202, 1965.
- [15] ASTM Standard D6671/D6671M, 2006, "Standard Test Method for Mixed Mode I-Mode II Interlaminar Fracture Toughness of Unidirectional Fiber Reinforced Polymer Matrix Composites," ASTM International, West Conshohocken, PA, 2006, DOI: 15.03/D6671-06, www.astm.org.
- [16] Mogadpalli, G. P. and Parameswaran, V., "Determination of Stress Intensity Factor for Cracks in Orthotropic Composite Materials Using DIC," Journal Compilation, Blackwell Publishing Ltd, Strain, vol 44, pp 446-452, 2008

- [17] McNeil, S.R. and Peters, W. H. and Sutton, M. A., “Estimation of Stress Intensity Factor by DIC,” *Engineering Fracture Mechanics*, vol. 28, Issue 1, pp. 101-112, 1987
- [18] Tippur, H.V. and Kiruguliege, M. S., “Measurement of Fracture Parameters for a Mixed Mode Crack Driven by Stress Waves using Image Correlation Technique and High-Speed Digital Photography,” *Journal Compilation*, Blackwell Publishing Ltd, *Strain*, vol 45, pp 108-122, 2008
- [19] Balzani, C. and Wagner, W. and Wilckens, D. and Degenhardt, R. and Reimerdes, G., “Adhesive joints in composite laminates—A combined numerical/experimental estimate of critical energy release rates.” *International Journal of Adhesion and Adhesives*, vol 32, pp. 23-38, 2012.
- [20] Tribikram, Kundu. “Fundamentals Of Fracture Mechanics,” Boca Raton, FL: CRC Press, Taylor & Francis Group, 2008. Print.
- [21] Virakthi, A. and Lee, S.W., “Unpublished Data” University of Maryland, College Park, 2012
- [22] Puishys, J. F. and Bruck, H.A. and Virakthi, A. and Lee, S.W., “Unpublished Progress Report,” University of Maryland, College Park, 2012
- [23] Liu, C. Rosakis, A.J., Ellis, RW. And Stout, A. “Study of the fracture behavior of unidirectional fiber reinforced composites using coherent gradient sensing.” *International Journal of Fracture*, vol. 90, pp. 335-382, 1998.
- [24] Shukla, A., Agarwal, B. D., and Bhushan, B. (1989) “Determination of stress intensity factor in orthotropic composite materials using strain gages.” *Engineering Fracture Mechanics*, vol. 332, pp. 467-477, 1989.

- [25] Maiti, S. and Geubelle, P.H., “A cohesive model for fatigue failure of polymers,” *Engineering Fracture Mechanics*, vol. 72, pp.691–708, 2005.
- [26] Munoz, J.J., Galvanetto, U. and Robinson, P., “On the numerical simulation of fatigue driven delamination with interface elements,” *International Journal of Fatigue*, vol. 28, pp.1136-1146, 2006.
- [27] Turon Travesa, A., “Simulation of delamination in composite under quasi-static and fatigue loading using cohesive zone models”, Ph.D Thesis, Universitat de Girona, ISBN: 978-84-690-4372-1, 2006.
- [28] Turon, A., Costa, J., Camanho, P.P. and Davila. C.G., “Simulation of delamination in composites under high-cycle fatigue,” *Composites: Part A*, vol. 38, pp. 2270–2282, 2007.
- [29] Kawashita, L.F., Jones, M.I., Trask, R.S., Hallett, S.R. and Wisnom, M.R., “Static and fatigue delamination from discontinuous plies - experimental and numerical investigations”, 17th International Conference on Composite Materials, Edinburgh, UK, 27-31 July 2009.
- [30] May, M. and Hallett, S.R., “A combined model for initiation and propagation of damage under fatigue loading for cohesive interface elements,” *Composite: Part A*, vol. 41, pp.1787-1796, 2010.
- [31] Landry, B. and LaPlante, G., “Modeling delamination growth in composites under fatigue loadings of varying amplitudes,” *Composite: Part B*, vol. 43, pp.533-541, 2012